ISSN:2538-516X

Journal of Civil Engineering Researchers

Volume: 7; Number: 1; March 2025

J-Researchers

J-Researchers

JOURNAL OF CIVIL ENGINEERING RESEARCHERS

Volume 7, Number 1, March 2025

Contents

J-Researchers

Journal of Civil Engineering Researchers

Journal homepage: www.journals-researchers.com

Optimizing Slope Stability Assessment Using Hybrid BPSO - SVC with Kernel Function Evaluation

Saurabh Kumar Anuragi,[a,*]

[a] *Department of Civil Engineering, Maulana Azad National Institute of Technology, Bhopal, India*

ABSTRACT

The complex nature of slope engineering presents considerable challenges in accurately predicting slope stability using traditional methodologies. Due to the serious implications that can arise from slope failures, it is crucial to implement the most effective techniques for assessing slope stability. This study investigates a hybrid approach that integrates BPSO with SVC to enhance predictive accuracy in slope stability assessment. The methodology employs BPSO to optimize the selection of features that are critical to the prediction process. Additionally, grid search technique is utilized for fine-tuning the hyperparameters of the SVC. The research evaluates the performance of three SVC kernel functions: linear, polynomial and rbf. For the predictive analysis, six features identified as potentially influential were selected: height of the slope (H), pore water ratio (ru), unit weight of the soil (Y), cohesion of the soil (c), slope angle (β), and angle of internal friction (ϕ). To enhance the generalization capability of the classification models, a 5-fold cross-validation (CV) approach was implemented. The effectiveness of the models was evaluated using various metrics, including the area under the curve (AUC) and overall accuracy of the predictions. The findings of the study indicate that the hybrid approach, particularly the SVC employing the rbf kernel, significantly outperformed the other models in terms of prediction accuracy, achieving an AUC of 0.735 and an accuracy rate of 0.725. This underscores the potential of the proposed hybrid method as a valuable tool for accurately predicting slope stability and mitigating risks associated with slope failures in engineering applications.

ARTICLE INFO

Received: December 22, 2024
Accepted: January 05, 2025

Keywords:
Support vector classifier
Machine learning
Slope stability
Binary particle swarm
Grid search

DOI: 10.61186/JCER.7.1.1
DOR: 20.1001.1.2538516.2025.7.1.1.7

1. Introduction

Slope stability evaluation represents a critical area of research within the field of slope engineering, as it directly influences the safety and effectiveness of various construction and geological projects. The processes underlying slope deformation and failure are inherently complex and involve intricate geological mechanisms. A multitude of factors contribute to slope stability, many of which are uncertain in nature, making it challenging to conduct accurate evaluations using conventional theoretical analyses and numerical methodologies. Traditional techniques, such as the finite element method [1], discontinuous deformation analysis [2], and limit equilibrium method [3], often fall short in accounting for the intricacies involved in slope behavior. Slope

* Corresponding author. Tel.: +91-94069-20449; e-mail: saurabh.1399@gmail.com.

engineering itself is characterized as a complex, non-linear, and dynamic system that is susceptible to various uncertainties. These uncertainties manifest through geological and engineering factors that exhibit randomness, fuzziness, and variability, all of which significantly influence the overall stability of slopes. One of the key challenges in analyzing slope stability is the highly non-linear relationship that exists between slope stability and the myriad influencing factors. Conventional deterministic approaches often fail to capture this non-linearity, leading to potentially inaccurate assessments. Consequently, there is a growing recognition within the research community of the necessity to move beyond traditional deterministic models. This shift aims to embrace a more holistic understanding of the uncertainties associated with the diverse parameters impacting slope stability [4–6]. Given the complex nature of slope engineering, it is vital to incorporate a broad spectrum of geological and engineering considerations, including the unpredictability and variability of these factors, when assessing stability. This evolving perspective emphasizes the urgency for researchers to adopt advanced methodologies that can systematically account for these uncertainties. Ongoing research efforts aim to refine numerical and analytical modeling techniques to better predict possible slope behaviors. By enhancing predictive accuracy, these efforts not only aim to improve understanding of slope stability but also seek to minimize potential losses and inform appropriate preventive measures.

With the advancement of computational techniques, there is a growing opportunity for researchers to implement diverse machine learning methods as alternative approaches for slope stability analysis. By evaluating critical parameters such as slope geometry and material properties, these techniques have the potential to deliver valuable insights and significantly enhance the accuracy of slope stability assessments. Nanehkaran et al. [7] conducted a comparative study evaluating various machine learning techniques for slope stability prediction. Their research included random forest, multilayer perceptron, support vector machines, and decision trees. Similarly, Bui et al. [8] employed five distinct machine learning approaches, namely support vector regression, Gaussian process regression, multilayer perceptron, multiple linear regression, and simple linear regression. Mahmoodzadeh et al. [9] proposed six machine learning techniques for factor of safety (FOS) prediction, which included deep neural networks, Gaussian process regression, support vector regression, k-nearest neighbors, long short-term memory, and decision trees. Nanehkaran et al. [10] further compared five machine learning techniques for FOS prediction, specifically k-nearest neighbors, support vector machines, decision trees, multilayer perceptron, and random forest. Moayedi et al. [11] conducted a comparative analysis among seven machine learning techniques for FOS prediction, including an improved support vector machine utilizing sequential minimal optimization, multiple linear regression, radial basis function regression, random tree, lazy k-nearest neighbor, multilayer perceptron, and random forest. Bai et al. [12] performed a comparative study among eight machine learning techniques for FOS prediction, which comprised gradient boosting decision tree, k-nearest neighbor algorithm, decision tree, guided clustering algorithm, artificial neural network, support vector machine, random forest, and AdaBoost algorithm.

Hybrid models are gaining popularity among researchers due to their ability to enhance accuracy and reliability by combining multiple algorithms. These models leverage the strengths of individual algorithms and compensate for their weaknesses, leading to improved performance across various datasets [13, 14]. For example, integrating optimization techniques like Binary Particle Swarm Optimization (BPSO), Genetic Optimization, Grid Search, Random Search etc. with machine learning classifiers such as Support Vector Classifiers (SVC), Random Forest (RF), XGBoost, CatBoost etc. allows for efficient feature selection while maintaining high prediction accuracy. Luo et al. [15] conducted an extensive slope stability analysis comparing the performance of three standalone machine learning algorithms—k-nearest neighbor (KNN), support vector machine (SVM), and classification and regression tree (CART)—with a hybrid algorithm, the particle swarm optimization-cubist algorithm (PSO-CA). Their study highlighted the potential advantages of integrating optimization techniques with machine learning models to enhance predictive accuracy. Koopialipoor et al. [16] investigated the efficacy of four hybrid machine learning techniques—genetic algorithm-artificial neural network (GA-ANN), artificial bee colony-artificial neural network (ABC-ANN), imperialist competitive algorithm-artificial neural network (ICA-ANN), and particle swarm optimization-artificial neural network (PSO-ANN)—for slope stability prediction. Their research demonstrated that hybrid models could surpass standalone methods by optimizing the training process and improving prediction reliability. Pham et al. [17] performed a comprehensive comparative study of eight machine learning models—decision tree (DT), k-nearest neighbor (KNN), artificial neural network (ANN), Gaussian process (GP), Gaussian naive Bayes (GNB), quadratic discriminant analysis (QDA), support vector machine (SVM), and stochastic gradient descent (SGD)—as well as their combinations in ensemble approaches for slope stability prediction. Their findings underscored the effectiveness of ensemble learning in capturing complex relationships within data. Gordan et al. [18] compared

artificial neural networks (ANN) with a particle swarm optimization-enhanced artificial neural network (PSO-ANN) for predicting the factor of safety (FOS) in homogeneous slopes. Their findings emphasized the superior performance of the hybrid PSO-ANN model in improving prediction accuracy. Zhang et al. [19] evaluated the performance of four machine learning models—XGBoost, support vector machine (SVM), random forest (RF), and logistic regression (LR)—in the context of slope stability prediction. Their results illustrated the applicability of contemporary algorithms, such as XGBoost, in achieving high predictive accuracy. Kardani et al. [20] developed a robust hybrid stacking model utilizing eleven machine learning techniques, including random forest (RF), decision tree (DT), k-nearest neighbor (KNN), extreme gradient boosting (XGB), logistic regression (LR), naive Bayes (NB), multilayer perceptron artificial neural networks (MLPANN), bagging classifier (BC), linear discriminant analysis (LDA), support vector classifier (SVC), and extremely randomized trees (ETs). The artificial bee colony (ABC) algorithm was employed to determine the optimal combination of base classifiers, leading to significant enhancements in the model's predictive performance. Qi et al. [21] introduced a hybrid model that integrates the firefly algorithm with six machine learning techniques—gradient boosting machine (GBM), logistic regression (LR), support vector machine (SVM), random forest (RF), multilayer perceptron neural network (MLP), and decision tree (DT)—to evaluate their effectiveness in precise slope stability prediction. Their approach underscored the advantages of metaheuristic algorithms in improving model accuracy and reliability. Zhou et al. [22] applied the gradient boosting machine (GBM) algorithm to slope stability prediction, demonstrating its effectiveness in managing complex datasets and providing accurate predictions. These collective studies reflect a growing trend in the use of advanced and hybrid machine learning models within geotechnical engineering, highlighting their potential to effectively address the challenges associated with slope stability analysis and prediction. These approaches reduce computational complexity and enhance the model's ability to generalize to unseen data. The rise of computational resources and advanced frameworks has made hybrid models increasingly applicable in real-world geotechnical problems, making them essential tools for predictive modeling in complex engineering scenarios.

The aforementioned machine learning models discussed play a vital role in advancing our understanding of slope behavior and the complex interactions that influence slope stability. However, the complexity of slope stability issues can vary, even when utilizing the same dataset. This variability is attributed to the inherent limitations of each model, as different algorithms operate under distinct assumptions and capabilities. The primary objective of slope stability analysis is to achieve accurate and reliable predictions, which necessitates the development and application of more sophisticated machine learning algorithms. To effectively address these challenges, it is essential to identify and utilize advanced hybrid machine learning algorithms that can provide better outcomes compared to traditional standalone models. The findings from the studies reviewed indicate that hybrid learning algorithms, which combine machine learning with optimization techniques, present a promising avenue for predicting slope stability. Nonetheless, there is a noticeable gap in the literature regarding the focused investigation of the various features influencing slope stability, which warrants thorough investigation. A detailed analysis of model behavior using different feature combinations can yield valuable insights into the dynamics of slope stability, ultimately enhancing model robustness. Optimization algorithms are instrumental in this regard, as they can facilitate the selection of the most significant features and refine model parameters to maximize performance. To further advance this field, future research should prioritize the exploration of innovative hybrid learning algorithms that integrate cutting-edge machine learning techniques with optimization strategies. This comprehensive approach can significantly improve predictive capabilities while deepening our understanding of the critical factors affecting slope stability, thereby contributing to the development of safer and more effective geotechnical solutions.

The objective of this study is to evaluate the performance of various kernel functions—specifically linear, polynomial, and radial basis function (RBF)—in the Support Vector Classifier (SVC) integrated with Binary Particle Swarm Optimization (BPSO), with the specific aim of predicting slope stability. The research will thoroughly explore and assess the effectiveness of SVC across different kernel functions and feature combinations. The selection of the SVC model is attributed to its growing prominence and application in engineering disciplines. This study aims to fill the existing gap in literature by providing a comprehensive evaluation of the performance and applicability of these methodologies.

2. Machine Learning Techniques

2.1. Support Vector Classifier

The Support Vector Classifier (SVC) is a sophisticated machine learning technique that utilizes a nonlinear transformation, characterized by an inner product function, to effectively map the input space into a higher-dimensional feature space. The theoretical underpinnings

of SVC center on key concepts such as linear separability, decision boundaries, and margin maximization. The seminal work of Vapnik and Chervonenkis (1963) introduced the concept of the Vapnik-Chervonenkis (VC) dimension, which serves as an essential framework for understanding the generalization capabilities of SVC [23]. The VC dimension quantifies the capacity or complexity of a hypothesis space, representing the set of potential decision boundaries that a learning algorithm can derive. Specifically, in the realm of SVC, the VC dimension indicates the maximum number of points that can be perfectly separated by the decision boundary established by the algorithm. This dimension is pivotal in evaluating the balance between model complexity and the capacity to generalize effectively to previously unseen data. Furthermore, the introduction of kernel functions by Boser et al. (1992) [24] significantly enhanced the ability of SVC to process non-linearly separable data. In 1995, Cortes and Vapnik [25] presented the formulation of the Support Vector Classifier, highlighting its ability to identify optimal separating hyperplanes characterized by maximum margins. This formulation incorporates two critical components: the slack variable, ξ, which quantifies the deviation of a data point from the ideal condition, and the penalty factor, C, which delineates the trade-off between the number of misclassifications in the training dataset.

The decision functions for different conditions are:

For Linearly Separable:

$$y_i[(w^T x_i) + b] - 1 \geq 0 \quad (1)$$

For Linearly Inseparable;

$$y_i[(w^T x_i) + b] \geq 1 - \xi_i \quad (2)$$

To minimize,

$$\frac{1}{2} w^T w + C \sum_{i=1}^{N} \xi_i \quad (3)$$

For Non-linear Classification:

Linear Kernel:

$$k(x_i x_j) = x_i^T x_j \quad (4)$$

Polynomial Kernel:

$$k(x_i x_j) = (\Upsilon x_i^T + r)^d, \Upsilon > 0 \quad (5)$$

Radial Basis Function (RBF):

$$k(x_i x_j) = e^{(\Upsilon ||x_i - x_j||^2)}, \Upsilon > 0 \quad (6)$$

Sigmoid Kernel:

$$k(x_i x_j) = \tan(\Upsilon x_i^T x_j + r) \quad (7)$$

Where w is an adaptive weight factor, x is an input vector, b is bias and w^T x is an inner product of w and x and Y, r and d are kernel parameters.

Numerous studies have concentrated on enhancing the training process and optimizing the performance of support vector classification (SVC). Platt (1999) [26] introduced a sequential minimal optimization algorithm that significantly improved the efficiency of training with large-scale datasets. Furthermore, Joachims (2006) [27] presented the concept of the Budgeted Support Vector Machine, which facilitated quicker training times by selecting a relevant subset of support vectors. Additional research has investigated the utilization of parallel computing, distributed learning, and active learning techniques to accelerate the training process and enhance scalability. From its foundational theoretical principles to its diverse applications across various domains, SVC has demonstrated notable performance and versatility. Despite existing challenges, such as parameter tuning and scalability, ongoing research endeavors aim to address these issues and further enhance the algorithm's effectiveness. An in-depth understanding of the advancements and future directions in SVC will enable researchers to contribute meaningfully to its continued development and explore its potential for tackling complex classification challenges.

2.2. Binary Particle Swarm Optimization (BPSO)

Binary Particle Swarm Optimization (BPSO) is a type of optimization algorithm used to solve binary optimization problems. In binary optimization problems, the goal is to find the binary string that maximizes or minimizes a given objective function. BPSO is a heuristic method that simulates the behavior of a swarm of particles in a multi-dimensional search space. In BPSO, the particles represent positions in a binary space where each element of a particle's position vector can only take on the values of 0 or 1. In other words, $x_i \in B^{n_x}$ or x_{ij} can only be 0 or 1. When a particle's position is updated, it means flipping one or more bits in the binary string representation of the particle. This effectively causes the particle to move to different corners of a hypercube in the binary search space. The flipping of bits can result in the particle moving closer or farther away from the optimal solution.

The binary PSO algorithm begins by randomly generating a population of particles, after which their positions and velocities are initialized. Following this, the fitness function is calculated for each particle, and the best positions of both the individual particles and the entire swarm are updated accordingly. The swarm best position refers to the position of the particle that has the best fitness function value across the entire population. Followed by the velocity and position of each particle is updated using the following equation:

$$V_{[i,j]} = w * V_{[i,j]} + c1 * rand\ 1 * \left(p_{best[i,j]} - x_{[i,j]}\right) + c2 * rand2 * \left(g_{best[i,j]} - x_{[i,j]}\right) \quad (8)$$

$$x_{[i,j]} = 1, if\ rand(0) < sigmoid\ (V_{[i,j]})$$

$$x_{[i,j]} = 0, otherwise$$

where $V_{[i,j]}$ is the velocity of the j^{th} dimension of the i^{th} particle, w is the inertia weight, c1 and c2 are the cognitive and social learning factors, rand1 and rand2 are random numbers between 0 and 1, $p_{best[i,j]}$ is the best position of the

i^{th} particle in the j^{th} dimension, and $g_{best[j]}$ is the best position of the swarm in the j^{th} dimension. The sigmoid function is used to convert the velocity into a probability of flipping the bit from 0 to 1.

The BPSO operates by defining velocities and particle trajectories in terms of the probability of each bit being set to 1 or 0. For instance, a velocity Vij (t) of 0.3 indicates a 30% chance of the corresponding bit being set to 1, and a 70% chance of it being set to 0. To ensure that velocities are interpreted as probabilities, they are typically restricted to the range of [0, 1]. There are various methods for normalizing velocities so that Vij ∈ [0, 1]. One common approach is to divide each v_{ij} by the maximum velocity, $V_{max,j}$. However, if $V_{max,j}$ is large and the actual velocity V_{ij} (t) << $V_{max,j}$ for all time steps, this will reduce the range of velocities, thereby decreasing the chances of a position to change to bit 1. For example, if $V_{max,j}$ = 10 and Vij (t) = 5, the normalized velocity V'_{ij} (t) would be 0.5, indicating a mere 50% chance that x_{ij} (t + 1) = 1. Using this normalization method can result in premature convergence to suboptimal solutions, as it limits the exploration abilities of the algorithm.

The velocity normalization is obtained by using sigmoid function

$$V_{ij}(t) = \text{sig}\left(V_{ij}(t)\right) = \frac{1}{1 + e^{-V_{ij}(t)}} \quad (9)$$

Using Eq. (9), the position update changes to

$$x_{ij}(t+1) = \begin{cases} 1. \ if \ r_{ij}(t) < sig\ (V_{ij}(t+1)) \\ 0. otherwise \end{cases} \quad (10)$$

Where r_{ij} is a uniform random number in the range [0,1]. The more detailed expressions can be referred at [28].

3. Materials and Methodology

3.1. Data Preprocessing

Developing a classification model for slope stability necessitates the careful selection of features that play a critical role in influencing the outcome. The process of feature selection is pivotal in reducing computational complexity and addressing challenges posed by high-dimensional data. By systematically identifying and retaining the most relevant features, we streamline the learning process, ensuring the model focuses on the essential factors impacting slope stability. This approach not only enhances the efficiency of model training but also mitigates issues like overfitting and redundant computations associated with excessive dimensionality. Ultimately, this strategy contributes to the creation of a robust and reliable classification model capable of accurately predicting slope stability.

Key features such as pore water pressure ratio (ru), slope height (H), unit weight (Y), cohesion (c), slope angle (β), and the angle of internal friction (ϕ) have been widely acknowledged as critical parameters for slope stability prediction. These features capture the essential geotechnical and physical properties influencing slope behavior. For this study, a dataset comprising 444 slope stability cases, categorized into stable (1) and unstable (0) classifications, serves as the foundation for analysis. An illustrative breakdown of these classifications is provided in Figure 1. To further refine the dataset and enhance the analysis, normalization is applied to all features, as described in Equation (11). By scaling the data to a uniform range, this step minimizes potential biases, improves the algorithm's convergence during training, and enhances the model's ability to generalize effectively to unseen cases. Consequently, the normalized dataset facilitates the development of a highly accurate classification model capable of delivering reliable slope stability predictions across diverse scenarios.

$$y_{normalization} = \frac{x - x_{min}}{x_{max} - x_{min}} \quad (11)$$

where, y is a normalized input parameter, x is the original input parameter, x_{max} is the maximum parameter and x_{min} is the minimum parameter.

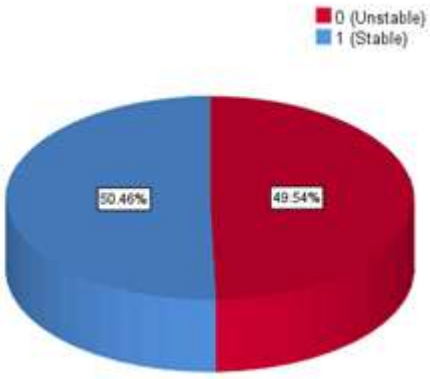

Figure 1. Dataset Pie Chart

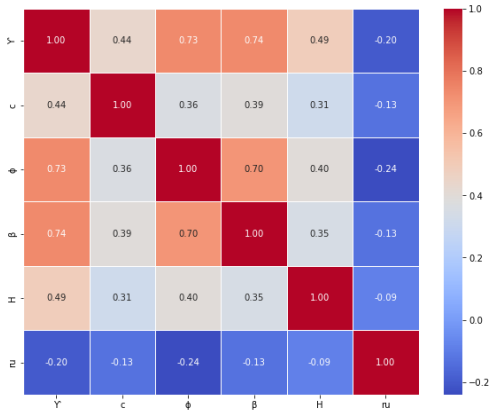

Figure 2. Correlation Matrix of Dataset

The variability and distribution of the input features depicted in Figure 2 demonstrate a strong positive correlation between the features Y and β. Additionally, a significant relationship is noted between ϕ and Y, suggesting that these features are interdependent and may jointly influence predictions related to slope stability. In contrast, the correlation matrix reveals that certain features, such as the ru and c, exhibit weaker correlations with other variables. This suggests that, while these features may have independent effects on slope stability, their interactions with other factors are limited.

Insights derived from the correlation matrix are essential for informed feature selection. Highly correlated features can introduce redundancy within the model, which may elevate computational complexity without substantially enhancing predictive accuracy. Conversely, features with low correlations, though less significant on their own, can still contribute to diversity and enhance the robustness of the model when utilized in combination. Striking a balance in feature selection is imperative for optimizing the feature set to maximize predictive performance while ensuring computational efficiency.

The violin plot illustrated in Figure 3 provides a comprehensive visualization of the distribution and density of the dataset across the various features under consideration. Each violin plot corresponds to a specific feature, with its shape offering valuable insights into the underlying data distribution. The width of the violin at any given point is indicative of the density of data at that value, wider sections signify areas with a higher concentration of data points, while narrower sections reflect regions of lower density. The horizontal line within each violin denotes the median value of the respective feature, serving as a reference for central tendency and aiding in the identification of symmetrical distribution or skewness in the data. Furthermore, the presence of tails at both ends of the violin provides a visual indication of the data's range, thus highlighting any potential outliers or extremes.

The variables Y, ϕ, β, and ru demonstrate a broad distribution, as evidenced by the diverse shapes of their corresponding violins. This broadness suggests a significant dispersion of data points across a wide range of values, indicating high variability in these features, which could be critical in influencing slope stability. In contrast, the variables c and H reveal a more narrowly shaped violin, implying that their data points are densely clustered around specific values. This concentration indicates lower variability and more consistent values compared to the previously mentioned features. The narrow shape highlights a higher frequency of data points near the median, with a reduced occurrence of extreme values.

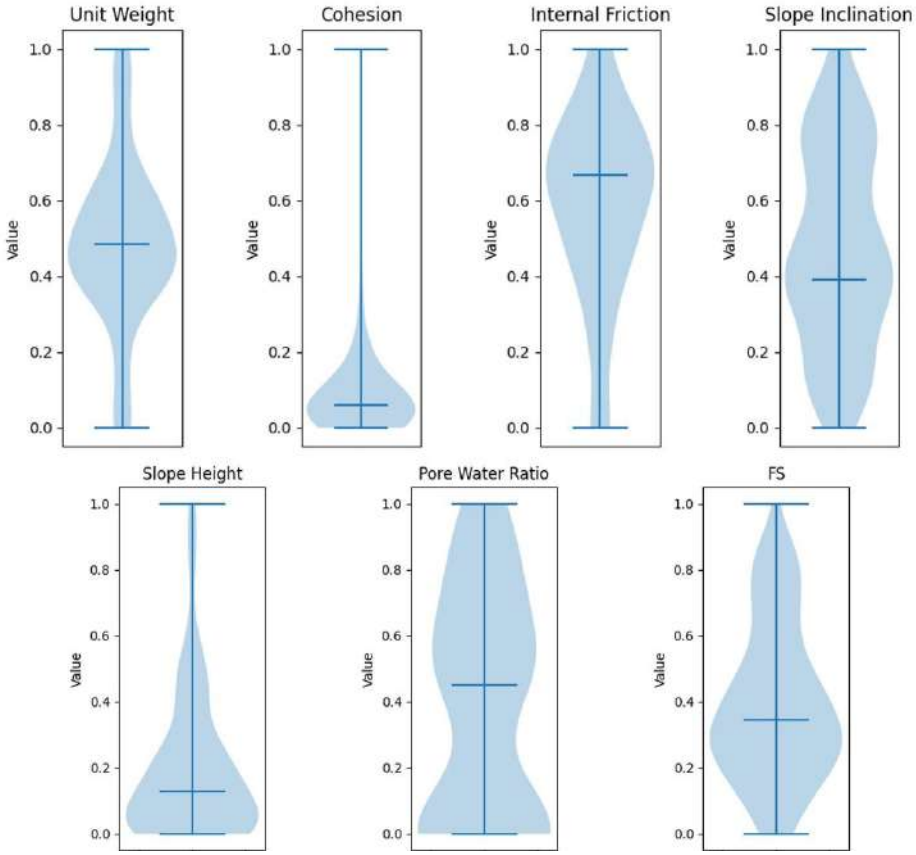

Figure 3. Violin Plots showing distribution of slope cases

This differentiation underscores that features like Ɣ and β may exert a broader influence due to their variability, while features such as c and H may contribute more stable and consistent inputs to the model. These insights are vital for understanding the significance of each feature in the analysis of slope stability and for optimizing overall model performance.

3.2. Model Development and Optimization

This study examines the applicability of SVC utilizing three distinct kernel functions: polynomial, linear, and radial basis function (RBF). The research employs Binary Particle Swarm Optimization (BPSO) for feature selection, as illustrated in Figure 4, which outlines the sequential process of BPSO-SVC. The primary objective of this approach is to enhance the effectiveness of SVC by integrating two critical tasks: the selection of relevant feature subsets from a dataset and the optimization of SVM parameters. In the BPSO framework, each particle in the swarm represents a potential feature subset, with a binary positional vector indicating the presence (1) or absence (0) of specific features. The classification accuracy of each subset is evaluated through a defined fitness function. Importantly, the fitness function that yields the highest accuracy is utilized to assess solutions and update particle positions throughout the iterative process. This methodology aims to identify feature subsets that significantly contribute to achieving precise classification outcomes. Once the best-performing subset is identified, SVC is employed. The optimized features derived from BPSO are subsequently applied to train and test the dataset (Table 1), utilizing the tuned SVC to facilitate improved classification results. The combination of hyperparameters utilized by BPSO are shown in Table 2.

For supervised classification problems, evaluating the performance of classification models on new data is critical to understanding their capacity for generalization.

Tale 1.

Feature optimization using BPSO

Models	Features					
	Ɣ	c	φ	β	H	ru
SVC_rbf	0	1	1	1	0	1
SVC_linear	1	1	1	0	1	0
SVC_poly	0	0	1	0	0	1
0 = Unselected feature			1 = Selected feature			

Table 2

Utilized Hyperparameters for feature optimization using BPSO

Parameters	Values
Acceleration coefficients (c1,c2)	[2,2]
Inertia Weight (w)	0.9
Number of dimensions (k)	7
Number of particles (n_particles)	50
Iterations (iter)	500
alpha	[1.0]

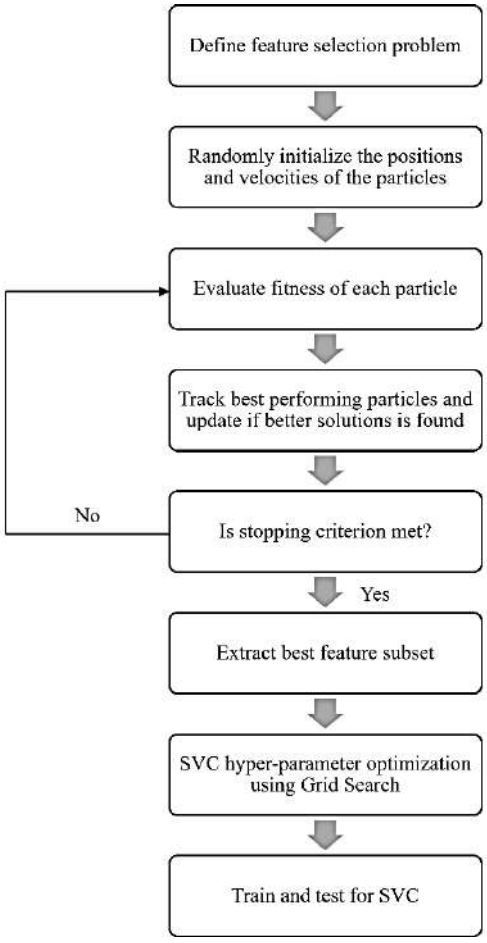

Figure 4. Flow Chart of the BPSO-SVC model

For supervised classification problems, evaluating the performance of classification models on new data is critical to understanding their capacity for generalization. Typically, the dataset is divided into two distinct subsets: the training set and the testing set. The training set, which comprises the majority of the data, is utilized to train the model and optimize hyperparameters. Conversely, the testing set, which constitutes a smaller portion of the dataset, is reserved exclusively for assessing the model's ability to generalize to new, unseen instances. In this study, 70% of the original dataset, amounting to 311 cases, has been designated as the training set, while around 30%, corresponding to 133 cases, has been allocated as the testing set. This division ensures that the model is trained on a diverse range of data while maintaining a separate, independent subset for a rigorous evaluation of its performance on unseen data. The training process for each kernel function involves the exploration of various combinations of hyperparameters, as detailed in the accompanying Table 3. By employing grid search technique, optimal hyperparameters of are identified,

facilitating the achievement of the best model performance. These optimal parameters are subsequently applied for making predictions on unseen data, thereby validating the model's effectiveness in real-world applications.

Table 3
SVC optimal hyperparameters using grid search

Model	Hyperparameters	Optimal Hyperparameters
SVC_poly	C = [1 – 200]; step size =5	186
	Degree = [1 – 6]	2
SVC_linear	C = [1 – 200]; step size =5	11
SVC_rbf	C = [1 – 200]; step size =5	41

The SVC model with different kernels is assessed using a technique known as 5-fold cross-validation. This approach enhances the robustness of the model and its ability to generalize to new data. The Area Under the Curve (AUC) metric serves as a comprehensive measure of the model's overall performance across both the training and testing sets. By considering the model's predictive capacity, particularly its ability to discriminate between classes under varying thresholds, the AUC metric enables a thorough examination and validation of the machine learning algorithm's capability to capture underlying patterns and generalize effectively to previously encountered instances.

4. Results and Discussion

The study employs a hybrid approach incorporating BPSO-SVC to assess its efficacy in predicting slope stability. The BPSO algorithm is utilized to determine optimal feature combinations for each SVC kernel function, and subsequent grid search optimization is conducted to fine-tune the hyperparameters of the SVC models. The performance of the classifiers is evaluated using various metrics, including the AUC scores. The findings indicate that the AUC scores for the models are as follows: SVC_linear at 0.671, SVC_poly at 0.681, and SVC_rbf at 0.735 (Figure 5). The observed differences in AUC values can be attributed to variations in the underlying algorithms, model complexity, and each classifier's capacity to capture the relationships between features and the target variable. Notably, SVC_rbf achieved the highest AUC score, signifying its superior discriminatory ability and overall performance in comparison to the other models.

A detailed analysis of the confusion matrices (as illustrated in Figure 6) highlights the misclassification counts for each model: SVC_linear exhibited 45 misclassifications, SVC_poly had 43, while SVC_rbf recorded the lowest number at 35. This reduced error rate

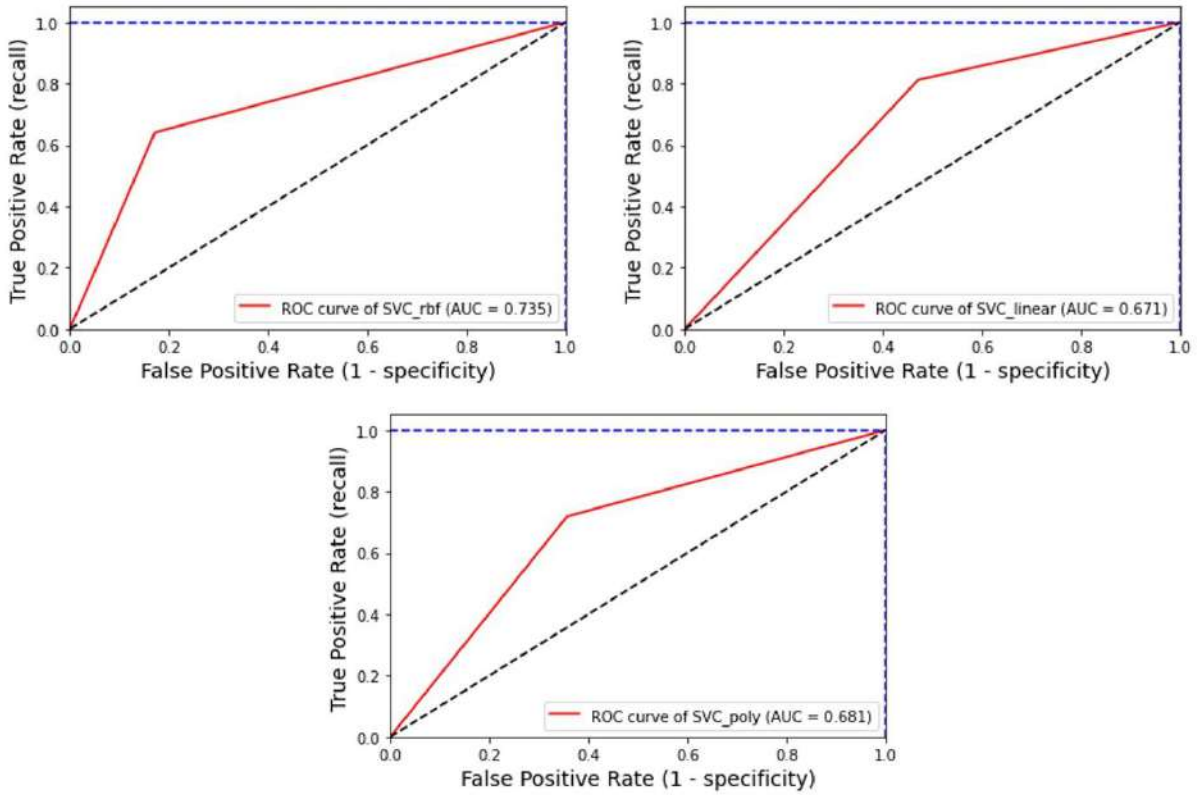

Figure 5. ROC curves of classification models

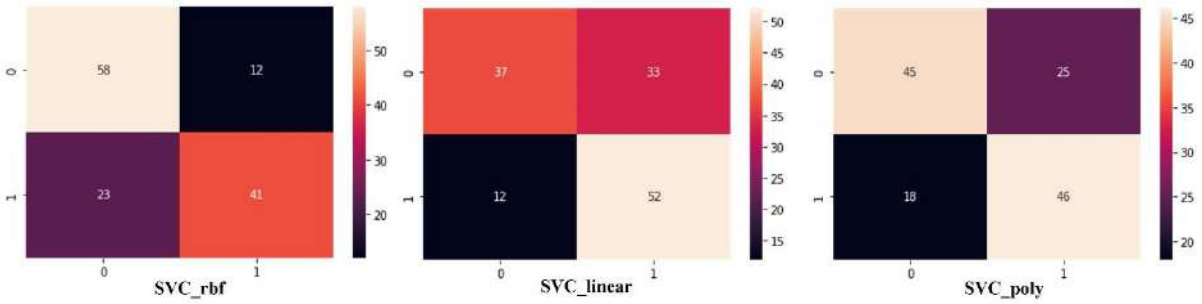

Figure 6. Confusion matrix of classification models

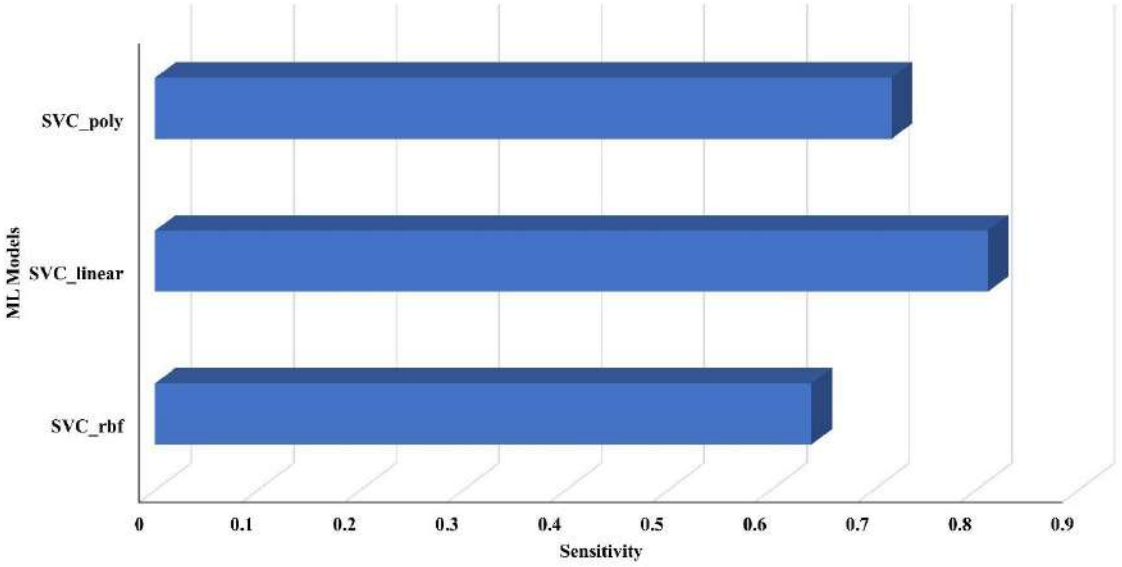

Figure 7. Sensitivity of classification models

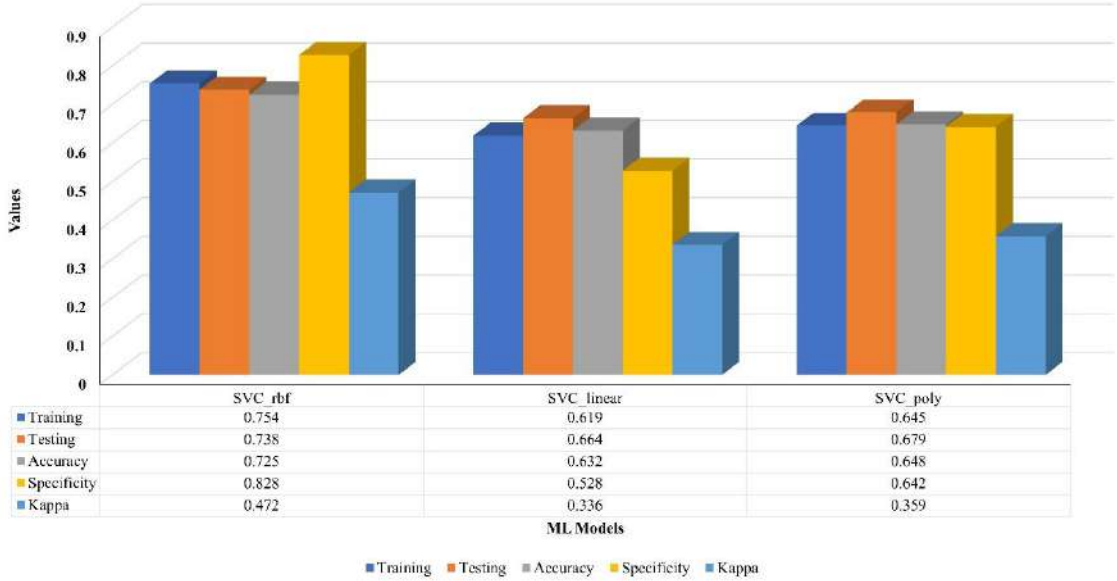

Figure 8. Evaluation metrics of classification models

for SVC_rbf further corroborates its effectiveness in accurately classifying slope stability cases. Furthermore, the sensitivity analysis (depicted in Figure 7) reveals notable performance disparities, with SVC_linear achieving the highest sensitivity score of 0.812, followed by SVC_poly at 0.718, and SVC_rbf at 0.640. Although SVC_linear excels in sensitivity, SVC_rbf demonstrates a more balanced performance across other critical metrics, including specificity (0.828), accuracy (0.725), and kappa (0.472) as shown in Figure 8. Consequently, SVC_rbf emerges as the most robust and reliable model for slope stability classification.

5. Conclusion

This study illustrates the efficacy of a hybrid approach that integrates Binary Particle Swarm Optimization (BPSO) with a Support Vector Classifier (SVC) for predicting slope stability. By employing BPSO to optimize feature selection and utilizing grid search for fine-tuning the hyperparameters of the SVC, the research assessed the performance of three distinct SVC kernel functions: linear, polynomial, and radial basis function (RBF). Notably, the SVC employing the RBF kernel consistently surpassed the other models across key performance metrics, achieving the highest Area Under the Curve (AUC) score of 0.735, the fewest misclassification errors (35), and the highest specificity rate of 0.828. These findings underscore its superior capability to effectively differentiate between stable and unstable slope conditions.

While the SVC with the linear kernel demonstrated the highest sensitivity at 0.812, it exhibited limitations in other metrics such as specificity and overall accuracy, rendering it less suitable for balanced classification tasks. The SVC with the polynomial kernel displayed intermediate performance, with an AUC of 0.681 and a comparatively lower number of misclassifications (43). However, the comprehensive performance profile of the SVC with the RBF kernel—characterized by strong discriminatory power and lower error rates—solidifies its status as the most reliable and robust classifier for this application. This research highlights the potential of hybrid methodologies like BPSO-SVC to advance predictive modeling in slope stability analysis through enhanced optimization of both feature selection and model parameters. Future investigations could benefit from exploring the integration of additional optimization algorithms, incorporating ensemble learning techniques, or evaluating alternative kernel functions to further improve model performance and generalizability. This study lays the groundwork for the application of hybrid approaches in addressing complex geotechnical challenges with greater accuracy and reliability.

References

[1] Duncan, James Michael. "State of the art: limit equilibrium and finite-element analysis of slopes." Journal of Geotechnical engineering 122.7 (1996): 577-596. https://doi.org/10.1061/(ASCE)0733-9410(1996)122:7(577)

[2] Zheng, Fei, et al. "Modified predictor-corrector solution approach for efficient discontinuous deformation analysis of jointed rock masses." International Journal for Numerical and Analytical Methods in Geomechanics 43.2 (2019): 599-624. https://doi.org/10.1002/nag.2881

[3] Liu, S. Y., L. T. Shao, and H. J. Li. "Slope stability analysis using the limit equilibrium method and two finite element methods." Computers and Geotechnics 63 (2015): 291-298. https://doi.org/10.1016/j.compgeo.2014.10.008

[4] Griffiths, D. V., and P. A. Lane. "Slope stability analysis by finite elements." Geotechnique 49.3 (1999): 387-403. https://doi.org/10.1680/geot.1999.49.3.387

[5] Matsui, Tamotsu, and Ka-Ching San. "Finite element slope stability analysis by shear strength reduction technique." Soils and foundations 32.1 (1992): 59-70. https://doi.org/10.3208/sandf1972.32.59

[6] Li, X. "Finite element analysis of slope stability using a nonlinear failure criterion." Computers and Geotechnics 34.3 (2007): 127-136. https://doi.org/10.1016/j.compgeo.2006.11.005

[7] Nanehkaran, Yaser A., et al. "Comparative analysis for slope stability by using machine learning methods." Applied Sciences 13.3 (2023): 1555. https://doi.org/10.3390/app13031555

[8] Tien Bui, Dieu, et al. "Predicting slope stability failure through machine learning paradigms." ISPRS International Journal of Geo-Information 8.9 (2019): 395. https://doi.org/10.3390/ijgi8090395

[9] Mahmoodzadeh, Arsalan, et al. "Prediction of safety factors for slope stability: comparison of machine learning techniques." Natural Hazards (2022): 1-29. https://doi.org/10.1007/s11069-021-05115-8

[10] Ahangari Nanehkaran, Yaser, et al. "Application of machine learning techniques for the estimation of the safety factor in slope stability analysis." Water 14.22 (2022): 3743. https://doi.org/10.3390/w14223743

[11] Moayedi, Hossein, et al. "Machine-learning-based classification approaches toward recognizing slope stability failure." Applied Sciences 9.21 (2019): 4638. https://doi.org/10.3390/app9214638

[12] Bai, Gexue, et al. "Performance evaluation and engineering verification of machine learning based prediction models for slope stability." Applied Sciences 12.15 (2022): 7890. https://doi.org/10.3390/app12157890

[13] Saurabh Kumar Anuragi, D.Kishan, S.K.Saritha. “Comparative Analysis of Ensemble Learning Approaches for Slope Stability Prediction”. SSRG International Journal of Civil Engineering 11.5 (2024) :168-180. https://doi.org/10.14445/23488352/IJCE-V11I5P116

[14] Saurabh Kumar Anuragi. “Utilizing Boosting Machine Learning Techniques for Slope Stability Prediction”. International Journal of Civil and Structural Engineering Research 12.2 (2024) : 53–58. https://doi.org/10.5281/zenodo.14274474

[15] Luo, Zhenyan, et al. "A novel artificial intelligence technique for analyzing slope stability using PSO-CA model." Engineering with Computers 37 (2021): 533-544. https://doi.org/10.1007/s00366-019-00839-5

[16] Koopialipoor, Mohammadreza, et al. "Applying various hybrid intelligent systems to evaluate and predict slope stability under static and dynamic conditions." Soft Computing 23 (2019): 5913-5929. https://doi.org/10.1007/s00500-018-3253-3

[17] Pham, Khanh, et al. "Ensemble learning-based classification models for slope stability analysis." Catena 196 (2021): 104886. https://doi.org/10.1016/j.catena.2020.104886

[18] Gordan, Behrouz, et al. "Prediction of seismic slope stability through combination of particle swarm optimization and neural network." Engineering with computers 32 (2016): 85-97. https://doi.org/10.1007/s00366-015-0400-7

[19] Zhang, Wengang, et al. "Slope stability prediction using ensemble learning techniques: A case study in Yunyang County, Chongqing, China." Journal of Rock Mechanics and Geotechnical Engineering 14.4 (2022): 1089-1099. https://doi.org/10.1016/j.jrmge.2021.12.011

[20] Kardani, Navid, et al. "Improved prediction of slope stability using a hybrid stacking ensemble method based on finite element analysis and field data." Journal of Rock Mechanics and Geotechnical Engineering 13.1 (2021): 188-201. https://doi.org/10.1016/j.jrmge.2020.05.011

[21] Qi, Chongchong, and Xiaolin Tang. "Slope stability prediction using integrated metaheuristic and machine learning approaches: A comparative study." Computers & Industrial Engineering 118 (2018): 112-122. https://doi.org/10.1016/j.cie.2018.02.028

[22] Zhou, Jian, et al. "Slope stability prediction for circular mode failure using gradient boosting machine approach based on an updated database of case histories." Safety Science 118 (2019): 505-518. https://doi.org/10.1016/j.ssci.2019.05.046

[23] Vapnik, Vladimir N., and A. Ya Chervonenkis. "On a perceptron class." Avtomatika i Telemkhanika 25.1 (1964): 112-120.

[24] Boser, Bernhard E., Isabelle M. Guyon, and Vladimir N. Vapnik. "A training algorithm for optimal margin classifiers." Proceedings of the fifth annual workshop on Computational learning theory. 1992. https://doi.org/10.1145/130385.130401

[25] Cortes, Corinna, and Vladimir Vapnik. "Support-vector networks." Machine learning 20 (1995): 273-297. https://doi.org/10.1007/BF00994018

[26] Platt, John. "Probabilistic outputs for support vector machines and comparisons to regularized likelihood methods." Advances in large margin classifiers 10.3 (1999): 61-74.

[27] Joachims, Thorsten. "Training linear SVMs in linear time." Proceedings of the 12th ACM SIGKDD international conference on Knowledge discovery and data mining. 2006. https://doi.org/10.1145/1150402.1150429

[28] Khanesar, Mojtaba Ahmadieh, Mohammad Teshnehlab, and Mahdi Aliyari Shoorehdeli. "A novel binary particle swarm optimization." 2007 Mediterranean conference on control & automation. IEEE, 2007. https://doi.org/10.1109/MED.2007.4433821

J-Researchers

Journal of Civil Engineering Researchers

Journal homepage: www.journals-researchers.com

Exit Strategies for Commercial Complexes in Economic Recession Periods (Case Study: Roya Mall Kish Commercial Complex)

Majid Motiolhagh, [a] Kamran Yeganegi, [b,*] Maryam Ebrahimi [a]

[a,] *Department of Management (Business-Marketing Management), Electronic Unit, Islamic Azad University of Tehran, Iran*

[b] *Department of Industrial Engineering, Zanjan Branch, Islamic Azad University, Zanjan, Iran*

ABSTRACT

The primary aim of this article is the identification and selection of the optimal strategy for the exit of a significant capital volume invested in the construction of commercial centers in the face of investment risk in the construction of commercial complexes, along with influential factors in challenging economic conditions such as exchange rate fluctuations, transregional power sanctions, stagflation, excessive supply and growth in commercial complex construction in the country, etc., specifically focused on the Royal Mall Kish project. Indeed, the effectiveness and reliability of formulating and selecting exit strategies based on successful implementation and the creation of a sustainable economic cycle for a commercial complex are deemed essential and prerequisite. The research method employed is qualitative. In the qualitative section of this study, through interviews, we identified the relevant factors affecting exit strategies, considering the current conditions and business environment to achieve ultimate goals. These factors are ultimately categorized into three dimensions: structural, behavioral, and contextual. The qualitative sample population includes active experts in this project. At theoretical saturation point, 8 experts were identified as participants in the research. Ultimately, 43 influential components on strategy selection and 5 exit strategies were identified in this project that can be determined as suitable strategies in the appropriate situation for decision-making regarding exit.

ARTICLE INFO

Received: December 26, 2024
Accepted: January 08, 2025

Keywords:
Exit Strategy
Content Analysis
Economic Recession Period
Commercial Centers
Structural Dimensions

DOI: 10.61186/JCER.7.1.12
DOR: 20.1001.1.2538516.2025.7.1.2.8

1. Introduction

The global economy has been facing numerous daily challenges, especially in the aftermath of recent crises such as the COVID-19 pandemic and global banking crises [1]. This pandemic has led to significant disruptions in the global supply chain, reduced consumer demand, and forced many businesses to temporarily close or reduce capacity, resulting in considerable economic losses worldwide [2]. Similarly, the global banking crises in the late 2000s resulted in widespread financial instability and economic recession, leading to numerous bankruptcies and job losses [3]. Analysis of the economic growth trend in Iran during the seasons of the years 1390 to 1400 shows an average growth rate of 0.35% per season and 1.4% per year in the Iranian economy. This level of economic growth indicates the inadequacy of the economic situation in Iran. Economic statistics indicate that in 7 periods, the country's economic

* Corresponding author. Tel.: +989121827383; e-mail: yeganegi@iauz.ac.ir (Assistant Prof. Kamran Yeganegi).

growth (seasonal) has recorded negative figures. The trend of economic growth highlights that in the two periods of 1391 and 1397, this figure has been severely negative. Examination of these two time periods indicates that the primary cause of this occurrence in this range may stem from transregional power sanctions. Although on the surface sanctions are the main cause of the decline in economic growth, it is necessary to examine the relationships between macro variables and economic growth and to make the sensitivity of economic growth to macro variables apparent so that the central bank and government can prevent economic growth decline by managing macroeconomic factors [4].

In order to confront these challenging economic conditions, it is necessary to formulate appropriate strategies that can help companies effectively navigate through crises [5]. In addition to the above, the issue of addressing inflation is one of the vital subjects in the economy of Iran. Based on economic statistics since the years following the Islamic Revolution, the average inflation rate in Iran has been around 20 percent. Considering the presented statistics, it can be acknowledged that the inflation rate in the Iranian economy is high, which can be one of the influential factors affecting speculative activities and hindering economic growth in Iran [6]. Formulating and implementing a strategy entail developing a clear action plan to achieve a specific goal and ensuring its effective execution [7]. However, decision-making regarding exit strategies during an economic recession can pose a challenging task for businesses, as they must balance their long-term objectives with short-term pressures to remain profitable [8].

Moreover, in recent years, we have witnessed a significant increase in the construction and launch of commercial complexes nationwide. However, in addition to the continuous growth in the number of these complexes, only a few have succeeded, with many undergoing changes and transformations in visitor units, while others are constantly evolving and changing their commercial units, and the continuation of this trend can lead to failures and changes in the use of commercial complexes, resulting in irrecoverable financial consequences [9].

The above instances indicate the risks associated with investing in the construction of commercial complexes. Risk management enables managers to balance their operational and economic expenses and helps them make the best decisions. When a suitable risk management technique is well implemented, it assists managers in identifying desirable control factors, thus ensuring the survival of the business and safeguarding the economic enterprise from both minor and major risks [10].

The main question of this research is what exit strategy is executable for commercial complexes. Commercial complexes face unique challenges during economic recessions such as reduced penetration, decreased consumer spending, and increased competition [11]. Therefore, identifying practical exit strategies that can help commercial complexes effectively navigate through economic recession and inflation is crucial.

2. Theoretical Foundations

2.1. Definitions and Concepts of Strategy

Strategy is a crucial concept in management that refers to planning, formulating, and implementing approaches and strategies to achieve the goals and of an organization or individual. Strategy is as a long-term roadmap for organizational or individual performance and determines how specific goals should be achieved.

In the business domain, strategy typically includes setting objectives, analyzing the internal and external environment, identifying opportunities and threats, selecting strategies, implementing strategies, and evaluating performance. While in the military and political domain, strategy refers to planning to achieve security and political objectives [12].

Strategies can be diverse and may change based on different conditions and perspectives. Some well-known strategies include growth strategy, defensive strategy, focus strategy, penetration strategy, and cooperation strategy. Additionally, based on the differentiation strategy, company activities focus on producing and delivering unique and high-quality products or services [10].

Strategies are usually determined based on a meticulous analysis of the internal and external environment of an organization or individual. This analysis involves assessing internal strengths and weaknesses, as well as identifying environmental opportunities and threats. Based on this analysis, strategies and approaches that yield the best results in achieving goals are selected [13].

2.2. Different types of exit strategies include:

- Initial Public Offering (IPO): When a private company sells its shares to the public for the first time, typically on the stock exchange. This allows the company to raise capital and expand its visibility, while providing founders and initial investors an opportunity to cash out their shares. However, IPOs are also costly, time-consuming, and risky, as they expose the company to increased regulations, thorough scrutiny, and market fluctuations [13].
- Acquisition: When one company acquires all or part of another company through cash, stocks, or

a combination of both. This can be a quick and profitable way for founders and investors to exit, especially if the acquirer is willing to pay a premium for the assets, technology, or customer base of the target. However, acquisitions can also involve complex negotiations, thorough due diligence, integration issues, as well as potential loss of control and cultural conflicts [14].

- Merger: This occurs when two or more companies combine their operations and assets into a new entity, usually with the aim of creating synergies and achieving economies of scale. It can be beneficial by increasing market share, diversifying their offerings, and reducing costs for both parties. However, mergers can also pose legal, financial, and operational challenges, as well as potential conflicts of interest and power struggles.
- Liquidation: This is when a company sells off all its assets and pays off its debts, usually because it is unable to continue its operations or fulfill its commitments. It can be the last resort for failed businesses that have no other suitable options. However, liquidation can also be a strategic choice for successful businesses looking to exit a mature or declining market and focus on other opportunities. Liquidation may result in minimal or negative returns for shareholders, but it can also free up resources and prevent further losses [15].
- Acquisition: This is when a group of investors or existing shareholders or managers purchase a company, usually with the help of financing through debt. It allows buyers to obtain full ownership and control of the company and implement their vision and strategy. However, acquisitions can be costly, risky, and stressful, as they require high levels of debt repayment and interest payments [13].

2.3. Exit strategies and crisis management

Every business faces risks and uncertainties that can threaten its survival and success. Whether it be a natural disaster, a cyber-attack, a pandemic, a legal dispute, or a market downturn, a crisis can occur at any time and disrupt the normal operations of a business.

An exit strategy is a plan that outlines how a business will end or reduce its involvement in a project, investment, or market. It can be used to minimize losses, maximize profits, or achieve other strategic objectives. An exit strategy can also be part of a crisis management plan, which provides a comprehensive and coordinated approach to dealing with a critical situation and mitigating its negative impacts [16].

A crisis management plan should include the following elements:

- Crisis Team: A group of individuals responsible for crisis management and communication with stakeholders. The team should have clear roles and responsibilities, as well as the necessary authority and resources to make decisions and take action.
- Crisis Assessment: A process for identifying and analyzing the nature, scope, and severity of the crisis, as well as its potential consequences and opportunities. The assessment should also evaluate the strengths and weaknesses of the business and its environment.
- Crisis Response: A set of actions taken to contain, control, and resolve the crisis, as well as to preserve the interests and reputation of the business. The response should be timely, effective, and aligned with the values and goals of the business.
- Crisis Communication: A strategy defining how a business communicates with its internal and external stakeholders during and after a crisis. Communication must be transparent, honest, empathetic, and proactive. It should address stakeholders' concerns and expectations, and provide accurate and relevant information [17].
- Crisis Evaluation: A process of examining and learning from the experience of a crisis and its outcomes. Evaluation should identify the root causes of the crisis, strengths and weaknesses of the crisis management plan, lessons learned, and best practices for future improvement.

An exit strategy can be integrated as an option or possibility in a crisis management plan. Depending on the circumstances, a business may decide to exit a project, investment, or market that is no longer sustainable or profitable due to another crisis. On the other hand, a business may utilize an exit strategy as a backup plan if the crisis worsens or becomes unmanageable.

A carefully planned and executed exit strategy ensures that desired outcomes are achieved and negative impacts on the business and its shareholders are minimized. Factors to consider in formulating an exit strategy include:

a) Business objectives and goals
b) Costs and benefits of exiting versus staying
c) Legal and contractual obligations and consequences of exit
d) Financial and operational feasibility and sustainability of exit
e) Market conditions and exit opportunities
f) Stakeholders' expectations and reactions to the exit [18].

Exit strategy and crisis management are essential skills for any business leader or entrepreneur. With a clear vision, flexible mindset, and proactive attitude, a business can navigate through any challenge and uncertainty that may arise on its journey.

3. Research Methodology

In this study, the qualitative section will involve examining the theoretical foundations and relevant background research using library research and content analysis methods. The first section will focus on targeted utilization of content analysis method based on identified indicators.

In this section, the questionnaire is researcher-designed. The Table 1 outlines the specifications of the data collection tools and the validity and reliability analysis methods for each research tool presented:

Table 1:

Research Tools and Validity and Reliability

Tool Name	Section Name	Validity	Reliability
Review Interview	Qualitative	Content	Cohen's Kappa Coefficient

The study population of this research comprises all experts, managers, and specialists of Roya Mal Kish. Roya Mal Kish is a grand construction project on Kish Island, encompassing luxury shops, restaurants, cafes, rooftop gardens, and other recreational amenities, as well as administrative units. The experts, managers, and specialists of Roya Mal Kish are individuals engaged in the design, construction, management, or marketing of this project, or possess the necessary knowledge and experience in this field. The research population is a limited population with a countable number of members.

The snowball sampling method is employed, and the sample size is determined at the theoretical saturation point. This means that the researcher, through personal connections, online sources, written materials, or other appropriate methods, seeks suitable initiators to begin their specific sampling process. After selecting the initiators, the researcher conducts brief and then in-depth interviews with them. In this research, a total of 8 experts have been identified at the theoretical saturation point as the research sample in this section. A qualitative model using content analysis methods will be presented in this study (Table 2-3).

Table 2

examines the status of position in the sample statistics

Position	Frequency (%)	Cumulative Frequency (%)
Deputy	44	44
Senior Specialist	19	63
Management	37	100
Total	100	

Table 3

Examines the status of work experience in the sample statistics

Work Experience	Frequency(%)	Frequency Cumulative (%)
5 to 10 years	13	13
10 to 15 years	19	32
15 years and above	68	100
Total	100	

4. Analysis Results of Data

4.1. Identification of text codes based on meaningful units

In this section, all interviews conducted in audio files were completely converted into text by us so that we could utilize them for code identification. Subsequently, the content of each text was meticulously and thoroughly transferred to the MaxQDA software, and considering that meaningful units existed in the texts in this research, meanings related to the main research question were extracted. In order to carry out this task, similar and related meaningful units were placed alongside each other and presented in the form of codes. Following that, some samples of the conducted interviews and the extracted codes were presented (Table 4).

Ultimately, other interviews conducted with 8 experts were coded and the results of these codes are presented below.

4.2. Extraction of sub-themes based on the extraction codes

In this stage of content analysis, the reviewed codes were first assessed in a focused manner, taking into the relationships between them and similar concepts. Additionally, repetitive codes were eliminated. Subsequently, selected codes were categorized based on the specified sub-themes.

To ensure the validity of the codes and the accuracy of the coding and identification of sub-themes, the experts were contacted again. The experts provided their opinions on the agreement or disagreement with the extracted sub-themes. For this survey, the CVR formula was utilized, and the value of this index for each sub-theme was reported in percentage.

In this research, the qualitative section utilizes a study of theoretical foundations and related background through a library method and content analysis. In the quantitative section, a field method and questionnaire tool are used for data collection.

In the first section, a focused content analysis method is used based on the identified indices.

Table 4
Sample Identification of Codes Based on Meaningful Units

Variable Name	Meaningful Phrases
Competitiveness of Managers	We inquired of the managers how they compete with their competitors at the Rooyamal Kish Complex and how they prioritize determining an exit strategy. They emphasized that competition in the market environment is fundamental, and in order to succeed in an exit strategy, they must be able to compete with their rivals.
The level of knowledge of managers	We inquired of the managers how they enhance their knowledge and expertise in the field of the Rooyamal Kish commercial complex and how they utilize their knowledge for strategic decision-making. expressed that continuous education and staying up-to-date with industry changes are crucial, and they leverage their knowledge for intelligent decision-making regarding exit strategies.
The team behavior of managers and employees	We inquired of the managers and employees how they manage their teams and how interactions between managers and employees impact strategic decision-making. They emphasized that effective communication and collaboration with work teams are of great importance, and in determining exit strategies, they need interaction and alignment with employees.
The communication culture of managers and employees	We asked managers and employees to discuss the communication culture in the Rooyamal Kish commercial complex and how this communication culture impacts exit strategy. They mentioned that an open and honest communication culture promotes trust and in strategic decision-making, there is a need for open communication with all team members.
The competitiveness of managers	We inquired of the managers about how they deal with managing competition in the market and how this competition impacts exit strategy. They emphasized that there is intense competition in the commercial market of Rooyamal Kish and the need for appropriate strategic decisions to compete with rivals.
The level of technological maturity	We asked the managers how they work with the level of technological maturity in the industry of Rooyamal Kish commercial complex and how they utilize technology as a tool for enhancing exit strategy. They expressed that in the information technology industry, the need for continuous progress and utilization of technology wherever possible is crucial.
Market demand and customer preferences	We inquired with managers and market experts on how they navigate changes in market demand and customer needs, and how they adjust exit strategies to align with these fluctuations. They emphasized that market understanding and analysis of customer changes are of paramount importance, and strategies should be tailored based on market demand and customer needs.
Fluctuations in financial markets	We inquired with the managers on how fluctuations in financial markets impact exit strategies and what actions they take to manage risks associated with these fluctuations. They emphasized that fluctuations in financial markets can have direct impact on financial decision-making and exit, highlighting the need precise planning and the use appropriate financial tools.
International sanctions	We inquired with the managers on how international sanctions and changes in the environment impact their strategies and how they consider these constraints when planning exit strategies. They mentioned the importance of being familiar with changes in laws and international sanctions, and adjusting their exit strategy accordingly.

Table 5
Research Validity and Reliability Tools

Name of the Tool	Name of the Section	Validity	Reliability
Literature Review	Qualitative	CVR	Cronbach's Alpha
Review Interview	Qualitative	Substantive	Cronbach's Alpha
Questionnaire for status determination and model fitting	Quantitative	Confirmatory Factor Analysis	Cronbach's Alpha
Alpha coefficient	Construct validity	Title of the concept	Row
0.84	Confirmation	Structural dimensions	1
0.74	Confirmation	Environmental dimensions	2
0.72	Confirmation	Behavioral dimensions	3

In the final section, a Likert-type five-option spectrum is used to examine the model fit of the questionnaire. In this section, the questionnaire is researcher-developed. The characteristics of the data collection tool and the validity and reliability analysis method for each research tool are presented in the Table 5.

The questionnaire for this study consisted of 50 questions, and the distribution of these questions is presented in the Table 6.

According to the table by Lawshe and colleagues, based on the opinions of 8 experts, a value above 0.59 or 59% indicates the validity confirmation of the sub-dimension in question.

4.3. Extraction of main based on sub-concepts

At this stage, by revisiting the codes and identified sub-concepts, the sub-concepts were re-examined. Based on the semantic and conceptual similarities and proximity of the sub-concepts to the main concepts of the initial conceptual model, these sub-concepts were divided into three different

Table 6
Research Questionnaire

Name of the questionnaire	Number of questions	Range of questions	Source of questions
Behavioral dimensions	14	Five-option Likert	Extraction from research findings
Environmental dimensions	9	Five-option Likert	Extraction from research findings
Organizational dimensions	22	Five-option Likert	Extraction from research findings
Components of exit strategy	5	Five-option Likert	Extraction from research findings

Table 7
Extraction of sub-themes from identified codes

Row	Behavioral factor	CVR	Row	Structural factor	CVR
1	Competitiveness of managers	100	3	Physical and spatial infrastructures	100
2	Level of managerial knowledge	100	4	Organizational goals	100
3	Interactions between managers and employees in a team setting	100	5	Current market strategies and outlooks	100
4	The communication culture between managers and employees	100	6	Access to resources	100
5	Experience in the market	100	7	Appropriate ratio of human resources	100
6	Skills in equity ownership	100	8	Decision-making processes	100
7	Motivations of shareholders	100	9	Organizational culture	100
8	The level of market knowledge among shareholders	100	10	Financial performance	100
9	The level of risk tolerance	100	11	Cost efficiency	100
10	Correct understanding of market dynamics	100	12	Adequate revenue	100
11	Strategic skills of managers	100	13	Operational efficiency	100
12	Acceptance and management of change	100	14	Agility of processes	100
13	Understanding environmental opportunities	100	15	Diversity of services	100
14	Understanding and mastery of customer communication	100	16	Financial resources	100
Row	Environmental factor		17	Ease of environmental access	100
1	Laws and regulations	100	18	Satisfying stakeholders needs	100
2	Population and regional needs	100	19	Efficient financial management and accounting	100
3	Government policies	100	20	Organizational and operational risks	100
4	The level of competition in the market	100	21	Reward, salary, and compensation system	100
5	The level of technological maturity	100	22	Formal and organizational communications	100
6	Market demand and customers	100		Exit strategies	
7	Fluctuations in financial markets	100	1	Market exit	100
8	International sanctions	100	2	Sale of the complex	100
9	Social and cultural changes	100	3	Mergers and acquisitions	100
Row	Structural factor		4	Resource reallocation management	100
1	Organizational structure	100	5	Strategy realignment	100
2	Technologies utilized in service provision	100	6	Business closure	100

categories. If a sub-concept did not belong to any of these three categories, a new classification was created. Thus, all sub-concepts were divided into three main categories. In the table below, the concepts of each main concept along with their frequency are mentioned. Based on this criterion, 45 sub-concepts were identified and classified into three different main concepts, and the details of this classification are provided in the Table 8.

Table 8
Selective coding for qualitative-exploratory study

Row	Concept Title	Frequency of Concept Repetitions
1	Structural Dimensions	14
2	Environmental Dimensions	9
3	Behavioral Dimensions	22

Based on the output of Table 3 and its results, the foundational structural and behavioral dimensions influencing exit strategy and their impact are elucidated:

Competitiveness of managers:

Managers with a competitive approach may be inclined to utilize exit strategies such as mergers and ownership changes to strengthen the organization's competitiveness in the market.

Level of managerial knowledge:

The knowledge and experience of managers in various fields can be determinants of the type of exit strategy. Managers with broader knowledge may be better equipped to decide whether exit strategies such as selling or merging are appropriate or not.

Team behavior of managers and employees:

Coordination and interaction between managers and employees can have a significant impact on the success or failure of the exit strategy. If the management team and employees act in unity and cohesively in relation to the exit strategy, a more successful implementation is achieved.

Communication culture of managers and employees:

The communication culture within the organization can be influential. If the organizational communication culture with customers and other connections is not correct and healthy, the exit strategy may face communication challenges.

Market experience:

The organization's experience in the market and deep understanding of customers, competitors, opportunities, and threats can influence decision-making regarding the exit strategy. Experience can help the organization choose strategies that yield desirable returns.

Shareholder skills:

Shareholders with better managerial and financial skills can make informed decisions regarding the exit strategy. They should have the ability to evaluate the financial performance of the organization and analyze the advantages and disadvantages of various strategies.

Shareholder motivations:

Shareholder motivations may vary. Some may seek to maximize profits from the exit, while others may seek to retain their participation in the company. Their motivations can play a vital role in selecting the exit strategy.

Risk Tolerance Level:

The risk tolerance level of shareholders and managers can influence decisions related to the exit strategy. Individuals more inclined towards risk may prefer exit strategies with higher risks, while those less risk-tolerant may lean towards less risky strategies.

Understanding Market Shifts Properly:

Managers must have a proper understanding of market shifts and industry trends to choose an appropriate exit strategy. Considering technological, competitive, and environmental changes is crucial.

Strategic Skills of Managers:

The strategic skills of managers in determining and executing exit strategies can ensure effective decision-making. Managers with the ability to analyze the environment and formulate new strategies can lead the organization to a successful exit.

Acceptance and Management of Change:

The ability to manage necessary changes for implementing the exit strategy can be vital. Managers should be capable of transitioning the organization from its current state to a desirable one.

Understanding Environmental Opportunities:

Understanding environmental opportunities can have an influential role in selecting an exit strategy. Recognizing market opportunities and environmental facilities can assist the organization in making appropriate decisions.

Skills and Customer Relationship Understanding:

Understanding the needs and preferences of customers can be impactful in selecting exit strategies and adapting to them. Effective communication with customers and the ability to create positive relationships can help in the success of the exit strategy.

Laws and Regulations:

Governmental and industrial laws and regulations can impact decisions related to the exit strategy. There may be regulations that impose prohibitions or restrictions on exit strategies or even encourage market exits through tax determinations, financial facilities, and other tools.

Population and Regional Needs:

Understanding the needs and preferences of the population and specific regional requirements can shape decisions related to the exit strategy. Organizations may choose exit strategies tailored to the region to align with these needs and satisfy local customers.

Government Policies:

Government policies can influence the exit strategy. Governments may affect exit strategies through tax designations, financial incentives, and other tools.

Market Competition Level:

The level of market competition can influence decisions regarding the exit strategy. In highly competitive markets, organizations may require more exit strategies to remain in the market.

Technological Maturity Level:

In industries with advanced technology, technological maturity level can determine the exit strategy. Organizations may need to master new technologies or quickly exit the market.

Market and Customer Demand:

Market demand and customer needs can determine the exit strategy. If demand for products or services decreases, organizations may require exit strategies.

Financial Market Fluctuations:

Risk Tolerance Level:

The risk tolerance level of shareholders and managers can influence decisions related to the exit strategy. Individuals more inclined towards risk may prefer exit strategies with higher risks, while those less risk-tolerant may lean towards less risky strategies.

Understanding Market Shifts Properly:

Managers must have a proper understanding of market shifts and industry trends to choose an appropriate exit strategy. Considering technological, competitive, and environmental changes is crucial.

Strategic Skills of Managers:

The strategic skills of managers in determining and executing exit strategies can ensure effective decision-making. Managers with the ability to analyze the environment and formulate new strategies can lead the organization to a successful exit.

Acceptance and Management of Change:

The ability to manage necessary changes for implementing the exit strategy can be vital. Managers should be capable of transitioning the organization from its current state to a desirable one.

Understanding Environmental Opportunities:

Understanding environmental opportunities can have an influential role in selecting an exit strategy. Recognizing market opportunities and environmental facilities can assist the organization in making appropriate decisions.

Skills and Customer Relationship Understanding:

Understanding the needs and preferences of customers can be impactful in selecting exit strategies and adapting to them. Effective communication with customers and the ability to create positive relationships can help in the success of the exit strategy.

Laws and Regulations:

Governmental and industrial laws and regulations can impact decisions related to the exit strategy. There may be regulations that impose prohibitions or restrictions on exit strategies or even encourage market exits through tax determinations, financial facilities, and other tools.

Population and Regional Needs:

Understanding the needs and preferences of the population and specific regional requirements can shape decisions related to the exit strategy. Organizations may choose exit strategies tailored to the region to align with these needs and satisfy local customers.

Government Policies:

Government policies can influence the exit strategy. Governments may affect exit strategies through tax designations, financial incentives, and other tools.

Market Competition Level:

The level of market competition can influence decisions regarding the exit strategy. In highly competitive markets, organizations may require more exit strategies to remain in the market.

Technological Maturity Level:

In industries with advanced technology, technological maturity level can determine the exit strategy. Organizations may need to master new technologies or quickly exit the market.

Market and Customer Demand:

Market demand and customer needs can determine the exit strategy. If demand for products or services decreases, organizations may require exit strategies.

Financial Market Fluctuations:

Internal decision-making processes can shape decisions related to the exit strategy. Organizations with more optimized decision-making processes may make better decisions.

Organizational Culture:

Organizational culture can influence decisions regarding the exit strategy. In organizations focused on innovation and change, the implementation of exit strategies may be better accepted.

Financial Performance:

The financial performance of an organization can determines decisions related to the exit strategy. Adequate revenue and cost efficiency can have a significant impact on the execution of exit strategies.

Cost Efficiency:

Cost efficiency can be influential in achieving the exit strategy and reducing associated costs. Cost reduction can assist in the development of exit strategies.

Appropriate Revenue:

Gaining appropriate revenue from exit strategies is crucial. Organizations must have sufficient financial resources to cover the costs of exit and necessary changes.

Operational Efficiency:

The operational efficiency of an organization can affects decisions related to the exit strategy. Improving efficiency and processes can help reduce costs and enhance performance in implementing exit strategies.

Process Agility:

Process agility and the ability to make decisions and implement exit strategies quickly can be crucial. Organizations with more agile processes can respond more rapidly to changes.

Service Diversity:

Service diversity can have an impact on the selection of exit strategies. Organizations with a wide range of services may lean towards different strategies for market exits.

Financial Resources:

Access to the financial resources needed to execute exit strategies is vital. Organizations must be able to utilize the financial resources required to achieve exit strategies.

Ease of Environmental Access:

Easy access to new environments or markets can have an impact on the selection of exit strategies. Easy access to target markets may make exit strategies more attractive.

Meeting Stakeholder Needs:

Meeting stakeholder needs can be influential in choosing the exit strategy. Organizations must pay special attention to the needs and preferences of their customers, personnel, and other stakeholders.

Effective Financial Management and Accounts:

Effective financial management and accounts can influence decisions related to the exit strategy. Ensuring optimal allocation of financial resources for the implementation of exit strategies is important.

Organizational and Operational Risks:

Understanding and managing organizational and operational risks can determine decisions related to the exit strategy. Evaluating and reducing risks associated with market exits is important.

Reward Systems and Compensation:

Reward systems and compensation can be effective in incentivizing employees to execute exit strategies. Appropriate rewards can be motivating for positive performance.

Formal and Organizational Communications:

Formal and organizational communications can play a role in conveying important information related to the exit strategy and interacting with stakeholders.

Additionally, in response to formulating exit strategies, the following potential exit strategies have been proposed as suitable for the Royal Mall Kish project:

a) Market Exit:
- This strategy is appropriate when a company decides to exit the market due to lack of success or market changes.
- In this approach, the organization may sell its products or services or transfer them to someone else who can manage and develop them.
- This method can help reduce losses and improve efficiency in time and energy.

b) Asset Sale:
- This strategy is usually applied when a company owns a collection of projects or business units, which are sold as a complete unit to someone else.
- This allows the company to leverage cumulative value and the fact that running the company as an assembly creates the best outcome.
- This approach may allow the company to accelerate its exit and reallocate its resources to other projects.

c) Mergers and Acquisitions:
- This strategy involves merging or acquiring other business units which can help the company to increase its size and capabilities.
- Mergers enable companies to leverage resources, technology, and human capital and gain new products or services.
- Acquisitions enable companies to quickly add rival business units as a faster way to enter the market.

d) Resource Reallocation Management:
- This strategy typically involves changing the pattern of resource utilization in projects.
- It may involve reducing resources in less productive projects or concentrating more resources in successful projects.
- This strategy helps improve efficiency and increase profitability.

e) Strategy Realignment:
- When market conditions or corporate goals change, it may be necessary to review the overall project's strategy.
- This allows companies to align with the external environment by adjusting strategies and setting new goals.

f) Business Closure:
- This strategy is suitable when a company needs to close its business due to financial issues or the inability to continue the project.
- Business closure allows the company to make the best use of its resources and prevent further losses.

Each of these strategies may be suitable depending on specific project conditions and goals; therefore, it is important to make careful selections based on the current circumstances.

In selecting the optimal exit strategy at the Royal Mall Kish commercial complex, internal organizational factors also play a crucial role. Subsequently, recommendations will be provided for each of these factors.

5. Conclusion

As expressed in this study, the main objective has been to identify the influential factors on exit strategies and determine suitable exit strategies. Consequently, in this research, factors and dimensions have been identified within 14 structural dimensions, 9 environmental dimensions, and 22 behavioral dimensions.

Exit strategies in the business world are utilized to optimize the performance and resources of companies. One

of the methods of exit is through selling assets. This method involves selling all or part of the company's assets and activities to one or more other companies. This process allows the company to align its investors with its objectives and strategies.

Mergers and acquisitions are also a common exit strategy. In this scenario, the target company is either acquired by another company or merged with it. This action can enable the acquiring company to enter broader markets or benefit from new resources.

Resource reallocation is also a crucial strategy that involves enhancing performance and optimizing company resources. This includes selling non-essential assets, reducing costs, and reorganizing activities. This strategy enables the company to pursue financial efficiency and adapt to market challenges.

Based on these strategies, the conclusion may be drawn that selecting the appropriate strategy based on the company's conditions and objectives can contribute to success and financial improvement. Decisions regarding market exit or mergers and acquisitions should be made carefully, considering market information and financial conditions. Additionally, resource reallocation and refining strategies can assist the company in implementing continuous improvements along the path of market exit and taking advantage of new opportunities.

References

[1] Barrero, Jose Maria, Nicholas Bloom, and Steven J. Davis. COVID-19 is also a reallocation shock. No. w27137. National Bureau of Economic Research, 2020.

[2] Baker, Scott R., et al. Covid-induced economic uncertainty. No. w26983. National Bureau of Economic Research, 2020.

[3] Rossi, Cesare, et al. "The strategic assessment of intellectual capital assets: An application within Terradue Srl." Journal of Business Research 69.5 (2016): 1598-1603. https://doi.org/10.1016/j.jbusres.2015.10.024

[4] Haterad, Saman, et al. "Estimating the Impact of Liquidity Growth, Inflation Rate and Exchange Rate Growth on Iran's Economic Growth: Midas & MF-VAR Methods Approach." Iranian Journal of Trade Studies 27.107 (2023): 67-106. https://doi.org/10.22034/ijts.2023.1996415.3817

[5] Forbes, Kristin, Ida Hjortsoe, and Tsvetelina Nenova. "The shocks matter: improving our estimates of exchange rate pass-through." Journal of international economics 114 (2018): 255-275. https://doi.org/10.1016/j.jinteco.2018.07.005

[6] Asgharpur, Hossein, et al. "Investigating the Interaction Effects of Exchange Rate Regimes and Inflation on Iran's Economic Growth." Iranian Journal of Trade Studies 26.104 (2022): 47-74. https://doi.org/10.22034/ijts.2022.555537.3667

[7] Kunc, Martin. Strategic analytics: integrating management science and strategy. John Wiley & Sons, 2018.

[8] Hitt, Michael A., R. Duane Ireland, and Robert E. Hoskisson. Strategic management: Concepts and cases: Competitiveness and globalization. Cengage Learning, 2016.

[9] Bakhshizadeh, Alirezaa, et al. "Studying the Effects of Celebrities' Endorsement on Shopping Malls Success through Brand Credibility." Iranian Journal of Trade Studies 22.86 (2018): 65-88. https://dor.isc.ac/dor/20.1001.1.17350794.1397.22.86.3.2.

[10] Vaghfi, Seyed Hesam, Seyed Ehsan Hosseini, and Fatmeh Keshvari. "Investigating the Effect of Cost Management and Differentiation Strategies on Company Risk, with Emphasis on the Role of Intellectual Capital and Risk Management." Iranian Journal of Trade Studies 26.104 (2022): 157-180. https://doi.org/10.22034/ijts.2022.554331.3652

[11] Liu, Ligang. "Impact of the global financial crisis on China: Empirical evidence and policy implications." China & world economy 17.6 (2009): 1-23. https://doi.org/10.1111/j.1749-124X.2009.01171.x

[12] Jamaludin, Shahrizan, et al. "COVID-19 exit strategy: Transitioning towards a new normal." Annals of Medicine and Surgery 59 (2020): 165-170. 10.1016/j.amsu.2020.09.046

[13] Lemley, Mark A., and Andrew McCreary. "Exit strategy." BUL Rev. 101 (2021): 1.

[14] Precup, Mihai. "The Exit Behavior of Private Equity Firms in Eastern Europe." The Journal of Private Equity 22.4 (2019): 83-95. https://www.jstor.org/stable/26864438

[15] Gilbert, Marius, et al. "Preparing for a responsible lockdown exit strategy." Nature medicine 26.5 (2020): 643-644. https://doi.org/10.1038/s41591-020-0871-y

[16] Marziano, Valentina, et al. "Retrospective analysis of the Italian exit strategy from COVID-19 lockdown." Proceedings of the National Academy of Sciences 118.4 (2021): e2019617118. https://doi.org/10.1073/pnas.2019617118

[17] Bongardt, Annette, and Francisco Torres. "The European green deal: More than an exit strategy to the pandemic crisis, a building block of a sustainable European economic model." JCMS: Journal of Common Market Studies 60.1 (2022): 170-185. https://doi.org/10.1111/jcms.13264

[18] Alderighi, Marco, and Alberto A. Gaggero. "Entry and exit strategy of low-cost carriers and global crises." Research in Transportation Business & Management 45 (2022): 100845. https://doi.org/10.1016/j.rtbm.2022.100845

J-Researchers

Journal of Civil Engineering Researchers

Journal homepage: www.journals-researchers.com

Numerical Investigation of the Impact of Steel Profiles and Embedded Stiffeners in Circular and Square Concrete-Filled Steel Columns under Axial and Lateral Loading

Mohammad Reza Oliaei,[a,*] Mohammad Amin Hamidi Moghadam[a]

[a] *Department of Civil Engineering, Ram.C., Islamic Azad University, Ramsar, Iran*

ABSTRACT

Concrete-filled steel tube (CFST) columns are widely used in high-rise buildings around the world due to their numerous structural advantages, including high load-bearing capacity, favorable inherent ductility, substantial energy absorption capabilities, and the elimination of the need for formwork. However, in Iran, these structures have not yet been widely implemented in practice, highlighting the need for further research in this area. Additionally, challenges such as buckling and local delamination between the concrete and steel under loading remain key issues for these columns. Research indicates that circular CFST columns provide the strongest confinement for concrete, whereas square CFST columns exhibit higher local buckling under loading. Furthermore, embedded steel profiles significantly enhance the overall performance of these columns. In this study, a finite element model of CFST columns with embedded cruciform profiles is validated using Abaqus software and subsequently analyzed parametrically. The objective of this study is to evaluate the seismic and axial performance of the "primary column cross-sections" and the "embedded steel profiles" with equivalent areas. The findings of this research demonstrate that filling the internal space of steel columns with concrete substantially improves axial and lateral performance, although it slightly reduces lateral ductility. Additionally, stress analysis reveals that the type of embedded steel profile directly influences the enhancement of load-bearing capacity and lateral performance. Results also show that square CFST columns outperform their circular counterparts in terms of axial strength and stiffness, though they exhibit lower axial ductility.

ARTICLE INFO

Received: December 26, 2024
Accepted: February 23, 2025

Keywords:
Numerical development
Concrete-filled steel columns
Axial performance
Lateral performance
Steel profiles embedded in concrete

DOI: 10.61186/JCER.7.1.22
DOR: 20.1001.1.2538516.2025.7.1.3.9

1. Introduction

Concrete-filled steel tube (CFST) columns represent a novel type of composite structural element, first introduced and studied by Tomi et al. in 1985. Subsequently, Xiao et al. in 1986 discussed the design methods for reinforced concrete columns confined with steel, thereby advancing the engineering applications of such structures. However, certain limitations in the application of CFST structures, such as the complexity of beam-to-column connections,

* Corresponding author. Tel.: +989113924331; e-mail: m.r.oliaei@gmail.com.

local buckling of the steel tube, and poor fire resistance, have constrained their use in contemporary buildings [1].

In the past few decades, CFST structures have been widely adopted in modern buildings and bridges, even in seismically active regions [2,3]. These composite structures ideally combine the advantages of both steel and concrete columns—such as rapid construction and high strength. However, as span lengths and building heights increase, the cross-sectional area of these columns must often be significantly enlarged to provide the necessary load-bearing capacity. This has underscored the need for research aimed at improving the load-bearing capacity while reducing the cross-sectional dimensions of CFST columns [4]. As illustrated in Figure 1, steel columns can experience local buckling, which manifests as either inward or outward deformation. Shear failure is also evident in plain concrete columns, whereas outward buckling is primarily observed in CFST columns, with the internal concrete undergoing more ductile failure. Research has shown that the ultimate strength of CFST columns exceeds the combined strength of individual steel and reinforced concrete columns. Moreover, the ductility of CFST columns is significantly higher than that of steel or concrete columns alone [4].

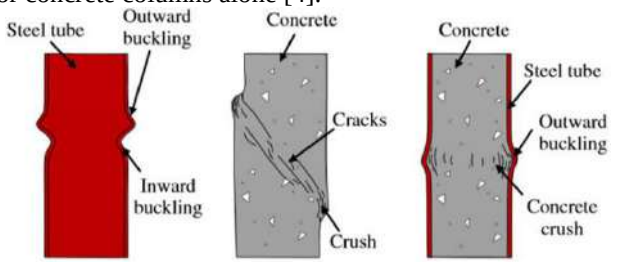

Figure 1: Schematic representation of failure modes for CFST columns, steel columns, and plain concrete columns［4］

Beyond conventional CFST columns, other variants have emerged, including CFST columns with embedded steel profiles and stiffeners. These have gained prominence in recent years due to their substantial enhancements in load-bearing and seismic performance. For example, Qing-Xiang Wang et al.［5］conducted experimental studies on the strength and ductility of 16 CFST columns with embedded cruciform steel profiles. They demonstrated that the embedded steel profile effectively prevents rapid propagation of shear cracks in concrete. Their results further revealed that increasing the structural steel index and confinement index improves the strength and ductility of the composite column. They also found that as the aspect ratio (length-to-diameter) increases, the composite column's strength decreases.

Meichun Zhu et al.［6］conducted experimental studies on square CFST columns filled with high-strength self-compacting concrete and reinforced with cruciform steel profiles under axial loading. Xu Chang et al.［7］performed numerical studies on the lateral strength of CFST columns with embedded cruciform profiles under combined axial and lateral loading, showing that the steel profile helps to bear lateral loads and reduces tensile stress in the concrete.

Numerical studies by Jingming Cai et al.［8,9］examined the mechanical behavior of circular and square CFST columns with embedded cruciform profiles under uniaxial compression, considering parameters such as steel tube ratio, embedded steel ratio, concrete strength, and steel yield strength. Fa-Xing Ding et al.［10］experimentally investigated the behavior of six square CFST columns with embedded cruciform steel profiles under axial loading, demonstrating that concrete strength and steel ratios influence ultimate load-bearing capacity and ductility.

Wang JZ et al.［11］studied the axial behavior and strength of 22 high-strength short concrete columns confined by steel tubes with embedded profiles through both experimental and numerical approaches, identifying the embedded steel profile's shape as a critical parameter in determining load-bearing capacity. Aizhu Zhu et al.［12］examined 30 cold-rolled square CFST columns with welded stiffeners along their inner surfaces. Moreover, Mizan Ahmed et al.［13］performed nonlinear analyses on short square CFST columns with embedded profiles, accounting for local buckling phenomena. Based on the reviewed literature, the most prominent finding regarding the axial and lateral performance of circular and square CFST columns with embedded profiles is the significant influence of cruciform embedded profiles on axial performance. Accordingly, this study proposes various circular and square CFST columns with different embedded steel profiles to evaluate their axial and lateral behavior. The results from axial and lateral loading tests on these proposed columns aim to enhance understanding and application in structural engineering, leading to the development of high-performance profiles with reduced cross-sectional areas. For validation, the experimental results of Tao Zhang et al.［14］on CFST columns with cruciform profiles will be analyzed using the finite element software ABAQUS［15］. Additionally, this study numerically investigates the impact of varying primary column cross-sections (circular/square) and embedded profiles. Axial and lateral performance criteria—including strength, stiffness, ductility, and deformation—are also examined comprehensively.

2. Validation of the Simulation Model

In this section, numerical modeling of an experimental CFST column tested under axial compressive loading by Tao Zhang et al.［14］is conducted to validate the

simulation process. The numerical analysis employs the Quasi-Static method, with nonlinear geometric configurations activated. All modeling steps, including part creation, assembly, and interactions, are accurately implemented in ABAQUS. In the loading module, the supports are modeled as fixed, and an incremental axial load is applied. For meshing, an optimal element size of 0.5 cm is utilized, ensuring precise meshing. Steel components are modeled with S4R shell elements, while concrete components use C3D8R solid elements with reduced integration to mitigate hourglass effects. Additionally, buckling modes are considered in the analysis. To evaluate the numerical model's performance, the axial displacement of the column's top section is considered as the displacement variable, while the reaction forces at the supports represent the load-bearing capacity. A load-displacement curve is extracted and compared with the experimental data from Tao Zhang et al. (Figure 2).

From Figure 2, a reasonably good agreement is observed between the finite element analysis (FEA) results and the experimental findings. The load-displacement curve from the ABAQUS model closely aligns with the experimental data, confirming the accuracy of the numerical modeling and the reliability of the simulation.

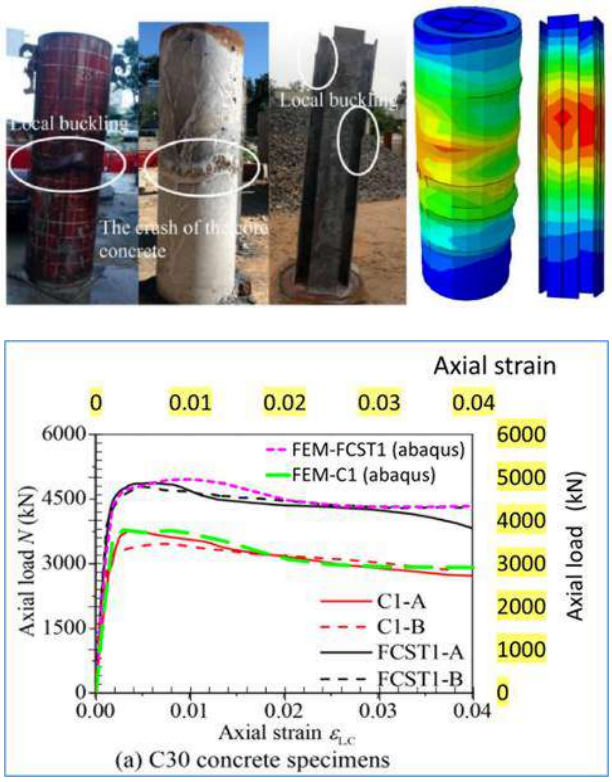

Figure 2: Comparison and validation between experimental load-displacement curve [14] and the numerical simulation results

3. Analysis of Results

To extend the experimental work by Tao Zhang et al. [14], a parametric numerical analysis is conducted in this study. This includes examining the following scenarios:

a) Behavior without concrete: The seismic and axial performance of a circular CFST column with an embedded cruciform profile is studied without the presence of concrete.

b) Comparison of circular vs. square cross-sections: The study investigates how seismic and axial behavior changes when using a square CFST column with an equivalent cross-sectional area to the circular CFST column. Similar analysis is performed for cases without concrete.

c) Introduction of innovative profiles: Five new embedded profiles are proposed to replace the validated cruciform profile ("Plus") within circular and square CFST columns. These innovative profiles are designed to examine their impact on seismic and axial performance. Figures 3 and 4 illustrate the equivalent cross-sectional dimensions for circular and square columns, as well as the new embedded profiles.

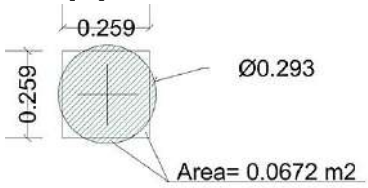

Figure 3: Equivalent dimensions of square and circular CFST columns with equal cross-sectional areas.

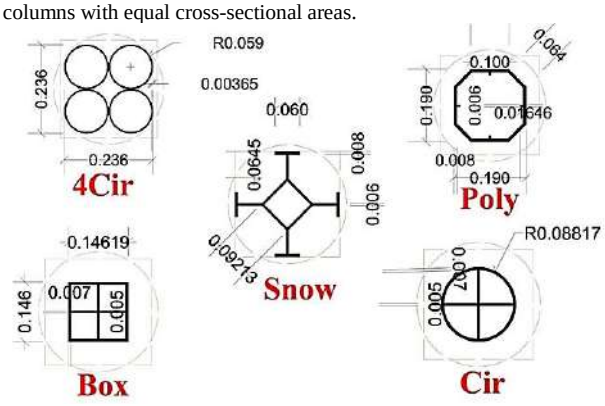

Figure 4: Proposed innovative profiles embedded in CFST columns (circular/square) with equivalent areas.

From Figure 3, the cross-sectional area of the circular column is calculated as 0.0672 m², corresponding to a diameter of 0.293 m. For the square column, a side length of 0.259 m is determined to provide an equivalent area. These dimensions are used in numerical simulations.

Figure 4 shows the five new profiles, which include:

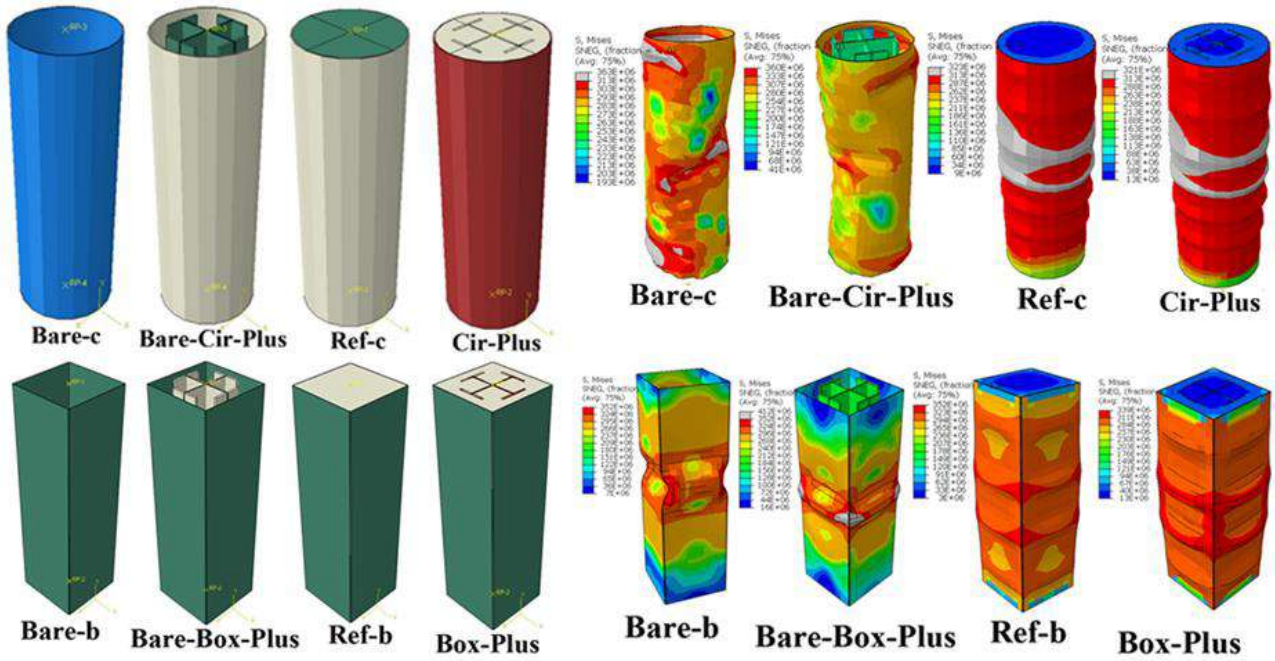

Figure 5: Modeling, Naming, and Axial Loading of Circular and Square CFST Columns (With and Without Concrete).

- 4Cir: Four circular segments.
- Poly: Polygonal profile.
- Snow: Snowflake-shaped profile.
- Box: Reinforced square profile.
- Cir: Reinforced circular profile.

These profiles are designed with areas equivalent to the validated cruciform profile ("Plus") and are analyzed for their influence on seismic and axial performance in CFST columns.

Classification of Profiles

The proposed profiles are categorized based on mass concentration:

- Centralized profiles: Profiles with mass concentrated at the center (e.g., Box and Cir).
- Peripheral profiles: Profiles with mass concentrated around the perimeter (e.g., Snow and 4Cir).
- Intermediate profiles: Profiles with mass distributed between the center and perimeter (e.g., Plus and Poly).

Further numerical simulations will explore the impact of these profiles on the behavior of circular and square CFST columns, aiming to identify high-performance designs with optimized cross-sectional areas.

3.1. The Effect of Concrete in Concrete-Filled Steel Tubes with Cross-Sectional Inserts

This section examines the axial and lateral behavior of circular concrete-filled steel tube (CFST) columns validated in the second part of this study when the concrete is removed. Similarly, the axial and lateral behavior of square steel tube columns without concrete is analyzed. Figure 5 illustrates the modeling and naming conventions for circular and square CFST columns, both with and without concrete. According to Figure 5, the "Bare" model represents hollow steel columns (without concrete), while the "Ref" model denotes reference steel columns (with concrete but without internal inserts). The second subscript "c" and "b" correspond to circular and square cross-sections, respectively. The "Cir-Plus" and "Box-Plus" models represent circular and square CFST columns with cross-shaped inserts, respectively.

Furthermore, Figure 5 shows the von Mises stress distribution and deformations under axial loading. The results indicate that stresses are primarily concentrated in the outer shell, and buckling deformations in the outer shell are evident in the hollow "Bare" models.

Under lateral loading, additional results are obtained. By aggregating these results into load-displacement curves and employing bilinear approximation using an equivalent energy approach, the axial and lateral performance of the models can be assessed. Figure 6 presents the load-displacement curves for the tested columns. Table 1

summarizes the axial and lateral performance metrics derived from analyzing the bilinearized load-displacement curves.

In Table 1:

- Δy and Vy indicate the displacement and load at the yield point, respectively.
- Δu represents the maximum effective displacement experienced by the columns.
- The maximum load sustained, denoted as P, serves as the resistance criterion.
- The initial stiffness, K, is obtained by dividing Vy by Δy, while ductility, μ, is calculated by dividing Δu by Δy.

The subscripts "ax" and "sh" in Table 1 represent axial and lateral performance, respectively. By comparing these performance metrics with the "Bare" circular and square models, the relative axial and lateral performance of CFST columns (with concrete) compared to hollow steel columns (without concrete) can be determined. These results are presented in Figure 7.

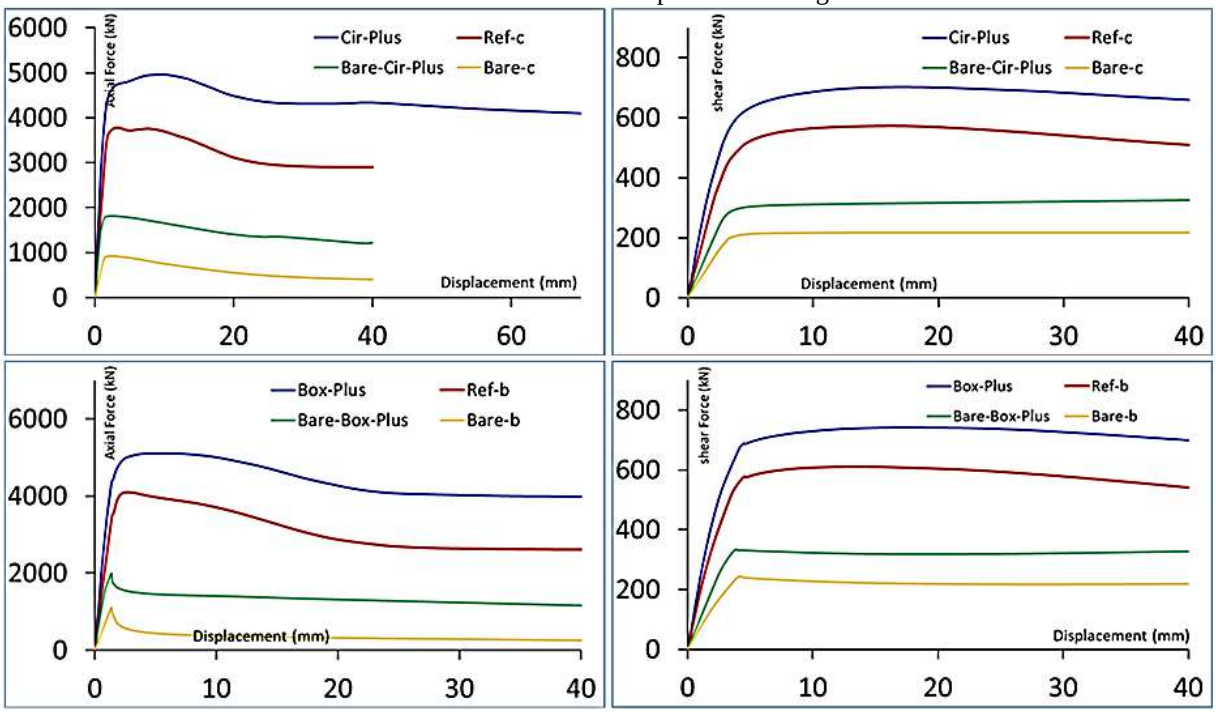

Figure 6: Load-Displacement Curves for Axial and Lateral Loading of Circular and Square CFST Columns (With and Without Concrete).

Table 1

Axial and Lateral Performance Metrics of Circular and Square CFST Columns (With and Without Concrete).

Spectrum	Δy (mm)	Vy (kN)	Δu (mm)	P_{ax} (kN)	K_{ax} (kN/mm)	μ_{ax}
Bare-c	1.22	829	12.94	929	680	10.6
Bare-Cir-Plus	0.94	1592	23.49	1811	1697	25.0
Ref-c	1.45	3245	40	3781	2246	27.7
Cir-Plus	1.45	4553	40	4961	3147	27.7

Spectrum	Δy (mm)	Vy (kN)	Δu (mm)	P_{sh} (kN)	K_{sh} (kN/mm)	μ_{sh}
Bare-c	3.39	216	40.00	217	64	11.8
Bare-Cir-Plus	3.30	315	40.00	325	96	12.1
Ref-c	3.47	547	40	572	158	11.5
Cir-Plus	3.42	679	40	702	199	11.7

Spectrum	Δy (mm)	Vy (kN)	Δu (mm)	P_{ax} (kN)	K_{ax} (kN/mm)	μ_{ax}
Bare-b	1.21	985	1.64	1106	817	1.4
Bare-Box-Plus	0.89	1625	3.49	1991	1833	3.9
Ref-b	1.43	3674	17	4093	2563	12.0
Box-Plus	1.26	4419	40	5102	3508	31.8

Spectrum	Δy (mm)	Vy (kN)	Δu (mm)	P_{sh} (kN)	K_{sh} (kN/mm)	μ_{sh}
Bare-b	3.21	222	40.00	241	69	12.5
Bare-Box-Plus	3.19	322	40.00	334	101	12.5
Ref-b	3.43	587	40	611	171	11.7
Box-Plus	3.46	723	40	741	209	11.6

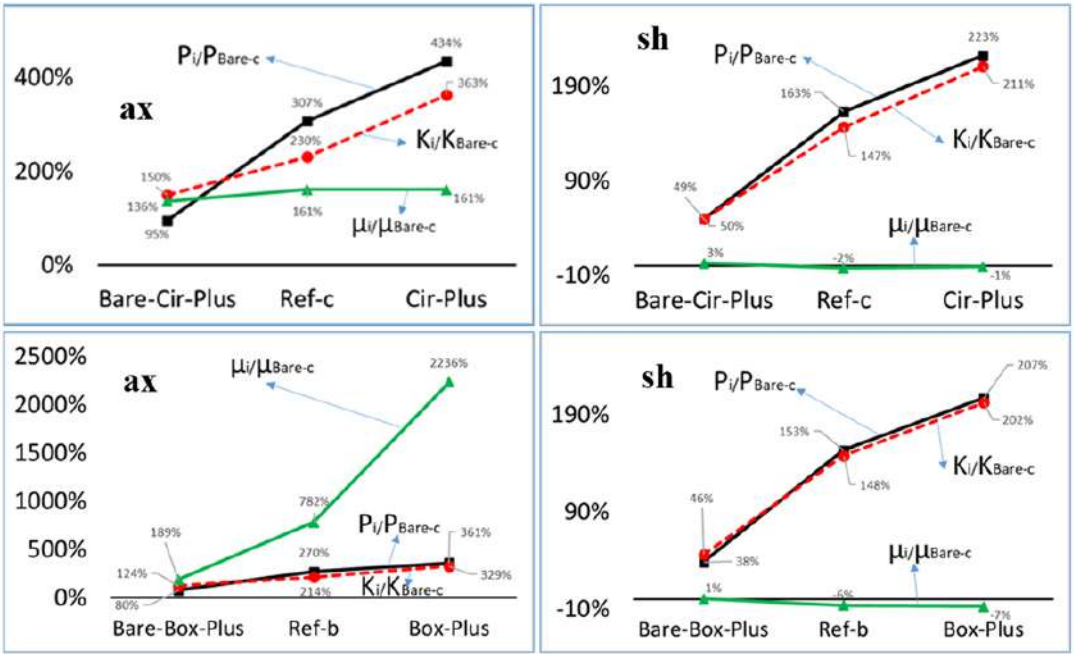

Figure 7: Relative Axial and Lateral Performance of Circular and Square CFST Columns Compared to Hollow Steel Columns.

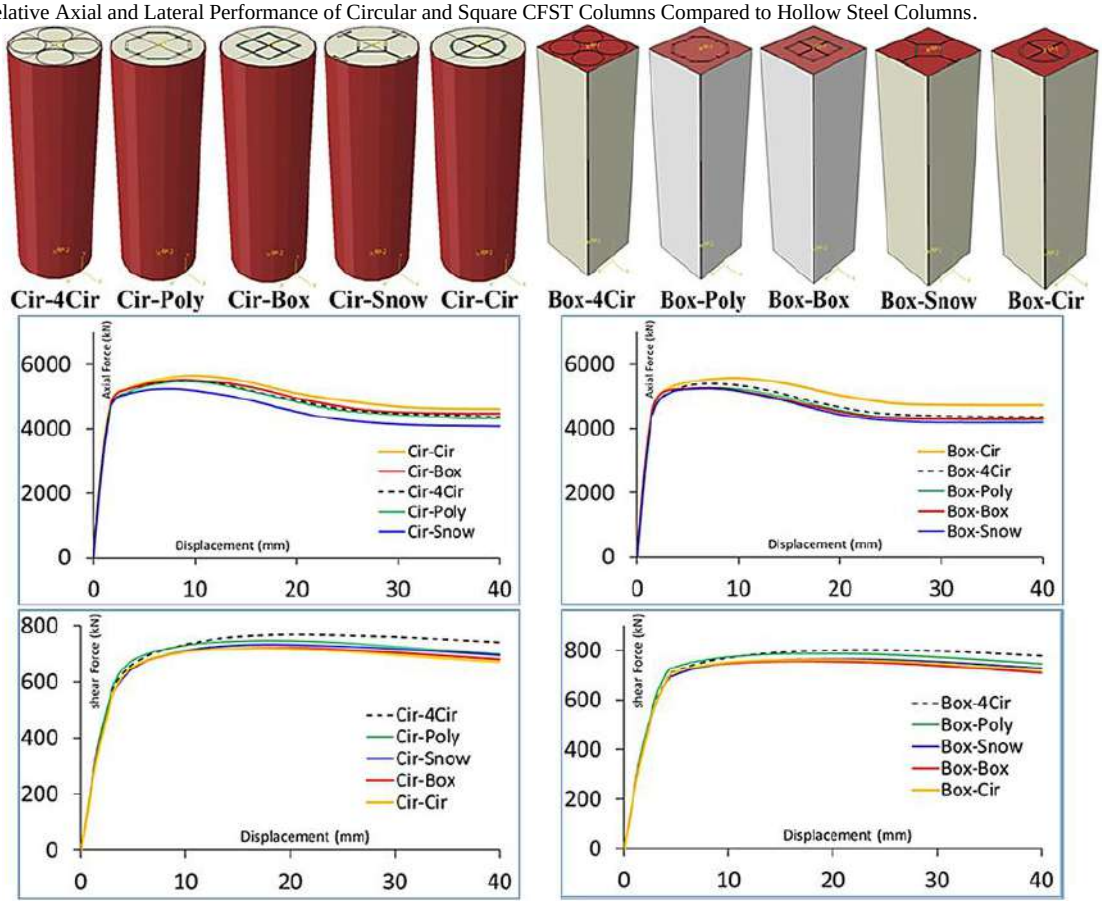

Figure 8: Modeling, naming, and axial and lateral load-displacement curves of circular and square concrete-filled steel columns with new internal sections.

Key findings from Figure 7 include the following:

- The axial resistance of the reference circular column filled with concrete ("Ref-c") is 307%

higher than the hollow circular column ("Bare-c"). Additionally, axial stiffness and ductility increase by 230% and 161%, respectively. The axial performance of the hollow circular column with a cross-shaped insert ("Bare-Cir-Plus") and the CFST column with the same insert ("Cir-Plus") shows improvement compared to the hollow column ("Bare-c").

- The lateral resistance of the reference circular column filled with concrete ("Ref-c") is 163% higher than the hollow circular column ("Bare-c"), with stiffness increasing by 147% and ductility decreasing slightly by 2%. For models with cross-shaped inserts, "Bare-Cir-Plus" and "Cir-Plus" exhibit enhanced lateral resistance and stiffness but reduced ductility compared to "Bare-c."
- The axial resistance of the reference square column filled with concrete ("Ref-b") is 270% higher than the hollow square column ("Bare-b"), with stiffness and ductility increasing by 214% and 782%, respectively. The axial performance of the hollow square column with a cross-shaped insert ("Bare-Box-Plus") and the CFST column with the same insert ("Box-Plus") also improves compared to "Bare-b."
- The lateral resistance of the reference square column filled with concrete ("Ref-b") is 153% higher than the hollow square column ("Bare-b"), with stiffness increasing by 148% and ductility decreasing slightly by 6%. The lateral performance of "Bare-Box-Plus" and "Box-Plus" shows increased resistance and stiffness but reduced ductility compared to "Bare-b."
- In the hollow circular column ("Bare-c"), the column collapses inward and slightly outward after loading. A similar behavior is observed in "Bare-Cir-Plus." However, when filled with concrete, stress and deformation are primarily concentrated in the outer shell, with outward buckling only.
- In the hollow square column ("Bare-b"), the column collapses inward and slightly outward at mid-height after loading. This behavior is also seen in "Bare-Box-Plus." When filled with concrete, stress and deformation are concentrated in the outer shell, with outward buckling only at mid-height.
- Stress and deformation patterns under lateral loading are generally similar across all tested models.
- In axial loading, hollow steel columns exhibit sudden drops in the load-displacement curves due to buckling and distortion. This behavior limits their effective axial performance, reducing ultimate load and ductility significantly.
- Concrete-filled columns, on the other hand, demonstrate significantly improved ductility due to the absence of severe buckling, particularly in axial loading. However, this improvement is less pronounced under lateral loading.

4. The Effect of Internal Sections on Circular and Square Concrete-Filled Steel Columns

This section investigates how axial and lateral performance changes when alternative internal sections (as depicted in Figure 4) are used in circular and square concrete-filled steel columns, replacing the cross-shaped section while maintaining the same cross-sectional area. Figure 8 illustrates the modeling of circular and square concrete-filled steel columns with new internal sections and their corresponding load-displacement curves for axial and lateral loading. Additionally, Table 2 presents the axial and lateral performance of these columns based on the bilinear analysis of the load-displacement curves.

4.1. Axial Performance of Circular and Square Concrete-Filled Steel Columns

By consolidating the axial performance data of circular and square concrete-filled steel columns, it is possible to compare these two shapes at different reinforcement levels. Figure 9 demonstrates the comparative axial performance of circular and square columns in terms of strength, stiffness, and ductility.

The following key findings are derived from Figure 9:

- Adding internal sections to circular or square concrete-filled steel columns enhances axial and lateral performance in terms of strength and stiffness. However, the impact on ductility is less definitive, as discussed below.
- Upon completion of axial loading tests, the numerical analysis reveals the axial performance of concrete-filled steel columns with various internal sections and stiffeners. Given the equal cross-sectional areas of the steel and concrete for both circular and square samples, these two shapes can be directly compared at each level of reinforcement.
- The square column exhibits higher axial strength than the circular column in both the bare and reference specimens. After reinforcement with internal steel sections, the circular column outperforms the square column in axial strength, except in the cross-shaped section ("Plus") where

Table 2
Axial and lateral performance of circular and square concrete-filled steel columns with new internal sections.

Spectrum	Δy (mm)	Vy (kN)	Δu (mm)	P_{ax} (kN)	K_{ax} (kN/mm)	μ_{ax}
Cir-4Cir	1.45	4878	40	5487	3366	27.6
Cir-Poly	1.42	4844	40	5465	3411	28.2
Cir-Box	1.39	4934	40	5528	3538	28.7
Cir-Snow	1.35	4586	40	5234	3398	29.6
Cir-Cir	1.43	5075	40	5646	3542	27.9

Spectrum	Δy (mm)	Vy (kN)	Δu (mm)	P_{sh} (kN)	K_{sh} (kN/mm)	μ_{sh}
Cir-4Cir	3.47	743	40	767	214	11.5
Cir-Poly	3.35	722	40	746	215	11.9
Cir-Box	3.55	702	40	723	198	11.3
Cir-Snow	3.44	710	40	733	207	11.6
Cir-Cir	3.47	697	40	721	201	11.5

Spectrum	Δy (mm)	Vy (kN)	Δu (mm)	P_{ax} (kN)	K_{ax} (kN/mm)	μ_{ax}
Box-4Cir	1.32	4755	40	5393	3595	30.2
Box-Poly	1.32	4659	40	5265	3542	30.4
Box-Box	1.24	4652	40	5262	3748	32.2
Box-Snow	1.28	4580	40	5236	3564	31.1
Box-Cir	1.38	5061	40	5573	3660	28.9

Spectrum	Δy (mm)	Vy (kN)	Δu (mm)	P_{sh} (kN)	K_{sh} (kN/mm)	μ_{sh}
Box-4Cir	3.54	782	40	803	221	11.3
Box-Poly	3.43	769	40	788	224	11.7
Box-Box	3.52	738	40	756	210	11.4
Box-Snow	3.46	747	40	765	216	11.6
Box-Cir	3.46	747	40	761	216	11.6

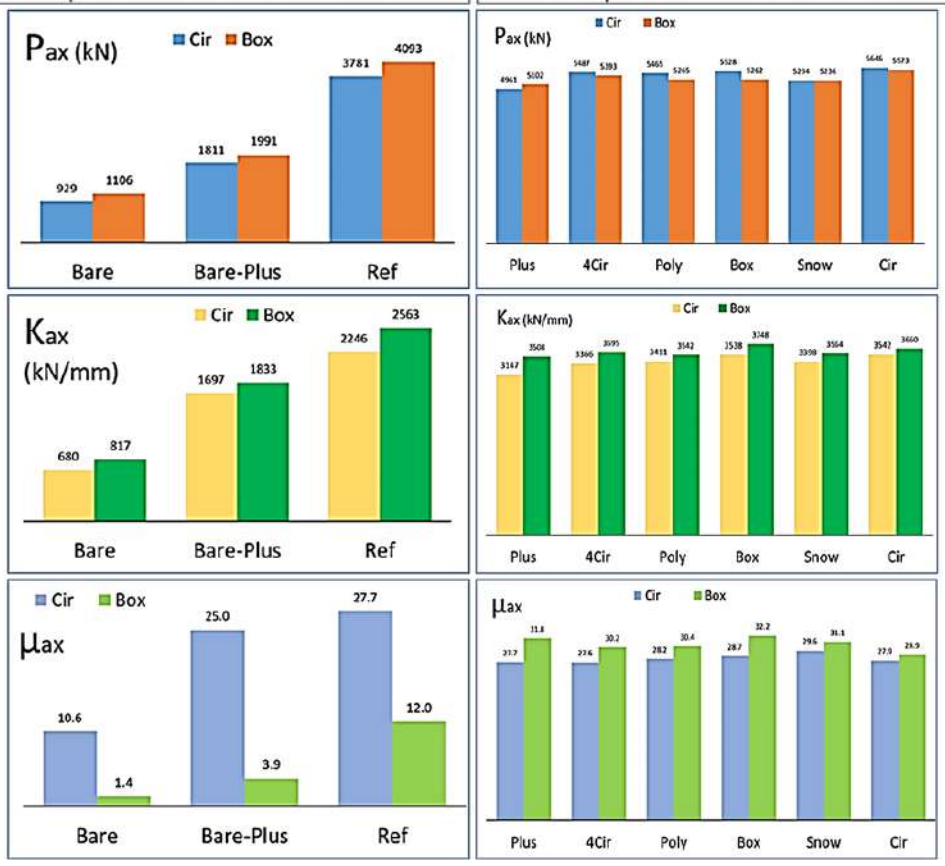

Figure 9: Comparative axial strength, stiffness, and ductility performance of circular and square columns in this study.

- the square column demonstrates superior axial strength.
- The square column shows higher axial stiffness than the circular column in both bare and reference specimens. Following reinforcement, the square concrete-filled steel column continues to exhibit greater axial stiffness compared to its circular counterpart.
- The square column has lower axial ductility compared to the circular column in both bare and reference specimens. After reinforcement, the circular column exhibits even lower axial ductility than the square column. In bare columns, the ductility difference is particularly pronounced due to the sudden axial strength drop caused by buckling in the square specimens.

- Under axial loading, bare square columns experience severe strength drops due to sudden buckling, which significantly reduces ductility. This phenomenon is mitigated in concrete-filled columns, where the increased ductility of circular and square columns becomes evident.
- Unlike axial performance, buckling does not have a pronounced effect on lateral loading, as abrupt instability is less likely in such scenarios. Thus, lateral performance trends differ from those observed under axial loading.

4.2. Lateral Performance of Circular and Square Concrete-Filled Steel Columns

By consolidating the data related to the lateral performance of circular and square concrete-filled steel columns, their lateral performance can be compared across various reinforcement levels. Figure 10 illustrates the comparison of lateral strength, stiffness, and ductility for circular and square columns investigated in this study.

From Figure 10, the following significant findings are derived:

- Square columns exhibit higher lateral strength than circular columns in both bare and reference specimens. After reinforcement with internal steel sections, square columns continue to show superior lateral strength compared to circular columns.
- Square columns demonstrate greater lateral stiffness than circular columns in both bare and reference specimens. This trend remains consistent after reinforcing the concrete-filled steel columns with internal sections.
- In bare and reference specimens, square columns display higher lateral ductility than circular columns. After reinforcement, circular columns generally achieve higher lateral ductility than square columns. However, in the reinforced samples, lateral ductility of circular and square columns becomes nearly equivalent.

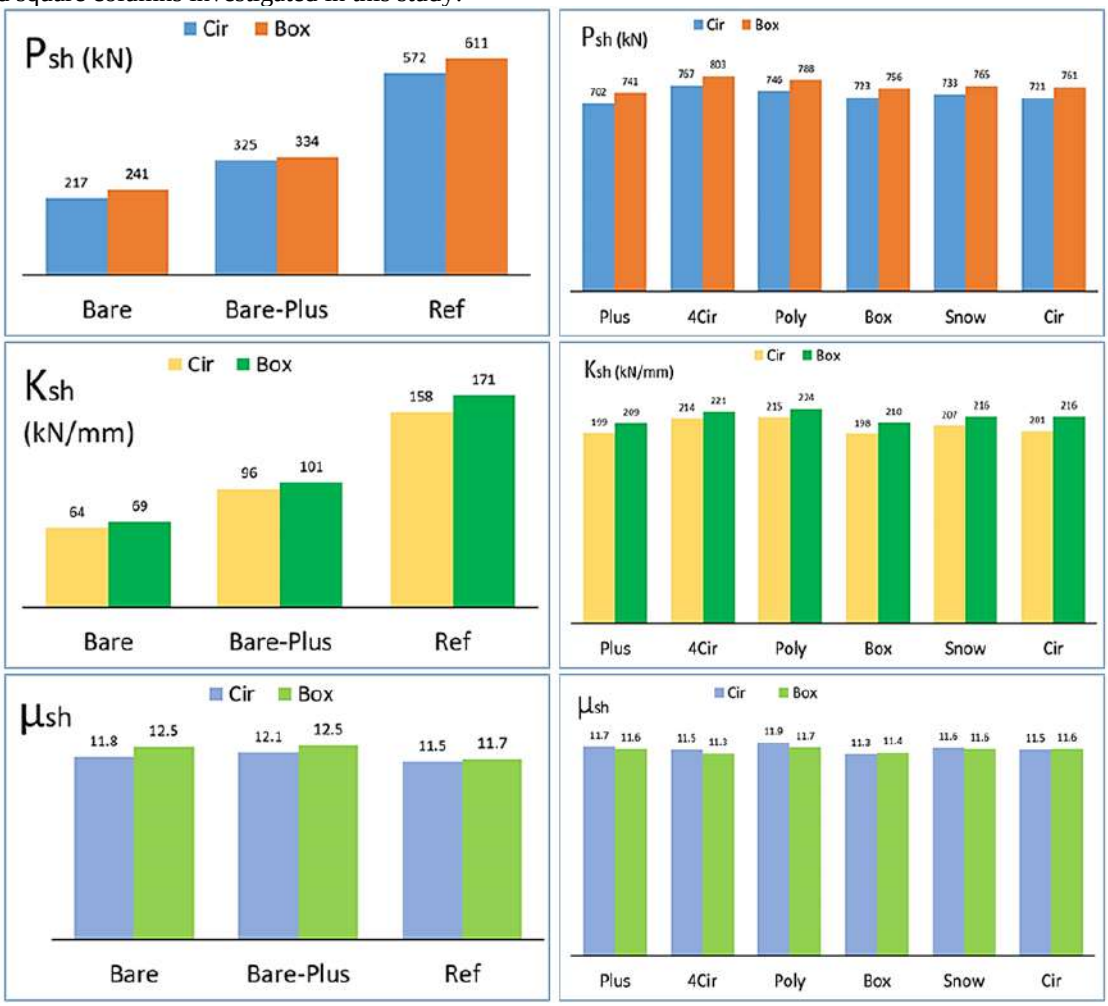

Figure 10: Comparison of lateral strength, stiffness, and ductility for circular and square columns in this study.

4.3. Comparative Relative Performance of Circular and Square Concrete-Filled Steel Columns

This section compares the relative performance of circular and square concrete-filled steel columns with various embedded steel sections and stiffeners. By expressing the relative axial and lateral performance in terms of percentage increase or decrease (sorted systematically), the overall behavior of these columns can be better understood. Relative performance is defined as the performance of each sample compared to its own reference case, i.e., the performance of circular samples relative to the circular reference column ("Ref-c") and square samples relative to the square reference column ("Ref-b"). Figure 11 presents the comparative relative axial and lateral performance of circular and square concrete-filled steel columns.

From Figure 11, the following major conclusions are drawn:

- "Cir-Cir" and "Cir-Box" samples show the highest increase in axial strength, with 49% and 46%, respectively. "Box-Plus" and "Box-Snow" samples exhibit the lowest increase in axial strength, with 25% and 28%, respectively. Overall, circular concrete-filled steel columns with embedded steel sections demonstrate higher relative axial strength compared to square columns.
- "Cir-Cir" and "Cir-Box" samples jointly achieve the highest increase in axial stiffness at 58%. "Box-Plus" and "Box-Poly" samples show the lowest increase in axial stiffness, with 37% and 38%, respectively. Circular concrete-filled steel columns exhibit superior relative axial stiffness compared to square columns.
- Square concrete-filled steel columns with embedded steel sections have significantly higher relative axial ductility than circular columns. This is due to the sudden buckling observed in bare square columns, which substantially reduces their axial ductility. Among square samples, "Box-Box" achieves the highest increase in relative axial ductility (169%), while "Box-Cir" has the lowest (141%). Among circular samples, "Cir-Snow" shows the highest increase in relative axial ductility (7%), while "Cir-4Cir" has the lowest (-0.3%).

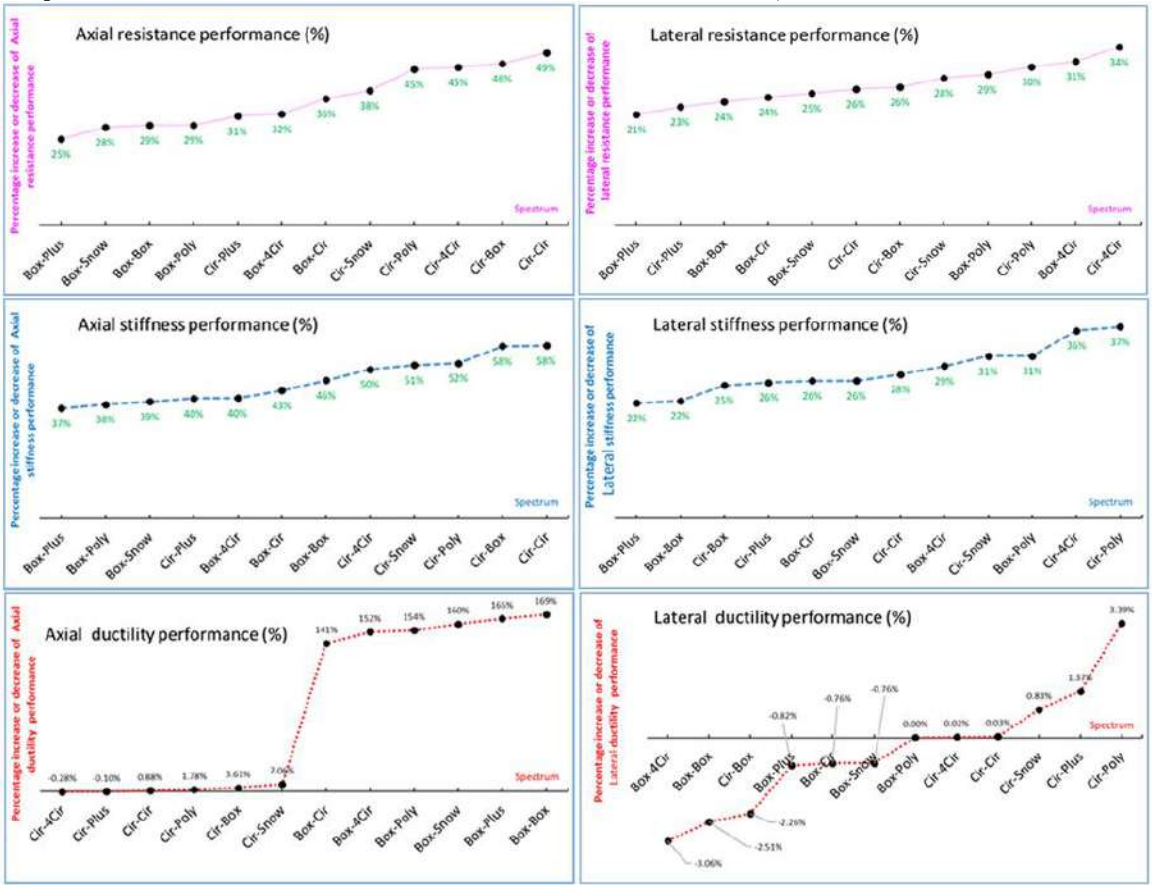

Figure 11: Comparative relative axial and lateral performance of circular and square concrete-filled steel columns.

- "4Cir-Cir" and "4Cir-Box" samples show the highest increase in lateral strength, with 34% and 31%, respectively. "Box-Plus" and "Cir-Plus" samples exhibit the lowest increase in lateral strength, with 21% and 23%, respectively. Overall, steel sections with profiles such as "4Cir" and "Poly" exhibit the highest relative lateral strength, while "Plus" profiles demonstrate the lowest.
- "Poly-Cir" and "4Cir-Cir" samples achieve the highest increase in lateral stiffness, with 37% and 36%, respectively. "Box-Plus" and "Box-Box" samples show the lowest increase in lateral stiffness, both at 22%.
- "Poly-Cir" and "Plus-Cir" samples achieve the highest increase in lateral ductility, with 3.4% and 1.4%, respectively. "Box-4Cir" and "Box-Box" samples exhibit the greatest reduction in lateral ductility, with -3.1% and -2.5%, respectively. Circular concrete-filled steel columns tend to demonstrate higher relative lateral ductility, while square columns are inclined toward lower relative lateral ductility.

In conclusion, circular concrete-filled steel columns generally outperform square columns in terms of ductility and stiffness, whereas square columns exhibit superior strength under certain conditions.

5. Conclusion

This research numerically analyzed the effects of steel sections and stiffeners embedded within circular and square steel columns filled with concrete under axial and lateral loading. The findings demonstrated that the incorporation of steel sections inside concrete-filled steel columns significantly enhances their axial and lateral performance. The numerical results closely aligned with experimental findings. Key conclusions based on the six types of internal embedded sections and two main steel column cross-sections are as follows:

- Filling the interior space of steel columns with concrete greatly improves axial performance (in terms of strength, stiffness, and ductility) and significantly enhances lateral performance (in terms of strength and stiffness). However, lateral ductility slightly decreases.
- The significant improvement in axial ductility due to concrete filling can be attributed to the prevention of premature distortion and buckling. In bare steel columns (without concrete), distortion and early buckling occur upon reaching yield strength under axial loading, reducing their effective ultimate displacement (ΔU). This issue is mitigated in concrete-filled steel columns, leading to higher axial ductility.
- Axial ductility improvement for square concrete-filled steel columns is 782%, and for circular ones, 161% compared to their bare counterparts. Conversely, since severe buckling does not occur under lateral loading, the lateral ductility of concrete-filled steel columns does not improve and may decrease slightly due to increased stiffness and yield points in strengthened samples.
- Stress distribution analysis showed that, under axial loading, the internal stiffener, outer shell, and concrete take the most load transfer responsibility in descending order. Under lateral loading, the outer shell, internal stiffener, and concrete take the most load in descending order, emphasizing the significant role of internal stiffeners in load transfer.
- Square concrete-filled steel columns outperform circular ones in axial strength and stiffness but have lower axial ductility.
- Reinforced square concrete-filled steel columns show higher axial stiffness and ductility than circular ones, albeit with lower axial strength.
- Square concrete-filled steel columns have superior lateral strength, stiffness, and ductility compared to circular columns in all cases (bare, reference, and reinforced).
- Reinforced square concrete-filled steel columns exhibit greater lateral stiffness and strength than circular ones but lower lateral ductility.
- Sections with centralized mass distribution (e.g., Box and Cir profiles) provide higher axial strength, stiffness, and ductility, while sections with distributed mass along the perimeter (e.g., Snow profiles) have the lowest axial performance metrics.
- Sections with mass concentrated near the perimeter (e.g., Cir4 and Poly profiles) enhance lateral strength and stiffness, while sections like Plus exhibit the lowest lateral strength and stiffness.
- Intermediate profiles (e.g., Plus and Poly) achieve the highest lateral ductility. Generally, circular columns have the highest relative lateral ductility and tend to increase lateral performance, while square columns exhibit the lowest relative lateral ductility and tend to decrease in this regard.

References

[1] Ayough, Pouria, NH Ramli Sulong, and Zainah Ibrahim. "Analysis and review of concrete-filled double skin steel tubes under compression." Thin-Walled Structures 148 (2020): 106495. https://doi.org/10.1016/j.tws.2019.106495

[2] Ezoji, Reyhaneh. "A review on behaviour and strength of concrete filled steel tubular columns." Journal of Civil Engineering Researchers 1.7 (2017): 12-16. https://www.journals-researchers.com/ojs/index.php/jcer/article/view/31

[3] Hosseinzadeh, Lobat. "Evaluation of Modified Seismic Model Using Shear Keys at Steel Beam Connections to Concrete Colum." Journal of Civil Engineering Researchers 4.1 (2022): 21-28. https://doi.org/10.52547/JCER.4.1.21

[4] Han, Lin-Hai, Wei Li, and Reidar Bjorhovde. "Developments and advanced applications of concrete-filled steel tubular (CFST) structures: Members." Journal of constructional steel research 100 (2014): 211-228. http://dx.doi.org/10.1016/j.jcsr.2014.04.016

[5] Wang, Qingxiang, Dazhou Zhao, and Ping Guan. "Experimental study on the strength and ductility of steel tubular columns filled with steel-reinforced concrete." Engineering Structures 26.7 (2004): 907-915. https://doi.org/10.1016/j.engstruct.2004.02.009

[6] Zhu, Meichun, et al. "Experimental research on square steel tubular columns filled with steel-reinforced self-consolidating high-strength concrete under axial load." Engineering Structures 32.8 (2010): 2278-2286. https://doi.org/10.1016/j.engstruct.2010.04.002

[7] Chang, Xu, You-Yi Wei, and Yan-Chun Yun. "Analysis of steel-reinforced concrete-filled-steel tubular (SRCFST) columns under cyclic loading." Construction and Building Materials 28.1 (2012): 88-95. https://doi.org/10.1016/j.conbuildmat.2011.08.033

[8] Cai, Jingming, Jinlong Pan, and Yufei Wu. "Mechanical behavior of steel-reinforced concrete-filled steel tubular (SRCFST) columns under uniaxial compressive loading." Thin-Walled Structures 97 (2015): 1-10. https://doi.org/10.1016/j.tws.2015.08.028

[9] Cai, Jing-ming, Jin-long Pan, and Yu-fei Wu. "Performance of steel-reinforced square concrete-filled steel hollow section (SRSCFSHS) columns under uniaxial compression." Advanced Steel Construction 12.4 (2016): 410-427. https://doi.org/10.18057/IJASC.2016.12.4.3

[10] Ding, Fa-xing, et al. "Behavior of steel-reinforced concrete-filled square steel tubular stub columns under axial loading." Thin-Walled Structures 119 (2017): 737-748. https://doi.org/10.1016/j.tws.2017.07.021

[11] JZ, Wang, Sun ML, and Jia JQ. "Axial load behavior and strength of tube-confined steel-reinforced short columns with ultra-high-strength concrete." Advances in Structural Engineering 21.3 (2018): 428-444. https://doi.org/10.1177/1369433217719983

[12] Zhu, Aizhu, et al. "Experimental study of concrete filled cold-formed steel tubular stub columns." Journal of Constructional Steel Research 134 (2017): 17-27. https://doi.org/10.1016/j.jcsr.2017.03.003

[13] Ahmed, Mizan, et al. "Nonlinear analysis of square steel-reinforced concrete-filled steel tubular short columns considering local buckling." Structural Concrete 25.1 (2024): 69-84. https://doi.org/10.1002/suco.202300402

[14] Zhang, Tao, et al. "Compressive behavior of steel-reinforced concrete-filled circular steel tubular stub columns." Structures. Vol. 28. Elsevier, 2020. https://doi.org/10.1016/j.istruc.2020.08.012

[15] ABAQUS-V6.16-1, “Finite Element Analysis Software”, Johnston, RI, USA. ABAQUS/Standard theory. Manual, Dassault Systèmes Simulia Corp., 2015

J-Researchers

Journal of Civil Engineering Researchers

Journal homepage: www.journals-researchers.com

Physical and Chemical Surface Modifiers of Carbon Nanotubes on the Mechanical and Physical Properties of Concrete

Mahsa Zarehparvar-Shoja,[a] Rasoul Shadnia,[a,*] Amin Kazemi Beydokhti[b,]

[a] *Department of Civil Engineering, Hakim Sabzevari University, Sabzevar, Iran*

[b] *Department of Chemical Engineering, Hakim Sabzevari University, Sabzevar, Iran*

ABSTRACT

This study utilizes nanofilament-based nanotechnology, such as carbon nanotubes (CNTs), to improve the mechanical characteristics of concrete as a building material. One of the important and effective factors in adding carbon nanotubes to cement composites is their proper dispersion in the mixture. Therefore, in this research, different methods of dispersing carbon nanotubes in cement mortar have been investigated. They were first functionalized through covalent bonding to prevent carbon nanotubes from accumulating in the water. To achieve the appropriate distribution of carbon nanotubes in water and maintain the stability of their dispersion, different surfactants including Polycarboxylate (PCE), Sodium dodecyl sulfate (SDS), Cetyltrimethylammonium bromide (CTAB), Polyethylene glycol (PEG) were employed. At that point, utilizing visual perception and UV test, PCE/PEG surfactant was presented as a reasonable surfactant for the scattering of carbon nanotubes. Once the most suitable dispersal technique was identified, the impact of incorporating multi-walled carbon nanotubes into concrete was investigated with varying weight proportions. The study revealed that even at low concentrations (0.015%, 0.030%, and 0.045%) relative to the cement weight, the inclusion of carbon nanotubes decreased the porosity of the concrete nanocomposite, resulting in a denser and more compact composite. As a result, it increases the concrete samples' compressive, tensile, and bending strength.

ARTICLE INFO

Received: December 28, 2024
Accepted: February 24, 2025

Keywords:
Dispersion method
Carbon nanotubes
Mechanical properties
Surfactant
Concrete

DOI: 10.61186/JCER.7.1.34
DOR: 20.1001.1.2538516.2025.7.1.4.0

1. Introduction

Concrete is a mixture of aggregate, cement, and water in proper proportions. Concrete is one of the most essential building materials for civil engineering projects worldwide. In any case, nanoscale cracks and pores in concrete create significant problems and diminish the mechanical performance and strength of concrete. Recently, nanomaterials have been used to increment the durability of concrete in concrete structures [1,2]. Nanomaterials have been used in various fields, including medicine, construction, the automobile industry, etc. Still, the construction field is one of nanomaterials' main and most beneficial uses. The use of these materials in concrete, steel, and glass can improve their properties and reduce environmental pollution [3]. It has been proved that

* Corresponding author. Tel.: +98000000000; e-mail: r.shadnia@hsu.ac.ir (R Shadnia).

carbon nanotubes (CNT) have better desirable properties among nanoparticles due to their resistance and high elastic modulus and are a more promising choice [1,2]. Carbon nanotubes are thin and long cylinders of carbon first discovered by Iijima in 1991 [3]. Carbon nanotubes possess a tubular configuration comprising coiled hexagonal lattice structures of graphene with tubes having nanometer-scale diameters. These tubes are categorized into two groups: single-walled (SWCNT) and multi-walled (MWCNT) [4]. With Young's modulus TPA of 1 and outstanding tensile strength in the range of 20-150 GPA, carbon nanotubes are considered the best candidates for cement and concrete reinforcement as they can prevent the propagation of small microcracks [5–7]. Carbon nanotubes (CNT) are increasingly being employed in concrete due to their high mechanical and electrical conductivity. Carbon nanotube concrete (CNTC) has been the subject of extensive research globally. Notably, they have shown that carbon nanotubes can bridge framework cracks, fill interior pores, and stimulate cement hydration responses in concrete. CNTs improve durability by optimizing the inner pore structure and increasing the interfacial transition zone (ITZ) [8,9]. Ahmed et al. and his colleagues discovered that nanomaterials such as CNT can make significant changes in cement composites, increasing cement quality and strength while decreasing the porosity [10]. Specifically, Shang and Song specified that the inclusion of CNT can increase the compressive and ductile strengths of concrete by 30.8% and 46%, respectively [11]. Kramer and colleagues examined the influence of incorporating 0.05 and 0.075% carbon nanotubes (CNT) in foam concrete. They noticed that the alteration in flexural strength after 28 days and the compressive strength of the concrete after 28 days were 40% and 7.5%, correspondingly [12]. In recent times, the influence of CNT in cement and concrete composites has been extensively studied., but there are contradictions in the reported results. Some results confirmed the improvement of mechanical properties in cement composites [13,14], while some did not show any improvement and in some other cases the mechanical properties even decreased [15–17]. The strengthening of concrete and cement matrices containing carbon nanotubes depends on various factors, including the type of carbon nanotubes, dispersion quality, interaction, and strength of their bond with the cement matrix [18,19]. According to Zijian Su, there are two primary obstacles for incorporating carbon nanotubes in cement mixtures: one is to standardize the distribution of CNTs within the cement mixture, and the other is to control the interaction of CNTs with substances produced during cement hydration [20]. It is challenging to evenly distribute CNTs throughout the cement matrix; Conversely, in order for CNTs to positively affect the mechanical characteristics of cement-based composites, proper dispersion of CNTs is necessary [21–23]. CNT aggregation occurs for several reasons. Due to their nanoscale diameter, the surface area of carbon nanotubes is high, as well as the interfacial attraction between CNTs. Dispersion problems can also arise from the tendency of CNTs to form bundles that are tightly bound by high van der Waals forces. In addition, the high aspect ratio of CNTs (length/diameter) combined with their flexibility allows for the formation of highly entangled agglomerates in the liquid phase. The incorporation of CNTs into cement also faces two major challenges: bonding and dispersion. Strong bonding between CNTs and the cement matrix as well as effective dispersion of CNTs are essential for effective load transfer to CNTs, which may act as reinforcements to improve the mechanical properties of cement composites. It is also believed that CNTs can provide significant mechanical reinforcement if the bonding between CNTs and the cement matrix can be controlled [23]. The proper dispersion of carbon nanotubes delays the growth of micro-cracks and reduces pores in nano-size, thus increasing the performance of concrete [24,25]. Therefore, an executive solution should be sought for this important matter. One of the available methods for proper dispersion is to use an additive in an aqueous solution and then in the concrete mixture. Many researchers have considered the use of different surfactants with different concentrations to disperse MWCNTs in cement materials [26,27]. A combination of physical (sonic) and chemical (surfactant-based) dispersion methods is the most recommended method for exfoliation of CNT agglomerates in water-mixed cement composites. Surfactants not only help in exfoliation of CNT bundles, but may also play a role in bonding with the cement matrix. Li et al. [4] claim that the surface interactions between surface-modified CNTs and hydration products provide high bond strength and enhance the efficiency of charge transfer from the cement matrix to the reinforcement [28]. Jang et al. studied the mechanical properties of MWCNT-reinforced cement pastes and their dispersion in cement pastes [29]. They used a water-reducing additive (ADVA Cast 575) as a surfactant and observed that MWCNTs tend to aggregate and precipitate immediately in distilled water without a surfactant. On the other hand, the presence of surfactants in MWCNTs improves their dispersibility. Additionally, Wang et al. employed gum Arabic as a surfactant and acknowledged its superiority as the optimal selection [30].

A review of the technical literature shows that only a few researchers have succeeded in properly dispersing carbon nanotubes in water [31]. In this study, to achieve the optimal scattering of oxidized multi-walled carbon nanotubes in distilled water, through a modification technique, the influence of employing various surfactants to enhance the scattering of carbon nanotubes and consequently enhancing the structural characteristics of

concrete was investigated and ultimately, a novel surfactant was introduced. For this purpose, various surfactants such as CTAB, sodium dodecyl sulfate (SDS), polyethylene glycol (PEG), and polycarboxylate (PCE) were used. Among the surfactants tested, combining polyethylene glycol and polycarboxylate provided good carbon nanotube dispersion and improved concrete mechanical properties. We have introduced a variety of polyethylene glycol and polycarboxylate as a new surfactant. This is because these two surfactants are compatible with the cement paste. Also, the dispersion of carbon nanotubes was more stable.

2. Materials and Methods

For concrete sample preparation, fine-grained and coarse-grained stones were used according to standard grading curves based on Iranian National Concrete Batching Plant. The ratio of fine grain used to the total fine grain and coarse grain used was calculated as 56%. The ratio of water to cement was chosen to be constant and equal to 0.48 for all samples. The characteristic compressive strength of the concrete was considered as 25 MPa. In this research, Portland type 2 Jovin cement with a strength class of 315 kg/cm^2 has been used. All the samples were processed in the same condition. The proportions and concrete mixing plants are given in Table 1. The samples containing carbon nanotubes with values of 0.015%, 0.030%, and 0.045% relative to the weight of cement (weight fraction) are named CNT0%, CNT0.015%, CNT 0.030%, and CNT0.045%. The used carbon nanotube is a multi-walled tube. Its length is 10-30 micrometers, and it is black. Carbon nanotubes are from Fine Nano company and made by US Nano. The complete information on multi-layered carbon nanotubes can be found in Table 2. Carbon nanotubes exist in a powdered state, initially undergoing acid modification to generate the functional group COOH. A novel surfactant, comprising polyethylene glycol and polycarboxylate, was employed to disperse the carbon nanotube powder in water. Polyethylene glycol is a polymer compound made from ethylene glycol (EG) that exhibits varying physical and chemical characteristics based on the quantity of EG units present in its molecular structure. These polymers are the most important commercial type of polyether and increase their hydrophilic properties. Additionally, a super lubricant based on polycarboxylate (PCE) obtained from Rezin Concrete Company has been utilized to enhance the distribution of carbon nanotubes in distilled water and cement paste, in order to achieve the desired consistency and flow...

Table 1.
Weight ratio of materials used in making concrete samples (For making 135 kg Concrete)

Sample	**1**	**2**	**3**	**4**
sample name	0	0.015% *cnt*	0.030% cnt	0.045% cnt
Cement (Kg)	27	27	27	27
Water (Kg)	12.5	12.5	12.5	12.5
Fine-grained agg. (Kg)	54.5	54.5	54.5	54.5
Coarse-grained agg. type 1 (Kg)	16	16	16	16
Coarse-grained type 2 (Kg)	25	25	25	25
carbon nanotube (gr)	0	4.05	8.1	12.1
Carbon nanotube /cement ratio%	0	0.015	0.030	0.045
amount of super lubricant in concrete production (gr) (0.5 percent of cement weight)	135	135	135	135
Amount of superlubricant in carbon nanotubes solution (gr) (Ratio of CNT to super lubricant 1:5)	0	20.25	40.5	60.5
Amount of polyethylene glycol in carbon nanotube solution (gr) (Ratio of CNT to PEG 1:5)	0	20.25	40.5	60.5

Table 2
Characteristics of carbon nanotubes used.

A type of carbon nanotube	Purity	Outer diameter (nm)	Inner diameter (nm)	length (micrometer)	specific surface $(\frac{m^2}{gr})$	True density $(\frac{gr}{cm^3})$
mutiwalled	>95	10-20	5-10	10-30	>200	~2.1

3. Functionalization of carbon nanotubes

To create carbon nanotubes hydrophilic, they are surface-modified using nitric acid (HNO3) and sulfuric acid (H2SO4) [32]. In order to alter and oxidize the exterior of multi-layered carbon nanotubes, the carbon exterior must initially be coated with nitric acid (HNO3, which causes oxidation of the exterior) and sulfuric acid (H2SO4, which creates a jagged exterior) [33]. Surface roughening of nanofibers is a procedure where carbon-carbon connections are fractured and imperfection sites are formed. This permits the nitric acid to generate a functional group on the nanofilaments. Then, according to Figure 1, a MWCNT solution paraffin bath with nitric acid and sulfuric acid was installed under the laboratory hood. Then, a balloon containing 30 ml of nitric acid, 90 ml of sulfuric acid, and 5 g of carbon nanotubes was placed inside the beaker along with a magnetic magnet. In this research, the ratio of sulfuric acid to nitric acid was 3:1 [34]. The ratio of nitric acid and sulfuric acid is crucial as altering the ratio of nitric acid to sulfuric acid either enhances or diminishes the extent of functionalization. Also, increasing the degree of functionalization disrupts the performance of carbon nanotubes and they are cut into smaller lengths. The duration of surface modification was considered as 3 h. Temperature is one of the important factors for oxidizing carbon nanotubes, because if the temperature exceeds a certain limit, the carbon nanotubes will shorten, and if it is lower than a certain limit, the carbon nanotubes will not be oxidized. The solution containing nitric acid, sulfuric acid, and carbon nanotubes was washed three times with Whatman paper with a diameter of 9 cm, which is connected to a vacuum pump. The pH of the solution is between 6.5 and 7, so the oxidized carbons are not acidic and don't cause the excessive arrangement of ettringite due to excess sulfate particles in the cement paste. Then, the carbon nanotubes placed on Whatman paper were placed in an oven set at 48 degrees for a day to dry. Thus, carboxyl functional groups are formed on the surface of carbon nanotubes, which are utilized as MWCNTCOOH. The carboxyl group is represented as COOH. Among the carboxyl, hydroxyl and carbonyl functional groups, the carboxyl functional group, due to its special conditions, causes a proper connection and bonding between the nanotubes and the concrete structure. Cement hydration is a complex process of interactions between water and the chemical phases of cement, tricalcium silicate (3CaO.SiO2 or C3S), dicalcium silicate (CaO.SiO2 or C2S), tricalcium aluminate (CaO.Al2O3) and tetracalcium alumino ferrite (CaO.Al2O3Fe2O3 or C4AF) which are hydraulic and occur as a result of interaction with water. Therefore, a range of hydrated phases are formed as a result of these interactions. Ca (OH) 2 and C-S-H are mainly produced as hydrated cement products. C-S-H gel and Ca(OH)2 are the two main products of the reaction of C3S and C2S with water. Therefore, in the structure of the hydration reaction products, namely calcium silicate hydrate and calcium hydroxide, there is a hydroxyl functional group, so through the carboxyl group, the nanotubes and the hydration reaction products are connected to each other [35].

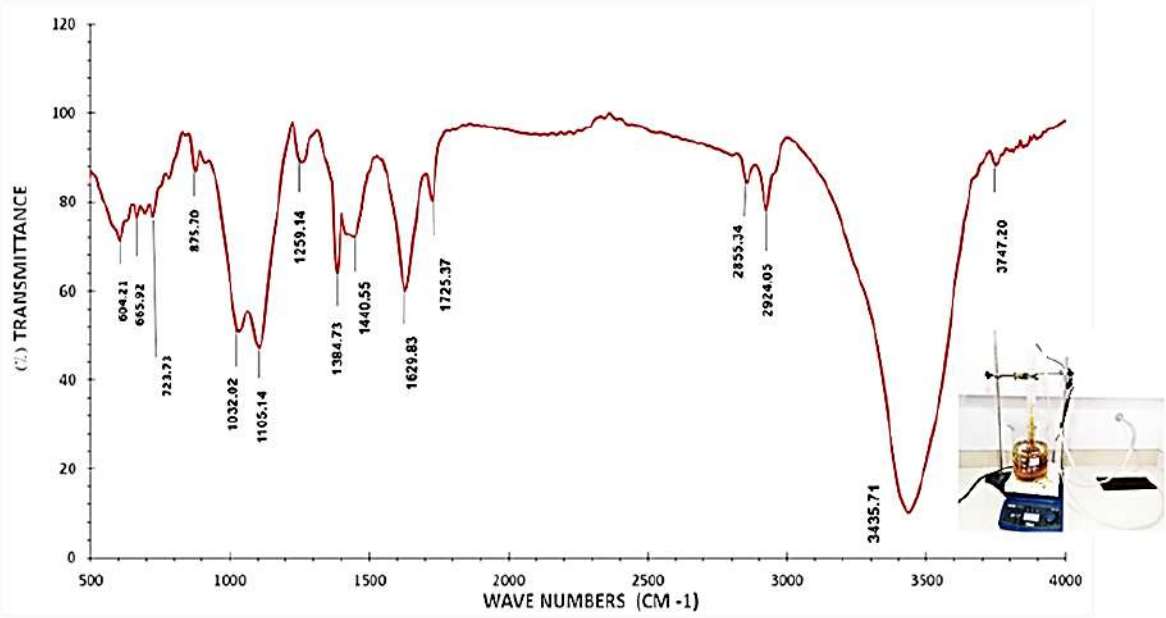

Figure 1: FTIR diagram of oxidized multi-walled carbon nanotubes

FTIR spectroscopy analyses were carried out on oxidized carbon nanotubes to qualitatively determine the hydroxyl and carboxyl groups linked to the surface of the carbon nanotubes and their level of functionalization [36], the findings of which are illustrated in Figure 1. In the mentioned diagram, each peak corresponds to a functional group and the intensity of each peak indicates that functional group in the carbon nanotube. Among the detectable absorption spectra in modified carbon nanotubes, the spectrum centered at wave number 3400 is observed, which indicates oxygen groups [37]. Additionally, the peaks associated with fluctuations in C=O stretching and C-O functional groups can be seen within the range of 1629.83, 1105.14, and 1384.73, respectively. These peaks are indicative of the existence of COOH-carboxyl groups. The results of FTIR spectroscopy clearly show that hydrophilic groups such as hydroxyl and carboxyl are well placed on the surface of functionalized CNTs.

4. Dispersion of carbon nanotubes

The dispersion of carbon nanotubes plays a crucial role in enhancing the mechanical characteristics of concrete. To prepare a homogeneous and uniform solution to have a favorable effect on concrete properties, carbon nanotubes should be well dispersed in water [38]. Modifications using covalent or ionic methods have been reported to disrupt the electronic band structure and intrinsic crystal structure of CNTs. Furthermore, CNT ropes or fragments can be observed in CNT-containing composites. Hence, physical adsorption of surfactants with long chains is commonly used in the dispersion of carbon nanotubes [39]. In this research, after the carbon nanotubes were surface modified using sulfuric acid and nitric acid and became hydrophilic, the modified carbon nanotubes were dispersed in a certain amount of water (30% of the total water required to make the samples) along with various surfactants (CTAB, SDS, polyethylene glycol (PEG) and polycarboxylate (PCE)). In this research, we functionalized carbon nanotubes with hydroxyl functional groups and the carbon nanotubes became hydrophilic, which functional group created in carbon nanotubes was confirmed in the FTIR test. Therefore, carbon nanotubes do not agglomerate and are easily dispersed in water. In this research, the carbon nanotubes hydrophilic were made using a hydroxyl functional group. It is worth mentioning that the carbon nanotubes with the functional group created in them, which was also confirmed in the FTIR test, are easily dispersed in water and do not agglomerate. However, in order for the dispersion of the water solution and carbon nanotubes to be durable and uniform, various surfactants have been used. It is important to note that the remaining blending water (70%) was utilized to saturate the aggregates and create concrete. In the first step, SDS was used as a surfactant, so that the ratio of SDS to carbon nanotubes was considered equal to 4:1, but no proper distribution and dispersion were observed. In the second step, CTAB (with a ratio of 1:1 compared to carbon nanotubes) was used as a surfactant. After 0.01g of carbon nanotubes and 0.01g of CTAB were poured into a certain amount of water and after 15 minutes of ultrasonic time, it was observed (immediately after ultrasonication) that the carbon nanotubes easily settled and separated from the solution. As can be seen in Figure 2, no sedimentation was observed until 90 minutes, indicating that the dispersion was improved; But as seen in Figure 2b, after one month, the solution containing CTAB settled, which shows that the dispersion of the solution containing CTAB surfactant was unstable. In the third step, polyethylene glycol (PEG), which is a hydrophilic polymer, increases the hydrophilicity of oxidized carbon nanotubes (the ratio of oxidized carbon nanotubes to PEG is 1:1, 1:3, and 1:5). be) was used. Ultrasonic was considered equal to 15 minutes. Observations indicate that by increasing the ratio of carbon nanotubes to PEG, the dispersity improves., but after 20 minutes, as seen in Figure 3, carbon nanotubes settled and agglomerated. In the fourth step, a solution containing oxidized carbon nanotubes, PEG, and polycarboxylate was prepared with a ratio of 1:5:5. The duration of ultrasonication was considered equal to 15 minutes and it was observed that a completely uniform solution was obtained. To observe the consistency of the solution, the solution was diluted at a 1:100 ratio, and no settling was observed again, indicating that the solution is very stable. As depicted in Figure 4, the solution remains consistent even after two months with no settling. Thus, the combination of polyethylene glycol and polycarboxylate is introduced as a novel surfactant. Generally, CNTs are dispersed using different surfactants, such as polycarboxylate-based superplasticizers, polyacrylic acid polymer, SDS, sodium dodecylbenzene sulfonate (SDBS or SDDBS), polyvinyl pyrrolidone (PVP), gum arabic (AG or GA), Pluronic F-127 and sodium deoxycholate (NaDC)[40]. CNTs adsorb the hydrophobic part of the surfactant on the side walls or ends of the tubes through van der Waals forces, π-π bonding or CH-π bonding, while the aqueous solubility and electrostatic repulsion are provided by the hydrophilic part of the surfactant [26]. The extent and strength of the electrostatic repulsion are determined by the density of polymers on the CNT surface and the length of the polymer chains. In the construction industry, polycarboxylate (PC)-based superplasticizers (SP) have been widely used to improve the workability and rheological properties of cement mixtures and reduce the amount of mixing water for cement. Polycarboxylate ester (PCE) is an example that has been successfully used for cement-based materials, and

can also be used as a surfactant for CNT dispersion due to its better adsorption ability to CNT compared to polycarboxylate (PC) superplasticizers. However, although PCE is commercially available and is highly compatible with cementitious materials, a well-dispersed CNT solution can be obtained with relatively higher PCE values. Polyethylene glycol (PEG) is a non-ionic hydrophilic polyether that is widely used to modify polymer membranes due to its hydrophilicity. Studies show that PEG-modified polymer membranes can effectively reduce membrane fouling. Compatibility between surfactants and the cement matrix is an important issue. Parvin et al. reported that Pluronic F-127 surfactants can reduce porosity and improve microstructure density [40]. These surfactants, containing polyethylene oxide side chains, act similarly to polycarboxylate-based superplasticizers, which can disperse cement particles and improve mortar fluidity [41].

The dispersion of carbon nanotubes was also examined using UV-VIS spectrophotometry. UV-VIS spectroscopy was employed to establish the correlation between the quality of CNT dispersion, the duration of sonication, and the concentration of surfactant. This method is based on the Beer-Lambert law. The UV-Vis range is used to allow comparison of dispersion methods using absorbance values recorded for different suspensions. .

(a) (b)

Figure 2. Dispersion of carbon nanotube oxidized with CTAB: (a) solution containing MWCNTCOOH and CTAB 90 minutes after ultrasonication (b) solution containing MWCNTCOOH and CTAB one month after ultrasonication

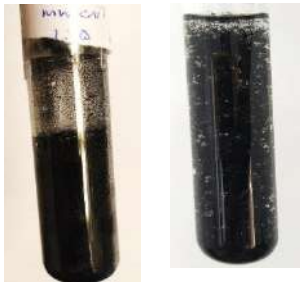

(a) (b)

Figure 3. Dispersion of carbon nanotubes oxidized with PEG with a ratio of 1:5 (a) solution containing MWCNTCOOH and PEG immediately after ultrasonication (b) solution containing MWCNTCOOH and PEG 20 minutes after ultrasonication

(a) (b)

Figure 4. Dispersion of oxidized carbon nanotubes with PEG/PCE (a) solution containing MWCNTCOOH and PEG/PCE two months after ultrasonication (b) solution containing MWCNTCOOH and PEG/PCE two months after ultrasonication in a diluted form to better observe the dispersion.

The greater the level of scattering of MWCNTs in water, the greater the absorbance value measured. The maximum absorption intensity of individual her MWCNTs was reported by previous researchers to be 200–300 nm [42]. Because the amount of light absorbed is directly proportional to the concentration of carbon nanotubes, the level of dispersion is quantified using the Beer-Lambert law [43]. The gathering of MWCNTs diminishes the strength of the absorption band. This conduct may subsequently be connected to the level of scattering and presents the potential for ascertaining the ideal scattering circumstances. The solutions were ultrasonicated for 10 minutes before scanning with a UV-Vis spectrophotometer. Considering that Lambert Beer's law is established with good accuracy only at lower concentrations, the solution was mixed with purified water at a ratio of 1:100 [43]. Absorption spectra for all three solutions are shown in Figures 5. The absorption peak intensity is different in different surfactants, so the highest absorption was observed in the solution containing polycarboxylate surfactant and polyethylene glycol, which indicates the best dispersion. It is evident that the highest point of absorption at a range of 200-300 nm can be observed in the solution containing multi-walled carbon nanotubes, polyethylene glycol, and polycarboxylate.

5. Preparation and mixing of concrete samples:

Before making concrete samples, a carbon nanotube dispersed solution must be prepared firstly. In this research, two surfactants CTAB and PEG/PCE were used to make concrete samples with carbon nanotubes because these two surfactants had the best dispersion and the most stability among the surfactants used. The procedure of blending substances to create all the examinations is as follows: Initially, a specific quantity of components is blended with

60% of the total blending liquid for three minutes, then cement is introduced and subsequently, the mixture prepared in the prior step (comprising 30% of total water with carbon nanotubes or lacking carbon nanotubes) is incorporated. After 8 min, the specified amount of polycarboxylate-based superplasticizer was mixed in 10% total water and added to the mortar. It is important to note that carbon nanotubes soak up a significant quantity of water because of their immense specific surface area (which is responsible for many of their notable characteristics). This can cause the concrete mix to dry out, and therefore the use of superplasticizers is essential. Consequently, the utilization of superplasticizers leads to a more consistent and simpler dispersion of the solution of carbon nanotubes in cement mortar. A total mixing time of 10 minutes was assumed to produce the concrete. The concrete was subsequently poured into metal molds in three phases and compressed with 25 strokes of a unique rod (16 mm in diameter, 60 cm in length). The occupied molds were shaken for 1 min and then their exterior was made even. Specimens were removed from the molds after 24 hours and treated in water for 7, 14, and 28 hours.

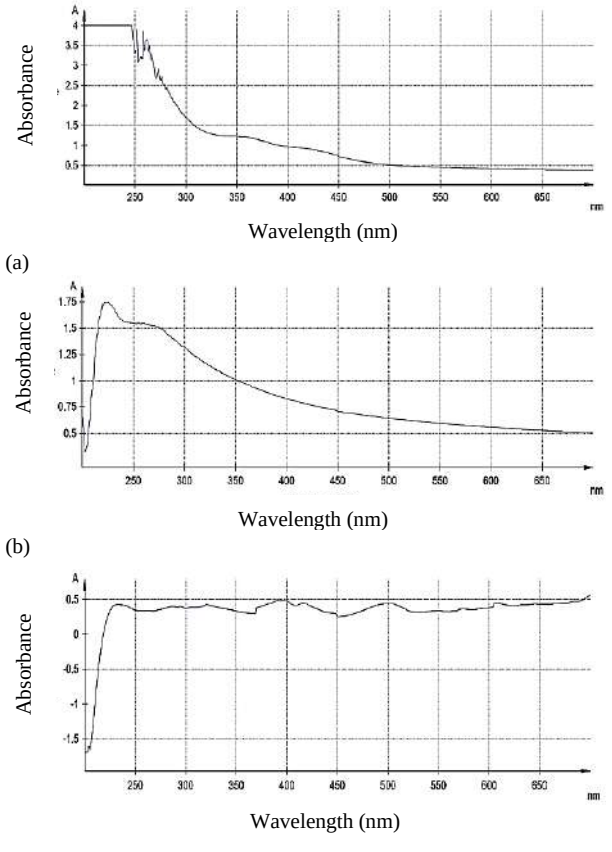

Figure 5: UV-vis test results:(a) for PEG/PCE (b) for CTAB (c) for PEG

6. Results and Discussion

6.1. Effect of carbon nanotube on compressive strength of concrete

This examination is the most prevalent examination that is conducted on the strength of concrete. The examination was conducted in accordance with the guidelines of ASTM C39 at the durations of 7, 14, and 28 days using a hydraulic jack and with a rate of loading of 1 mm/min. As seen in Figure 6, the load is uniformly applied to the sample by two heavy hydraulic jaws. To conduct the experiment, standard cubic samples (15x15x15 cm) were used and the effect of adding multi-walled carbon nanotubes with different proportions of 0.015%, 0.030%, and 0.045% to the weight of cement was investigated.

Figure 7(a) displays the outcomes of compressive strength examination of concrete specimens incorporating carbon nanotubes and CTAB surfactant. The results indicate that the addition of 0.015% carbon nanotube with CTAB surfactant reduces the compressive strength by -5%, -17%, and -9% for 7, 14, and 28-day samples, respectively. This reduction can be attributed to the irregular effect of the CTAB agent on cement hydration. This surface-active agent can increase the quantity of air trapped in the cement mixture, thereby reducing the strength. Additionally, these varieties of surface-active agents experience reactions with water-reducing additives that could impede the process of hydration and lead to reformation, further reducing the strength. This surface-active agent can increase the quantity of air trapped in the cement mixture. Additionally, these varieties of surface-active agents experience reactions with water-reducing additives that could impede the process of hydration and lead to reformation. Figure 7(b) shows the compressive strength of concrete samples containing varying proportions of carbon nanotubes, polyethylene glycol, and polycarboxylate surfactants. Regarding the 7-day concrete samples, a rise in compressive strength was solely noticed in samples encompassing 0.030% of carbon nanotubes. This increase is marginal and seems to be due to insufficient distribution of the carbon nanotubes. The escalation in the compressive strength of 14-day concrete samples encompassing carbon nanotubes with proportions of 0.015%, 0.030%, and 0.045% is 7.14%, 24.3%, and 26.19%, correspondingly. This increase is thought to be due to the effective dispersion of carbon nanotubes. It is thought that this rise in power is attributed to the effective distribution of carbon nanotubes, which, alongside occupying the pores, reduce the porosity of the framework and assist in creating more compact cement-based composites. The findings of Hawreen and Bogas demonstrate that the surge in compressive strength in concrete specimens containing CNT in comparison to standard concrete is linked to the

filling characteristics of CNT and their interconnection and bridging [44].

Figure 6. Compressive strength test on cubic sample

The findings also indicate that the highest rise in compressive strength in 28-day concrete samples is linked to samples containing 0.030% carbon nanotubes, thus resulting in a surge of approximately 27.4%. Importantly, concrete samples containing 0.015% and 0.045% carbon nanotubes exhibited a 14.14% and 23.4% boost in compressive strength at the 28-day mark, respectively. In simpler terms, as the quantity of carbon nanotubes increased, the upward trend in strength improvement ceased, and the optimal value of the 28-day compressive strength was observed in the samples containing 0.030 carbon nanotubes. It is important to note that excessively increasing the amount of carbon nanotubes may halt the process of increasing compressive strength, as high CNT concentrations may lead to the re-accumulation of carbon nanotubes. In other words, it can be said that smaller amounts of carbon nanotubes may disperse better and thus stop the propagation of microcracks and reduce nano-sized holes [45]. The decrease in strength of CTAB-containing concrete can be attributed to the incompatible effect of CTAB on cement hydration, which leads to a delay in the cement hydration process. This surfactant can increase the amount of air entrapped in the cement paste to the extent seen in the fresh mix. In addition, these types of surfactants undergo reactions with water-reducing admixtures that may delay hydration and cause re-agglomeration. As previously mentioned, the instability of the CTAB-containing solution resulted in the lack of proper dispersion of carbon nanotubes in water and cement mortar, resulting in a lack of improvement in the mechanical properties of concrete.

The higher strength achieved is believed to be due to the physical contribution of well-dispersed carbon nanotubes, which act as pore fillers and reduce matrix porosity, contributing to denser cementitious composites. The bridging effects of nanotubes can also enhance the ability of the materials to delay microcrack formation and increase the load-bearing capacity of the cement matrix by bridging adjacent hydration products. There are four main mechanisms by which carbon nanotubes strengthen cementitious matrices, the first of which is the crack-bridging mechanism mediated by carbon nanotubes. Carbon nanotubes can bridge nano- and micro-sized pores or gaps in the range of 10–103 nm in hydration products. This bridging effect of carbon nanotubes provides efficient charge transfer from the matrix to the carbon nanotubes within the composites, thereby delaying the growth of nano-sized pores or cracks and preventing the formation of micro-sized pores or cracks. Carbon nanotubes reduce the nano-porosity of the cement paste by filling the pores and cracks between the hydrate gel, thus CNTs enhance the mechanical properties [40]. In addition, carbon nanotubes can act as nucleating agents for C-S-H gels. The hydrophilic nature of the CNT structure due to the functional groups (or surfactants) allows water to be more effectively adsorbed onto it, thereby producing hydration products. There are two mechanisms of nucleating agents for enhancing mechanical properties. One is that such nucleating agents can improve the hydration process, leading to a denser and stronger microstructure. Furthermore, the C-S-H gel coated with CNT bundles leads to a much larger effective contact area between the CNT and the matrix, resulting in an extremely strong bond between them [46].

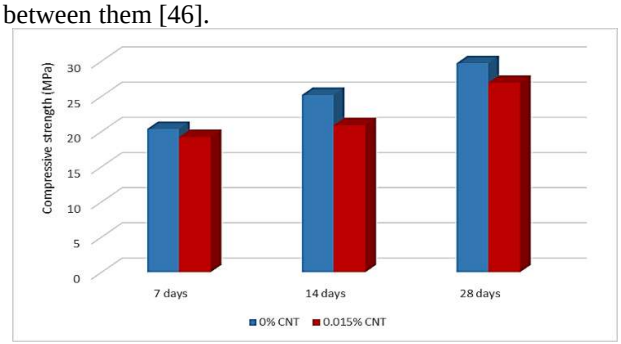

(a)

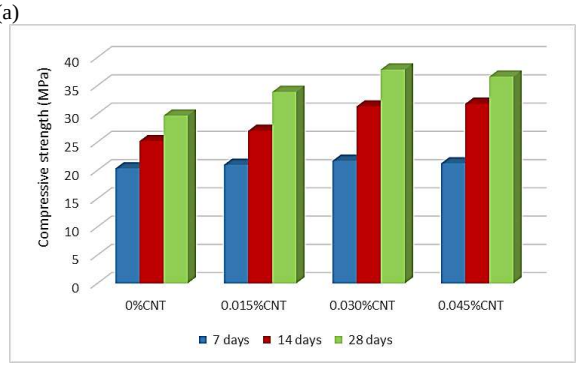

(b)

Figure 7. Compressive strength of concrete containing (a)carbon nanotubes and CTAB surfactant at different ages (b) Carbon Nanotubes, Polyethylene Glycol, and Carboxylic Acid Poly surfactant at different ages

6.2. The effect of carbon nanotube on the tensile strength of concrete

In this investigation, a technique of dividing shaped or cored cylindrical samples was employed to assess the pulling power of concrete. As depicted in Figure 8, applying a diagonal compressive force on 28-day cylindrical concrete samples (diameter 15 cm and height 30 cm) containing different amounts of carbon nanotubes, which are placed horizontally between two plates of the test device and the tensile strength is determined and compared.

Figure 9(a) shows the tensile strength of concrete samples containing varying amounts of carbon nanotubes with PEG and polycarboxylate surfactants at 28 days. It is evident that the tensile strength rises of the specimens with carbon nanotube concentrations of 0.015%, 0.030%, and 0.045% are 16.7%, 28.5%, and 19.7% correspondingly. As can be seen, the increasing trend in tensile strength stops for the samples containing carbon nanotubes as high as 0.045%. This is due to the redistribution of carbon nanotubes in the cement matrix. Table 3 presents a comparison between the ideal quantity of carbon nanotubes in this research and the ideal quantity of carbon nanotubes in earlier studies. It is evident that the optimal amount of carbon nanotubes in the current investigation is lower than the figure in the prior study., the reason can be the proper performance of the new combined surfactant in this research, which has led to a more favorable dispersion of carbon nanotubes. Figure 9(b) compares the tensile strength of concrete samples containing carbon nanotubes with CTAB surfactant, polyethylene glycol, and polycarboxylate surfactants. It is apparent that the pulling power of concrete with CTAB surfactant diminished by -4.17% in comparison to the standard sample.

Figure 8. Testing the tensile strength of the cylindrical sample

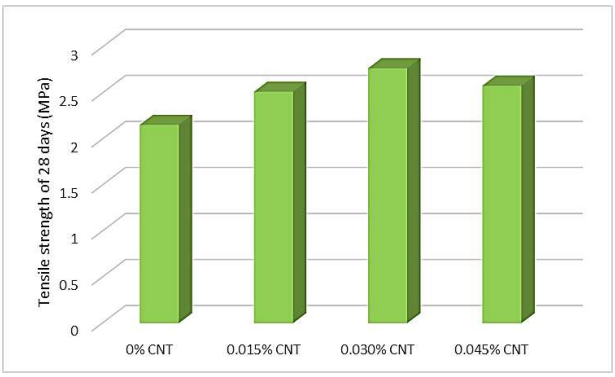

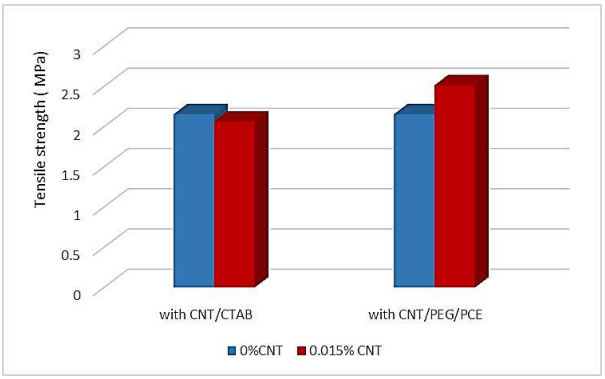

Figure 9. Tensile strength of concrete containing (a) different amounts of carbon nanotubes and polyethylene glycol and polycarboxylate surfactants (b) carbon nanotubes and CTAB surfactant with concrete containing carbon nanotubes and polyethylene glycol and polycarboxylate surfactants

Figure 10. Flexural strength test of prismatic beam

6.3. Effect of carbon nanotube on flexural strength of concrete

As depicted in Figure 10, the bending strength test is performed on a rectangular concrete cube of 100 x 100 x 500 mm for 28 days. This research test was performed based on the ASTM C293 standard using the three-point method.

Table 3
Comparison of optimal values of carbon nanotubes in different studies

The type of surfactant	Measured mechanical properties	Percentages of CNTs used (%)	Measured strength values (MPa)			Optimum percentage of CNT (%)	Reference
super lubricant	flexural strength	0.030% 0.08% 0.15% 0.25%	2.9 2.6 4 4.25			0.25%	[47]
super lubricant	compressive strength	0.06% 0.12%	31 25			0.06%	[21]
-	compressive strength Tensile strength	0.01% 0.02% 0.03%	compressive strength 31.2 33 35		Tensile strength 3.3 3.5 3.6	0.03%	[48]
Polyethylene glycol and polycarboxylate surfactant	compressive strength flexural strength Tensile strength	0.015% 0.030% 0.045%	compressive strength 33.6 37.86 36.6	flexural strength 7.2 8.1 7.42	Tensile strength 2.51 2.77 2.58	0.03%	current article

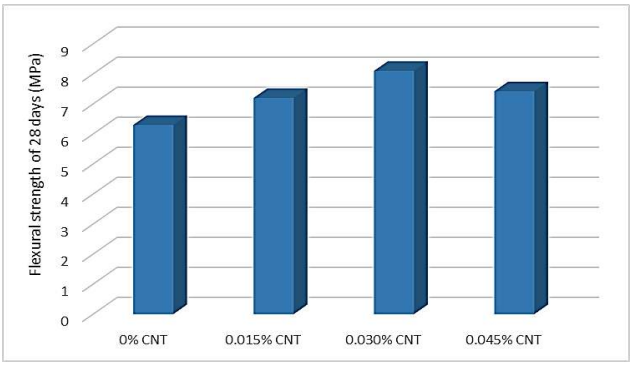

(a)

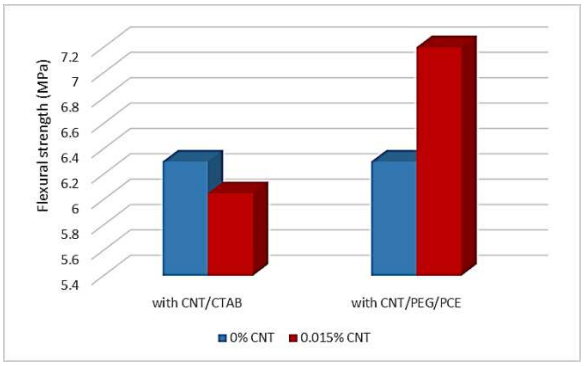

(b)

Figure 11. Flexural strength of concrete (a) containing different amounts of carbon nanotubes and polyethylene glycol and polycarboxylate surfactants (b) carbon nanotubes and CTAB surfactant with concrete containing carbon nanotubes and polyethylene glycol and polycarboxylate surfactants.

Figure 11(a) shows the flexural strength of concrete samples containing varying amounts of carbon nanotubes, polyethylene glycol, and polycarboxylate surfactants for 28 days. It has been noticed that augmenting the quantity of carbon nanotubes in concrete enhances the bending strength of the concrete. This increase in bending strength for samples containing 0.015%, 0.030%, and 0.045% of carbon nanotubes is equal to 14%, 28.5%, and 17.7%, respectively. These results confirm the findings of previous researchers. Put differently, approximately 70% or higher of prior research has indicated that the incorporation of carbon nanotubes enhances flexural strength by 50% or greater [49]. Current findings suggest that the impact of carbon nanotubes on enhancing the bending resistance of the cement structure is more significant compared to its influence on compressive strength. Sedagatdoost and Behfarnia have linked the improved bending resistance of the carbon nanotube mixture to its spatial arrangement,

which involves filling the gaps between C-S-H and decreasing the porosity of the cement structure [50]. The rise in flexural potency is thought to be caused not just by the filling of moistened pores but also by the linking impact of carbon nanotubes and the sealing of tiny fractures. This fortifies the framework and adds to the enhancement of bending strength [51]. The optimal amount of carbon nanotubes to produce maximum bending strength is 0.030% relative to the weight of the cement, and increasing amounts of carbon nanotubes stop the trend of increasing bending strength. Figure 11(b) displays the flexural strength of concrete samples incorporating carbon nanotubes and CTAB surfactant over a period of 28 days. It is observed that the inclusion of carbon nanotubes in conjunction with the CTAB surfactant resulted in a decrease of 3.9% in the flexural strength at the end of the 28-day period. Conversely, the utilization of polyethylene glycol and polycarboxylate surfactants led to an increase of approximately 16% in the 28-day flexural strength of concrete samples containing carbon nanotubes.

6.4. Effect of nanotube carbon on specific weight of concrete

Figure 12 shows the specific weight of concrete samples containing different amounts of carbon nanotubes and polyethylene glycol and polycarboxylate surfactants in two states of hardened concrete and fresh concrete. It is evident that the incorporation of carbon nanotubes decreases the specific density of concrete in comparison to the control concrete sample. These results support the findings of other researchers. These results confirm the findings of other researchers. The findings of a study conducted by Hawreen and Bogas similarly demonstrated that incorporating carbon nanotubes at a concentration of 0.1% of the cement mass had a minimal impact on the performance and density of the concrete, suggesting that the dispersion of carbon nanotubes was unaffected [44]. This figure shows that carbon nanotubes' specific gravity reduction effect is more significant in hardened concrete than in fresh concrete. The largest reduction in specific weight is observed for hardened concrete containing 0.030% carbon nanotubes, which is about 10%, while fresh concrete containing the same amount of carbon nanotubes has a specific gravity reduction of about 3%. Note that increasing concrete strength is usually accompanied by increasing specific gravity; However, the unique properties of carbon nanotubes also positively affect the compressive strength and specific weight of concrete. As one of the critical problems in building design and implementation is the dead weight of the building, reducing the dead weight of the building and using concrete with lower the specific weight and higher compressive strength in concrete structures has been the focus of many design engineers. This fact is important because the seismic force acting on a structure is proportional to the mass of the system, and reducing the group of the design is the most critical factor in mitigating the impact of earthquakes on the form [52]. Therefore, carbon nanotubes solve this need and produce concrete with high compressive strength and low specific weight.

7. Conclusion

Laboratory experiments demonstrate that adequate scattering of carbon nanotubes enhances the structural characteristics of concrete. In this study, by means of the surface alteration technique, carbon nanotubes were oxidized and discovered to possess hydrophilic characteristics; Nevertheless, the ideal scattering and steadiness of carbon nanotube dispersion in water were insufficient. Therefore, different surfactants (such as CTAB, SDS, PEG, and PCE) were used. Finally, the

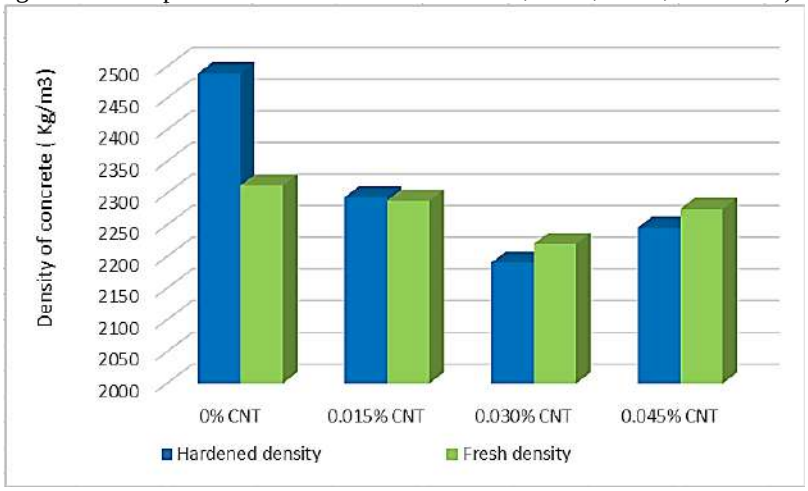

Figure 12. Specific weight of 28-day concrete samples containing different percentages of carbon nanotubes and polyethylene glycol and polycarboxylate surfactants

CTAB surfactants and PEG/PCE combination caused better dispersion and homogeneous distribution of carbon nanotubes. Observations showed that the solution containing PEG/PCE surfactant is more stable than the solution containing CTAB surfactant. In other words, the solution containing CTAB surfactant settled after one month, while the solution containing PEG/PCE surfactant did not settle after two months. Therefore, two surfactants, CTAB and PEG/PCE were used to make concrete samples due to their uniform distribution and optimal dispersion. The findings indicated that the compressive strength of concrete samples incorporating CTAB surfactant did not experience significant enhancement; the reason for this can be the incompatibility of the CTAB surfactant with the cement matrix, this slows down the hydration process and destabilizes the dispersion of solutions containing carbon nanotubes with CTAB surfactant, which results from the uneven dispersion of carbon nanotubes in cement mortar. Finally, a PEG/PCE surfactant combination was selected as a suitable surfactant for carbon nanotube dispersion to improve concrete's mechanical and physical properties. So, in summary, we can say that using different surfactants gives different results. The remedy with the ideal quantity of 0.030% of carbon nanotube and PCE/PEG surfactant enhanced the compressive, bending, and tensile resistance of concrete by 27.49%, 28.57%, and 28.53%, and the higher the amount of carbon nanotube, the increasing trend of compressive strength decreased. The carbon nanotubes also had a favorable effect on the specific gravity of concrete, decreasing the specific gravity of hardened concrete by about 10% and that of fresh concrete by about 3%. The suggestions for future research could include as: investigating the mechanism of chemical adsorption and the effect of different molecular weights of polycarboxylate and polyethylene glycol, adsorption on the outer walls of nanotubes and surfactant agents on nanotubes following high ultrasonic intensity on dispersion, investigating methods for improving the dispersion of nanotubes for large-scale cement applications (because the use of nanocomposites for large-scale structural applications is encouraging), and investigating the effect of carbon nanotubes on thawing and freezing, shrinkage, creep, corrosion, and chloride infiltration of concrete.

Acknowledgements

Hakim Sabzevari University concrete research center laboratory and respected officials of this university are grateful for providing the equipment and the possibility of using it.

References

[1] Adhikary, Suman Kumar, Žymantas Rudžionis, and R. Rajapriya. "The effect of carbon nanotubes on the flowability, mechanical, microstructural and durability properties of cementitious composite: An overview." Sustainability 12.20 (2020): 8362. https://doi.org/10.3390/su12208362

[2] Alrekabi, S., et al. "Experimental investigation on the effect of ultrasonication on dispersion and mechanical performance of multi-wall carbon nanotube-cement mortar composites." International Journal of Civil, Environmental, Structural, Construction and Architectural Engineering 111.3 (2016): 268-274. http://waset.org/publications/10003884

[3] Vidivelli, B., and B. Ashwini. "A study on carbon nanotube (cnt) in concrete." Int Res J Eng Technol 5.7 (2018): 481-489.

[4] Song, Xiaobin, Yeqi Li, and Chenzhi Li. "Bond behavior between steel bars and carbon nanotube modified concrete." Construction and Building Materials 255 (2020): 119339. https://doi.org/10.1016/j.conbuildmat.2020.119339

[5] Reales, Oscar Aurelio Mendoza, and Romildo Dias Toledo Filho. "A review on the chemical, mechanical and microstructural characterization of carbon nanotubes-cement based composites." Construction and Building Materials 154 (2017): 697-710. https://doi.org/10.1016/j.conbuildmat.2017.07.232

[6] Zhang, Shukun, et al. "Preparation and load-deformation characterization of carbon nanotube-reinforced foam concrete." Construction and Building Materials 254 (2020): 119294. https://doi.org/10.1016/j.conbuildmat.2020.119294

[7] Foldyna, Josef, Vladimír Foldyna, and Michal Zeleňák. "Dispersion of carbon nanotubes for application in cement composites." Procedia engineering 149 (2016): 94-99. https://doi.org/10.1016/j.proeng.2016.06.643

[8] Jayakumari, Breetha Yesudhas, Elangovan Nattanmai Swaminathan, and Pachaivannan Partheeban. "A review on characteristics studies on carbon nanotubes-based cement concrete." Construction and Building Materials 367 (2023): 130344. https://doi.org/10.1016/j.conbuildmat.2023.130344

[9] Dinesh, A., et al. "Influence of carbon nanotube on the mechanical and electrical characteristics of concrete–A review." Materials Today: Proceedings (2023). Dinesh, A., et al. "Influence of carbon nanotube on the mechanical and electrical characteristics of concrete–A review." Materials Today: Proceedings (2023). https://doi.org/10.1016/j.matpr.2023.03.549

[10] Ahmed, Hawreen, et al. "Dispersion and reinforcement efficiency of carbon nanotubes in cementitious composites." Magazine of Concrete Research 71.8 (2019): 408-423. https://doi.org/10.1680/jmacr.17.00562

[11] Shang, Su Su, and Xiao Bin Song. "Experimental research on mechanicals performance of carbon nanotubes reinforced concrete." Applied Mechanics and Materials 858 (2017): 173-178. https://doi.org/10.4028/www.scientific.net/AMM.858.173

[12] Krämer, Christina, et al. "CNT-stabilized foam concrete on the basis of ultra highperformance concrete (UHPC)." 14th International Congress on the Chemistry of Cement. 2015.

[13] Xu, Shilang, Jintao Liu, and Qinghua Li. "Mechanical properties and microstructure of multi-walled carbon nanotube-reinforced cement paste." Construction and Building Materials 76 (2015): 16-23. https://doi.org/10.1016/j.conbuildmat.2014.11.049

[14] Yazdani, Nur, and Vinoth Mohanam. "Carbon nano-tube and nano-fiber in cement mortar: effect of dosage rate and water-cement ratio." International Journal of Material Science 4.2 (2014): 45.

[15] Hu, Yu, et al. "Fracture toughness enhancement of cement paste with multi-walled carbon nanotubes." Construction and Building

Materials 70 (2014): 332-338. https://doi.org/10.1016/j.conbuildmat.2014.07.077
[16] Kim, H. K., Il Woo Nam, and H-KJCS Lee. "Enhanced effect of carbon nanotube on mechanical and electrical properties of cement composites by incorporation of silica fume." Composite Structures 107 (2014): 60-69. https://doi.org/10.1016/j.compstruct.2013.07.042
[17] Teymouri, Ali, et al. "A review on carbon nanofiber production and application in cementitious mixtures." Journal of Building Engineering 84 (2024): 108519. https://doi.org/10.1016/j.jobe.2024.108519
[18] Hawreen, A., J. A. Bogas, and A. P. S. Dias. "On the mechanical and shrinkage behavior of cement mortars reinforced with carbon nanotubes." Construction and Building Materials 168 (2018): 459-470. https://doi.org/10.1016/j.conbuildmat.2018.02.146
[19] Bajad, Mohankumar N. "Cement-based composites containing carbon nanofibers and carbon nanotubes." Current Materials Science: Formerly: Recent Patents on Materials Science 17.3 (2024): 240-250. https://doi.org/10.2174/2666145416666230517164939
[20] Su, Zijian, Wei Hou, and Zengqing Sun. "Recent advances in carbon nanotube-geopolymer composite." Construction and building materials 252 (2020): 118940. https://doi.org/10.1016/j.conbuildmat.2020.118940
[21] Lelusz, Małgorzata. "Carbon nanotubes influence on the compressive strength of cement composites." Technical Transactions 2014.Civil Engeneering Issuet 1-B (5) 2014 (2015): 5-11.
[22] Carriço, A., et al. "Durability of multi-walled carbon nanotube reinforced concrete." Construction and Building Materials 164 (2018): 121-133. https://doi.org/10.1016/j.conbuildmat.2017.12.221
[23] Sobolkina, Anastasia, et al. "Dispersion of carbon nanotubes and its influence on the mechanical properties of the cement matrix." Cement and Concrete Composites 34.10 (2012): 1104-1113. https://doi.org/10.1016/j.cemconcomp.2012.07.008
[24] Zhang, Peng, et al. "Influence of carbon nanotube on properties of concrete: A review." Construction and Building Materials 369 (2023): 130388. https://doi.org/10.1016/j.conbuildmat.2023.130388
[25] Dinesh, A., et al. "Development of Self-Sensing Cement Composite using Nanomaterials for Structural Health Monitoring of Concrete Columns–A Comprehensive Review." Sustainable Materials and Smart Practices: NCSMSP-2021 23 (2022): 191. https://doi.org/10.21741/9781644901953-23
[26] Collins, Frank, John Lambert, and Wen Hui Duan. "The influences of admixtures on the dispersion, workability, and strength of carbon nanotube–OPC paste mixtures." Cement and concrete composites 34.2 (2012): 201-207. https://doi.org/10.1016/j.cemconcomp.2011.09.013
[27] Lin, Daohui, and Baoshan Xing. "Adsorption of phenolic compounds by carbon nanotubes: role of aromaticity and substitution of hydroxyl groups." Environmental science & technology 42.19 (2008): 7254-7259. https://doi.org/10.1021/es801297u
[28] Konsta-Gdoutos, Maria S., Zoi S. Metaxa, and Surendra P. Shah. "Highly dispersed carbon nanotube reinforced cement based materials." Cement and concrete research 40.7 (2010): 1052-1059. https://doi.org/10.1016/j.cemconres.2010.02.015
[29] Jang, J. G., et al. "Resistance of coal bottom ash mortar against the coupled deterioration of carbonation and chloride penetration." Materials & Design 93 (2016): 160-167. https://doi.org/10.1016/j.matdes.2015.12.074
[30] Wang, Baomin, et al. "Mechanical and morphological properties of highly dispersed carbon nanotubes reinforced cement based materials." Journal of Wuhan University of Technology-Mater. Sci. Ed. 28.1 (2013): 82-87. https://doi.org/10.1007/s11595-013-0645-1
[31] Gao, Yibo, et al. "Dispersion of carbon nanotubes in aqueous cementitious materials: A review." Nanotechnology Reviews 12.1 (2023): 20220560. https://doi.org/10.1515/ntrev-2022-0560
[32] Shadnia, Rasoul, Mahsa Zarehparvar Shoja, and Amin Kazemi Beydokhti. "The Effect of Dispersion Method of Nanotube Carbon on the Compressive Strength of Concrete." Journal of Concrete Structures and Materials 7.1 (2022): 60-75. https://doi.org/10.30478/JCSM.2022.346473.1272
[33] Kim, Taehoon, et al. "A universal surface modification method of carbon nanotube fibers with enhanced tensile strength." Composites Part A: Applied Science and Manufacturing 140 (2021): 106182. https://doi.org/10.1016/j.compositesa.2020.106182
[34] Kazemi-Beydokhti, Amin, et al. "Surface modification of carbon nanotube: Effects on pulsating heat pipe heat transfer." Chemical Engineering Research and Design 152 (2019): 30-37. https://doi.org/10.1016/j.cherd.2019.09.023
[35] Chen, S. J., et al. "Carbon nanotube–cement composites: A retrospect." The IES journal part a: Civil & structural engineering 4.4 (2011): 254-265. https://doi.org/10.1080/19373260.2011.615474
[36] Kazemi-Beydokhti, Amin, Saeed Zeinali Heris, and M. R. Jaafari. "Experimental investigation of thermal conductivity of medical nanofluids based on functionalised single-wall carbon nanotube and conjugated cisplatin." Micro & Nano Letters 10.5 (2015): 241-247. https://doi.org/10.1049/mnl.2014.0593
[37] Yudianti, Rike, et al. "Analysis of functional group sited on multi-wall carbon nanotube surface." The Open Materials Science Journal 5.1 (2011): 242-247. http://dx.doi.org/10.2174/1874088X01105010242
[38] Batiston, Eduardo, et al. "Effect of Carbon Nanotubes (CNTs) aspect ratio on the rheology, thermal conductivity and mechanical performance of Portland cement paste." Revista IBRACON de Estruturas e Materiais 14.5 (2021): e14510. https://doi.org/10.1590/s1983-41952021000500010
[39] Mc Carthy, B., et al. "Microscopy studies of nanotube-conjugated polymer interactions." Synthetic Metals 121.1-3 (2001): 1225-1226. https://doi.org/10.1016/S0379-6779(00)00906-1
[40] Parveen, Shama, et al. "Microstructure and mechanical properties of carbon nanotube reinforced cementitious composites developed using a novel dispersion technique." Cement and Concrete Research 73 (2015): 215-227. https://doi.org/10.1016/j.cemconres.2015.03.006
[41] Yamada, Kazuo, et al. "Effects of the chemical structure on the properties of polycarboxylate-type superplasticizer." Cement and concrete research 30.2 (2000): 197-207. https://doi.org/10.1016/S0008-8846(99)00230-6
[42] Safdari, Masoud, and Marwan S. Al-Haik. "Synergistic electrical and thermal transport properties of hybrid polymeric nanocomposites based on carbon nanotubes and graphite nanoplatelets." Carbon 64 (2013): 111-121. https://doi.org/10.1016/j.carbon.2013.07.042
[43] Ikeda, Atsushi, et al. "Water-solubilization of nucleotides-coated single-walled carbon nanotubes using a high-speed vibration milling technique." Organic letters 8.6 (2006): 1153-1156. https://doi.org/10.1021/ol053089s
[44] Hawreen, A., and J. A. Bogas. "Influence of carbon nanotubes on steel–concrete bond strength." Materials and Structures 51 (2018): 1-16. https://doi.org/10.1617/s11527-018-1279-8
[45] Hawreen, A., and J. A. Bogas. "Creep, shrinkage and mechanical properties of concrete reinforced with different types of carbon nanotubes." Construction and Building Materials 198 (2019): 70-81. https://doi.org/10.1016/j.conbuildmat.2018.11.253
[46] Singh, Avanish Pratap, et al. "Multiwalled carbon nanotube/cement composites with exceptional electromagnetic interference shielding properties." Carbon 56 (2013): 86-96. https://doi.org/10.1016/j.carbon.2012.12.081
[47] Mohsen, Mohamed O., et al. "Carbon nanotube effect on the ductility, flexural strength, and permeability of concrete." Journal of

Nanomaterials 2019.1 (2019): 6490984. https://doi.org/10.1155/2019/6490984

[48] Ruan, Yanfeng, et al. "Carbon nanotubes reinforced reactive powder concrete." Composites Part A: Applied Science and Manufacturing 112 (2018): 371-382. https://doi.org/10.1016/j.compositesa.2018.06.025

[49] Wang, Zhongkun, et al. "Corrosion behavior of steel rebar embedded in hybrid CNTs-OH/polyvinyl alcohol modified concrete under accelerated chloride attack." Cement and Concrete Composites 100 (2019): 120-129. https://doi.org/10.1016/j.cemconcomp.2019.02.013

[50] Sedaghatdoost, Arash, and Kiachehr Behfarnia. "Mechanical properties of Portland cement mortar containing multi-walled carbon nanotubes at elevated temperatures." Construction and Building Materials 176 (2018): 482-489. https://doi.org/10.1016/j.conbuildmat.2018.05.095

[51] Li, Geng Ying, Pei Ming Wang, and Xiaohua Zhao. "Pressure-sensitive properties and microstructure of carbon nanotube reinforced cement composites." Cement and Concrete Composites 29.5 (2007): 377-382. https://doi.org/10.1016/j.cemconcomp.2006.12.011

[52] Yasar, Ergül, Cengiz Duran Atis, and Alaettin Kiliç. "High strength lightweight concrete made with ternary mixtures of cement-fly ash-silica fume and scoria as aggregate." Turkish Journal of Engineering and Environmental Sciences 28.2 (2004): 95-100.

J-Researchers

Journal of Civil Engineering Researchers

Journal homepage: www.journals-researchers.com

Comparison of the Mechanical Behaviour of Concrete Reinforced with Industrial Metal Fibers and Recycled Chips in Acidic Environments

Hadi Faghihmaleki,[a,*] Mehrshad Jafariyan Jolodar[a]

[a] *Faculty of Civil Engineering, Ayandegan Institute of Higher Education, Tonekabon, Iran*

ABSTRACT

In recent years, most of the laboratory research on the comparison of the mechanical behaviour of reinforced concrete containing industrial metal fibers and recycled chips has been carried out abroad, and it is necessary to carry out special studies on reinforced concrete with domestic materials, so that we can produce a recycled reinforced concrete from metal waste and recycled chips that is resistant to acid attack and can be used in the construction industry. First, we prepare the materials and fibers required for the test, then we design an optimal mixing plan in which industrial metal fibers and recycled chips are used in different percentages. The recycled chips are added to the concrete mix in such a way that the amount of chips we add reduces the amount of fine-grained sand, and the chips replace a small percentage of the sand. Concrete samples are then taken according to the mix design and tested after curing at a specified age. We compare concrete samples containing industrial metal fibers and recycled chips after exposure to an acidic environment with a concrete sample without fibers exposed to an acidic environment to understand how much the presence of fibers and chips in the concrete mix has increased the resistance of the concrete to acid.

ARTICLE INFO

Received: December 08, 2024
Accepted: February 27, 2025

Keywords:
Mechanical behaviour
Reinforced concrete
Industrial metal fibers
Recycled chips
Acidic environment

DOI: 10.61186/JCER.7.1.48
DOR: 20.1001.1.2538516.2025.7.1.5.1

1. Introduction

Concrete is known as one of the most widely used construction materials in construction projects, and due to its widespread use in all construction projects, it requires a lot of mining, which causes serious damage to the environment, and after a while the mines run out, creating a serious problem in the construction industry [1]. To solve this problem, the use of waste construction materials in concrete has become popular in recent decades, replacing some of the main concrete materials to create a concrete that can be used in buildings and construction projects, and this type of concrete is called recycled concrete [2,3].

Concrete has many weaknesses and is damaged in adverse weather conditions, acidic environments, etc., which is a problem in construction projects [4]. For this reason, in recent years, fibers have been used in concrete, which is called fiber concrete. The use of fiber concrete has received attention in recent years [5-7]. Ordinary concrete has a small amount of porosity, which causes the

* Corresponding author. Tel.: +98 9112923228; e-mail: h.faghihmaleki@gmail.com (Associate Prof. Hadi Faghihmaleki).

penetration of destructive factors into the concrete. The presence of fibers in concrete not only increases its resistance but also improves its performance against destructive factors. Because it reduces the porosity of the concrete and prevents the penetration of destructive factors into the concrete. Yossari et al. [8] showed that fiber-reinforced concrete (such as steel, polypropylene, and glass fibers) performs better than conventional concrete against acid attacks and leaching processes. This study indicates that adding fibers to concrete can increase the service life of concrete structures in highly corrosive and acidic environments. They also found that the type and quantity of fibers directly affect the concrete's resistance to these conditions.

Wang et al. [9] demonstrated that basalt fiber reinforced concrete exhibits high corrosion resistance in acidic environments. This type of concrete shows particularly high resistance to acids such as sulphuric acid, suffering less structural strength loss. The results of this study suggest that using basalt fibers as reinforcement can be an effective option for producing concrete used in acidic environments, such as refineries or chemical plants. Tigerjan et al. [10] showed that the mechanical behaviour of fabric-reinforced concrete differs significantly between acidic and alkaline environments. In acidic environments, this type of concrete can exhibit good resistance, but its mechanical properties deteriorate in alkaline environments. This research highlights that fabric-reinforced concrete can be an effective solution for applications requiring resistance to corrosive environments. Moreover, specific environmental conditions can influence the performance of this type of concrete, necessitating more careful design for each specific application. Kim et al. [11] found that the type of fiber used has a significant impact on the durability properties of concrete. In particular, fibers like glass and steel improve the concrete’s resistance to environmental stresses, abrasion, and corrosion. This research emphasizes that choosing the right fiber type for each project can enhance the concrete’s performance against specific environmental challenges, including acid attacks, temperature fluctuations, and humidity. Additionally, the study showed that the use of fibers in concrete can extend the lifespan of structures and reduce maintenance needs. Achudhan et al. [4] demonstrated that the use of FRP (fiber-reinforced polymer) can effectively enhance the mechanical properties of concrete beams, particularly in harsh and damaging environmental conditions, such as acidic environments. The inclusion of FRP in reinforced concrete increases its flexural and tensile strength, as well as its resistance to corrosion from various environmental factors. This research could be valuable for investigating the behaviour of different reinforcements under harsh environmental conditions, including acidic ones.

Al-Ajarma et al. [12] examined hollow concrete columns, which are commonly used in tall and heavy structures due to their reduced weight and concrete consumption. Their research showed that using GFRP (glass fiber reinforced polymer) as reinforcement can increase the strength and resistance of these columns to flexural and tensile loads, particularly in acidic environments, which often cause corrosion and shorten the lifespan of structures. These results can assist in comparing different reinforcement options and selecting the best solution for acidic environments.

In recent decades, the use of fiber concrete in construction has become popular and various fibers are used in concrete. One of the fibers used in concrete is metal fiber. Metal fibers are used in concrete in different types and materials and increase the strength of concrete. One of the metal fibers used in concrete is industrial metal fiber, which, in addition to increasing the strength of concrete, also helps the environment because the problem of disposing of these industrial metal fibers is very damaging to the environment. The use of these fibers in concrete increases the resistance of concrete to acidic destructive factors, provided that the fibers are added to the concrete in appropriate percentages, because the presence of excessive metal fibers in concrete causes metal fibers exposed to an acidic environment to corrode over time, and acidic and chemical agents to penetrate the concrete, and over time the concrete loses its effectiveness. Recycled sawdust has been used as a partial replacement for sand in concrete, which in addition to improving the strength of the concrete, reduces the problem of industrial waste disposal and causes less damage to the environment [8].

Table 1
Specifications of cement used

Description	Result
Initial Setting Time	185 minutes
Final Setting Time	230 minutes
Specific Gravity of Cement	3.15 g/cm³
Normal Consistency of Cement	26%

2. Research Methodology

2.1. Materials used

2.1.1. Cement

Portland cement type 2 from Bojnourd Cement Company was used in this study. This cement has a medium resistance to sulphate attack due to the amount of aluminate phase. On the other hand, it can be used in almost bulky concrete due to its medium heat of hydration. This cement has a minimum compressive strength of 440 kg/cm^2 at 28 days. This cement is also known as modified cement by the buyers. This cement has the ability to resist heat and salt, which makes the reinforcement resistant to

rust. The Table 1 shows the specifications of the cement used.

2.1.2. Coarse sand

The sand used in this thesis is factory-made broken sand that is crushed by a crusher and graded by successive sieves. 60 to 70 percent of the total aggregate grains in concrete are sand and play the role of the concrete skeleton. The use of broken grains is very suitable due to the presence of sharp corners and increases the strength of concrete. The specifications of the sand used are given in the Table 2.

Table 2
Coarse sand specifications

Category Name Sand	Seed diameter size (mm)
Coarse	25 to 60
Almond	12 to 25
Peanut	5 to 12

Figure 1: Coarse sand

2.1.3. Fine grained sand

The sand used in this paper is of the mineral type, which is crushed by a machine in the factory and sedimented several times to remove the silt and clay it contains and to make the resulting sand free of impurities so that it can be used in the production of high-strength concrete. Sand makes up 30 to 40 percent of concrete aggregates.

2.1.4. Water in concrete

Drinking water has been used in this study. Water and cement are chemically combined, and as a result of this combination, cement paste is obtained, in which neutral particles and grains of sand and gravel remain suspended until the cement paste sets. Water also acts as a lubricant between the fine particles and grains of sand and gravel, giving the concrete its workability and application properties and making it easy to pour.

The use of inappropriate water in concrete construction leads to the following issues and problems:

- The setting time of the cement is delayed, the concrete becomes slow.
- It causes a reduction in the final strength of the concrete. (Sometimes the strength is reduced by up to 30 per cent).
- Causes corrosion and gradual deterioration of reinforcing steel.
- Causes stains on the surface of the final dried concrete, which is particularly problematic in concrete used on facades.

Figure 2: Consumable sand

Table 3
Stone material specifications

Sieve size (mm) and (micrometer)	Residual weight on each sieve (g)	Percentage of residual fraction per sieve (%)	Percentage of residual fraction per sieve (%)
5/9	0	0	100
75/4	20	2	98
36/2	45	5/4	5/95
18/1	85	5/8	5/91
600	120	12	88
300	185	5/18	5/81
150	230	23	77
pan	315	5/31	5/68
Total	1000	-	-

2.2. Superplasticiser

This chemical has many uses and its standard use in concrete also brings many benefits. Superplasticisers have many uses and can be used to produce higher quality concrete. Due to its properties, concrete shrinks in cold weather and loses the required fluidity, so by adding superplasticiser to the concrete, it is made fluid to the required extent. Another use of these materials is in prefabricated concrete moulds. In addition to the mould, superplasticisers are also used in the concrete material to produce concrete with high strength and durability.

2.2.1. Use of concrete superplasticisers

Superplasticisers were used for making hard and strong concrete, production of micro-silica concrete, increasing concrete efficiency, reducing the water-cement ratio, increase concrete flow and increase production speed.

2.2.2. Main constituents of concrete superplasticisers

Concrete superplasticisers consist of lignosulphonates, melamine formaldehyde sulphonate, naphthalene formaldehyde sulphonate, synthetic polymers and water-soluble copolymers.

2.2.3. MTOCRETEN-480 Concrete Superplasticiser

MTOCRETEN-480 is a chloride-free concrete superplasticizer based on melamine formaldehyde and is used to produce strong concrete. This product is available in two forms: solution and powder, the powder to be dissolved in water before use. Strong concrete is completely fluid, but the adhesion of its elements is maintained even at a slump of 200 mm, and this type of concrete is self-dense and at the same time free from segregation. This superplasticiser was used in this experiment because, in addition to reducing the water/cement ratio and increasing resistance to chemical agents, it also increases the strength of the concrete to a certain extent.

Table 4
Lubricant properties and specifications

Description	Specifications
Superplasticizer paint	Clear to slightly cloudy liquid
Specific gravity	1.1 g/cm^3
Input air	Airless

2.3. Recycled shavings

Iron shavings were used in this research. The shavings are obtained from the machining of industrial parts and some shavings are used to replace aggregate in concrete to increase the strength of the concrete. The shavings are in the form of fine grains and are combined in a sand and gravel mixture and then added to the cement paste.

Figure 3: Consumable chips

2.3.1. Steel Fibers in Concrete

The use of various types of steel fibers in concrete is used as concrete or mortar reinforcement to increase concrete strength, reduce shrinkage, control cracking, increase durability and improve mechanical properties of concrete, and as alternative reinforcing fibers for thermal bars in concrete structures. In this study, steel fibers were used at different percentages as woven fibers in concrete.

2.3.2. Effect of steel fibers in concrete

Stee fibers increase the tensile, flexural and shear strength of concrete, increase in impact resistance and energy absorption, reduced installation costs due to the price of concrete steel fibers, decrease in manpower and project implementation time.

Table 5
Steel fiber specifications

Fiber Type	Density (Kg/m^3)	Maximum Strain at rupture	Tensile Strength (Mpa)	Diameter	Length (mm)
Ind. Steel	7850	8/0	1050	<4	50
Ind. Steel	7850	8/0	1050	<4	25

2.3.3. Acid Destructive of Concrete

In this study, battery water was used as a substance that endangers concrete, which acts like carbonic acid and causes concrete to lose its strength over time. The attack of carbonic acid is mild and gradually destroys concrete.

2.4. Laboratory program

In this research we first studied the materials used, then we mixed these materials at different percentages and took concrete samples and tested them. The tests include testing the compressive and tensile strength of the concrete.

The concrete is tested after being immersed in acid and its resistance is determined.

2.4.1. Mixing ratios used

In this study, 5 series of concrete specimens are tested, 4 of which are concrete specimens containing metal fibers and recycled chips at certain percentages, and 1 series of ordinary concrete specimens without fibers. The test results of the fiber concrete samples made of steel fibers and recycled chips are compared with ordinary concrete without fibers after exposure to acid to find out what is the optimum mixing plan for making acid-resistant concrete containing steel fibers and recycled chips.

In this mix design, (10, 15, 20, 25) kilograms of steel fibers per cubic metre are used, a superplasticiser is also used to increase the fluidity of the concrete and its resistance to acid, and recycled chips are also added to the concrete mix in fine form as a partial replacement for fine-grained sand.

2.4.2. Sample making method

To make the samples in this study, we first prepared 15 cm moulds and then greased them with oil to prevent the

Table 6
Optimal mixing plan Kg/m^3

Sample Name	Cement	Sand	Gravel	Water	Recycled Chips	Plasticizer	Steel Fibers
Plain Concrete	450	1000	710	260	0	0	0
Concrete (M1)	450	993	710	260	7	4.5	10
Concrete (M2)	450	988.5	710	260	11.5	5.85	15
Concrete (M3)	450	983.5	710	260	16.5	6.75	20
Concrete (M4)	450	980	710	260	20	9	25

concrete from sticking to them. After preparing the moulds, we mix the concrete according to the desired mixing schedule. The concrete mixing process takes between 3 and 5 minutes to mix the desired fibers well into the concrete paste and distribute them throughout the concrete. After mixing the steel fibers, recycled chips and lubricant, we pour the concrete into the cube moulds in 3 stages, hitting them 25 times at each stage to remove the air in the concrete, then smoothing it out and leaving it in place for 24 hours without moving it. Then we remove the samples from the mould and cure the concrete.

Figure 4: Cubic mold

2.4.3. Curing

Concrete curing is a process that prevents the loss of moisture in the concrete and maintains its temperature as much as possible. This is done at the start of sampling at an early age to maintain the moisture content of the concrete and ensure that the final hardened concrete is of the highest quality and strength.

2.5. Concrete testing

2.5.1. Slump test

Concrete slump, or inverted slump cone, is determined by a relatively simple test using a very simple instrument. This instrument consists of a hollow incomplete cone with a handle, a steel rod for compaction, a steel base plate and a tape measure for measurement. Concrete slump testing is one of the methods used to determine the workability and flowability of fresh concrete. This test is usually carried out in a concrete laboratory under specific environmental conditions or on site using a slump testing machine.

The conventional slump test is one of the easiest tests to perform on concrete. It is very inexpensive and the results are immediate. For this reason, the slump test has been the most widely used and common test for determining the workability and flowability of concrete since 1922.

2.5.2. Concrete Compressive Strength Test

The purpose of a compressive strength test is to determine the compressive strength of a cylindrical or cubic concrete specimen. The compressive strength of any material is its resistance to failure under compressive loading. For concrete in particular, compressive strength is an important parameter in determining the performance of the concrete throughout the life of the structure.

The compressive strength of concrete is determined in the batching plant laboratory for each batch in order to maintain the desired quality of concrete during the curing period.

The strength of concrete members is required. Concrete specimens are prepared and tested under compressive load to determine their compressive strength. In very simple terms, compressive strength is calculated by dividing the failure load by the area of application of the load, usually after 28 days of concrete storage and curing.

To determine the compressive strength of concrete, a minimum of two samples are selected for each test and are soaked in water for 24 hours prior to testing. The samples are then tested in a testing machine and the compressive strength of the sample is calculated by dividing the maximum load applied by its cross-sectional area.

The lower the water/cement ratio, the higher the compressive strength. The strength of concrete is expressed in the United States in psi per square inch and in the SI unit in megapascals. For typical applications, the compressive strength of concrete is between 0.1 and 61 MPa.

Figure 5: Jack for compressive strength testing

Table 7
Compressive strength test results in MPa

Sample name	Compressive strength of the sample 7 days	Compressive strength of the sample 28 days	Compressive strength of concrete exposed to acid
Fiberless concrete	46/25	73/34	71/30
Concrete 10 m1	87/25	71/36	69/32
Concrete 15 m2	49/28	84/39	68/38
Concrete 20 m3	76/21	47/33	46/28
Concrete 25 m4	83/19	34/22	78/21

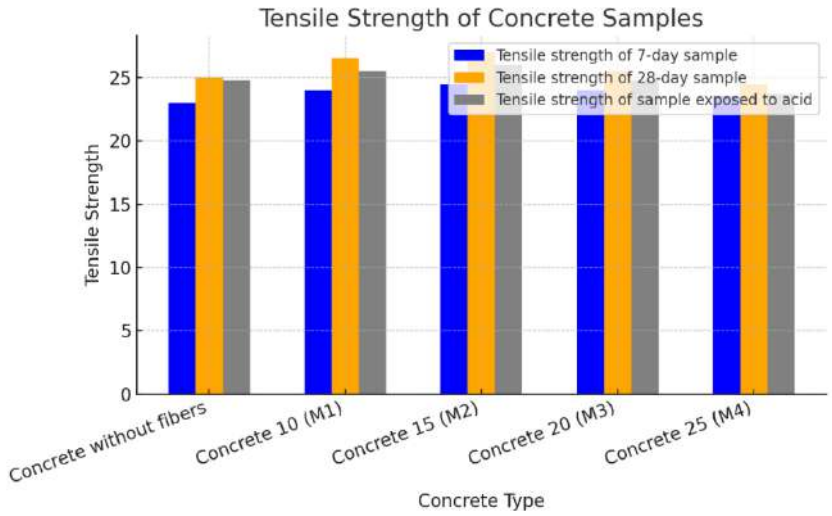

Figure 11: Tensile strength test results

2.5.3. Testing Concrete Tensile Strength

Concrete tensile strength is one of the most fundamental and important properties that significantly affects the cracking rate of structures. In addition, concrete is very weak in tension due to its brittle nature, so it is not expected to withstand direct tension, so if the tensile strength of the concrete is exceeded, cracks will form in the concrete. To determine the amount of force that is likely to cause cracking in a concrete member, it is necessary to determine the tensile strength of the concrete. Tensile testing of concrete by dividing or halving a cylindrical specimen is one method of determining the tensile strength of concrete.

3. Results

3.1. Compressive strength

In this research, after sampling and curing the samples, which were placed in water for 28 days to reach their final strength, the samples were tested using a concrete compressive strength testing machine. From each concrete sample, a 7-day sample and a 28-day sample were tested and also a sample after curing was placed in acid and tested again to record the final strength. The results are shown in the Table 7.

3.1.1. Slump test

In general, the addition of industrial metal fibers and recycled chips to the concrete mix will reduce the slump of the concrete. The high percentage and large surface area of the fibers can collect more cement paste around them, increasing the viscosity of the concrete mix and reducing slump.

Because recycled chips have a fine cross section, they absorb more water and increase the water-to-cement ratio. To reduce the water-to-cement ratio, we used a superplasticiser in the concrete mix. In this study it was observed that adding more fibers and recycled chips reduced the slump of the concrete, with the control sample having the highest slump and the sample containing 25 kg of industrial metal fibers having the lowest slump.

4. Results discussions

From tests carried out on reinforced concrete containing industrial metal fibers and acid-resistant recycled chips, it was found that concrete with suitable fibers up to a certain percentage had good resistance to acids, but as more fibers were added to the concrete, the resistance decreased somewhat. Acids increase the porosity of concrete due to the corrosion of metal materials in the samples, which is

the main factor in reducing the strength of concrete. Also, in concrete structures, if the porosity increases, destructive factors will penetrate into the concrete, and if rebar is used in it, it will also cause corrosion of the rebar, which will cause the concrete structure to fail.

In this test, by adding the right amount of fibers, we were able to create a strong recycled concrete that does not harm the environment and uses a lower percentage of aggregate than normal concrete.

5. Conclusion

The following results were obtained from the conducted study:

- The use of metal fibers and recycled chips in concrete resulted in the creation of a recycled fiber concrete, which uses industrial waste to create a quality product in the construction industry.
- Industrial fibers and recycled chips are abundant in Iran, so it does not require much money to prepare them, which increases their use in concrete.
- The use of metal fibers and recycled chips in concrete increased the resistance of concrete to mechanical behaviour and improved the properties of ordinary concrete.
- The use of metal fibers in concrete together with recycled chips in certain percentages turned ordinary concrete into a reinforced concrete that is resistant to acid attacks and can withstand chemical attacks that are a destructive factor for concrete.
- Optimal use of recycled chips in concrete can result in less use of fine-grained materials in concrete and less damage to sand and gravel resources.
- The use of industrial waste reduces the problems associated with the disposal of these materials and can be used directly.

References

[1] Faghihmaleki, Hadi. "Comparison of concrete and steel jacket methods for reinforcing a concrete bridge pier by numerical and experimental studies." Makara Journal of Technology 25.2 (2021): 2. https://doi.org/10.7454/mst.v25i2.3909

[2] Faghihmaleki, Hadi, and Reza Abbasghorbani. "Investigating the Effect of Silica Foam on the Mechanical Properties of Concrete Containing Recycled Glass Shards." Journal of Civil Engineering Researchers 6.4 (2024): 22-31. https://doi.org/10.61186/JCER.6.4.22

[3] Khazraie, Donya, and Hossein Razzaghi. "Investigating the compressive and tensile strength of concrete containing recycled aggregate with polypropylene fibers." Journal of Civil Engineering Researchers 4.4 (2022): 20-32. https://doi.org/10.61186/JCER.4.4.20

[4] Achudhan, Deepavarsa, and Shalini Vandhana. "Strengthening and retrofitting of RC beams using fiber reinforced polymers." Materials today: proceedings 16 (2019): 361-366. https://doi.org/10.1016/j.matpr.2019.05.102

[5] Parvinnejad, Zahed. "The effect of steel and hybrid fibers on the impact resistance of concrete enclosed with FRP sheets." Journal of Civil Engineering Researchers 4.2 (2022): 41-45. https://doi.org/10.52547/JCER.4.2.41

[6] Jamshidi, Morteza. "The Effect of Polypropylene Fibers on the Behavior of Fiber Self-Compacting Concrete." Journal of Civil Engineering Researchers 5.4 (2023): 56-62. https://doi.org/10.61186/JCER.5.4.56

[7] Kameli, Sanaz, Amin H. Shahi, and Amir Mahboob. "Investigating the Mechanical Properties of Natural Fiber-Reinforced Concrete with Kenaf, Jute, and Coconut Fibers." Journal of Civil Engineering Researchers 6.4 (2024): 32-39. https://doi.org/10.61186/JCER.6.4.32

[8] Youssari, Fatima Zohra, Omar Taleb, and Ahmed Soufiane Benosman. "Towards understanding the behavior of fiber-reinforced concrete in aggressive environments: Acid attacks and leaching." Construction and Building Materials 368 (2023): 130444. https://doi.org/10.1016/j.conbuildmat.2023.130444

[9] Wang, Zhenshan, et al. "Study on corrosion law and characteristics of composite modified basalt fiber concrete in acid environment." Polymer Testing 128 (2023): 108201. https://doi.org/10.1016/j.polymertesting.2023.108201

[10] Thiyagarajan, Hemalatha, Ramesh Gopal, and Smitha Gopinath. "Textile reinforced concrete subjected to acidic and alkaline environment: Experimental study." Journal of Materials in Civil Engineering 34.8 (2022): 04022156. https://doi.org/10.1061/(ASCE)MT.1943-5533.0004307

[11] Kim, B., A. J. Boyd, and J-Y. Lee. "Durability performance of fiber-reinforced concrete in severe environments." Journal of composite materials 45.23 (2011): 2379-2389. https://doi.org/10.1177/0021998311401089

[12] AlAjarmeh, O. S., et al. "Hollow concrete columns: Review of structural behavior and new designs using GFRP reinforcement." Engineering structures 203 (2020): 109829. https://doi.org/10.1016/j.engstruct.2019.109829

J-Researchers

Journal of Civil Engineering Researchers

Journal homepage: www.journals-researchers.com

Analysis of box-girder bridge Considering Translational and Rotational Components of Earthquake

Mohamadreza Abdollahi Kakroudi, [a,*] Morteza Hosseinali Beygi, [a] Leila Kalani Sarokolayi [b]

[a] *Department of Civil Engineering, Babol Noshirvani University of Technology, Babol, Iran*

[b] *Department of Civil Engineering, Tabari Institute of Higher Education, Babol, Iran*

ABSTRACT

Due to the importance of bridges as vital arteries and the huge investment of countries in building bridges, the need for more accurate seismic analysis of bridges to better understand their structural behavior is inevitable. Like many structures, the effect of the rotational components of the earthquake on bridges has been less noticed by researchers and designers. This research has evaluated the effect of the rotational components of the earthquake to better understand the seismic behavior of bridge. For this purpose, in addition to three translational components, the rotational components of the earthquake, including two rocking components and one torsional component, have been considered in the three-dimensional seismic analysis of box-girder concrete bridges. By creating the rotational component of the earthquake by the Hong-Nan Li method, three box-girder bridges with pier heights of 12, 30, and 45 meters were subjected to the combined effect of six translational and rotational components, as well as three translational components were separately subjected to under a far-field earthquake with different soil and shear wave velocity. The results of the analysis show that the effect of the earthquake's rotational components on the response of stresses and displacement, depending on the type of earthquake and the characteristics of the bridge structure, can be particularly important.

ARTICLE INFO

Received: July 09, 2024
Accepted: February 28, 2025

Keywords:
Box-girder bridge
Rotational component of the earthquake
Linear dynamic analysis
Far field earthquake
Concrete bridge

DOI: 10.61186/JCER.7.1.55
DOR: 20.1001.1.2538516.2025.7.1.6.2

1. Introduction

Bridges are the oldest structures and passageways to cross valleys and rivers [1-2]. Also, the continuous expansion of highways worldwide, mainly due to the significant increase in traffic, population, and the extensive growth of urban and metropolitan areas, makes using bridges inevitable. The special impact of the bridge on intracity and suburban communication, as well as the importance of these structures in terms of safety, has forced engineers to design it accurately under earthquake. The occurrence of numerous earthquakes and the damages they cause make a more detailed study of the impact of

* Corresponding author. Tel.: +989358914697; e-mail: mohamadreza.abdollahi76@gmail.com.

earthquake components on all kinds of structures inevitable.

Many studies have been carried out on all types of structures under the translational components of an earthquake to better understand the performance of structures under an earthquake and also the amount of damage inflicted on them. The earthquake comprises six components, including three translational and three rotational components. The translational components are divided into two horizontal components and one vertical component, and the rotational components are divided into two rocking components (rotation around two horizontal axes) and one torsional component (rotation around the vertical axis). The analysis of structures and bridges under rotational components has been less considered than translational components. For this reason, in this study, bridges with box-girder are examined under the translational and rotational components of the earthquake to determine the impact of rotational components on the response of the behavior of this structure.

Observations made on the rotation of tombstones and chimneys have drawn researchers' attention to the effect of the rotational component of the earthquake [3]. Using theoretical relationships, researchers found two methods to calculate the rotational component. The first method uses the equation of the theory of elasticity, and the second method uses the equation of the theory of elasticity along with the theory of wave propagation. Newmark performed the first method, which provided a simple relationship between the earthquake's translational and rotational components and caused more researchers to investigate this field [4]. Other researchers also used this method after the Newmark study. The methods of calculating the rotational components are diverse; some are divided into direct methods using parallel seismographs, ring lasers, and chemical explosions. Another set uses earthquake translational components based on the elastic theory method and is divided into time derivation, finite difference, and geodetic methods. In this study, we calculate the rotational component using an improved method by Hong Nan Lee, which uses wave propagation theory and elasticity theory [5]. In the Hang Nan Lee method, the wave velocity and the angle of the incident wave are used to calculate the rotational component.

According to the existing methods for calculating the rotational components of the earthquake, various studies have been conducted on different types of structures under rotational components. In 1984, Abdul Ghaffar and Rubin examined the torsional response of the Golden Gate suspension bridge and concluded that this structure's response was necessary for higher mode, and the displacement and cable tensions are under little torsion stimulation, but the flexural stresses are high [6]. Kalani and Navayi Neya studied the effect of spatially varying the rotational and translational components of the earthquake on concrete gravity dams using the Hang Nan Li method. The results of their study express the increasing effect of the rotational component on the instruments' responses. Also, the rotational component impacts the destroyed concrete areas and the crack zone [7]. Kalani et al. investigated the translational and rotational components on the elevated Water Storage Tanks and concluded that the rotational components of ground motion can increase the structure's response, and ground motion analysis with six components can be essential for design control [8]. The results of studies on structures such as cooling towers [9], self-centering base-rocking walls [10], and progressive collapse of steel structures [11] under rotational components of earthquake express the impact of this component on the response of structural behaviour and require consideration of rotational components. The studies of Raghem Moayed [12], Özşahin and Pekcan [13], respectively, on steel girder bridges and skew highway bridges under rotational components, pointed out the increasing effect of rotational components on the response of structures, such as displacement and stress and stated the need to consider the rotational component. Dehmardeh et al.'s study was devoted to examining the effects of the torsional component on the response of buildings and the adequacy of accidental eccentricity, which concluded that the accidental eccentricity to consider Getting the effects of the torsional component is not enough and leads to unreliable responses [14]. The impact of rotational components on the response of structures makes it necessary to investigate this component on bridges. For this purpose, box girder bridges under both the translational and rotational components of the earthquake have been studied in this research.

2. Calculation of earthquake rotational components

According to the six-component analysis, rocking and torsional components will need to be produced because the codes do not mention a direct method for calculating it. For this purpose, this research calculates the rotational components using the Hang Nan Li method [7], which uses the translational component and the theory of elasticity and wave propagation, which is calculated with the help of programming in MATLAB software. Using relationships 1 and 2, respectively, can obtain the time history of rocking and torsional components in which the R domain, θ_w is the frequency phase calculated from the frequency content spectrum w and ω is the angular velocity of the wave, and C_x is the apparent velocity of the waves.

$$\varphi_{gy} = \varphi_{gx} = \frac{i\omega}{C_x} w = e^{\frac{\pi}{2}i} \frac{\omega}{C_x} R_w e^{i\theta_w} = \left(\frac{\omega}{C_x} R_w\right) e^{\left(\frac{\pi}{2}+\theta_w\right)i} \quad (1)$$

$$\varphi_{gz} = \frac{i\omega}{2C_x} v = e^{\frac{\pi}{2}i} \frac{\omega}{2C_x} R_v e^{i\theta_v} = \left(\frac{\omega}{2C_x} R_v\right) e^{\left(\frac{\pi}{2}+\theta_v\right)i} \quad (2)$$

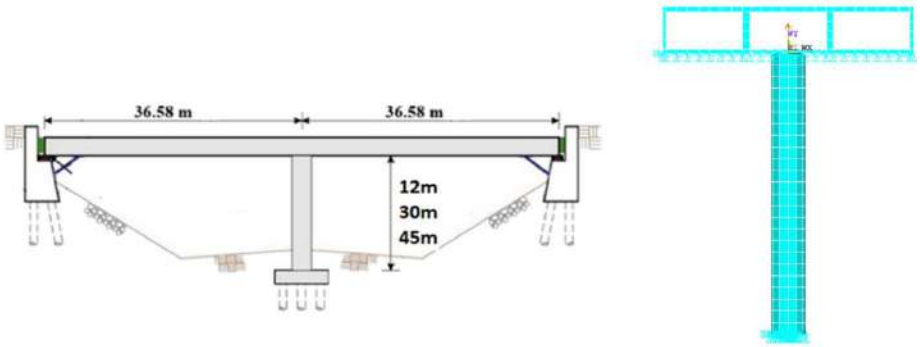

Fig. 1. The geometry of the bridge

3. Numerical modeling of bridges

To investigate the effect of the earthquake's rotational components on bridges, the geometry of the bridge was selected from a reference [15], and it is shown in Figure 1. The examined concrete box-girder bridge is 73.16 meters long, has a pier height of 12 meters, and a deck width of 10.75 meters. To thoroughly investigate the behavior of the bridge under the rotational components of the earthquake and compare it with the translational components, two other bridges were modeled by increasing the pier height to 30 and 45 meters. Table 1 presents the geometry of the bridges, and Table 2 provides the specifications of the materials used.

Table 1.
Geometrical characteristics of the investigated bridge per meter unit

Model	Pier height	Pier diameter
1	12	1.52
2	30	2.5
3	45	3.00

Table 2.
Specifications of the investigated bridge materials

Type of material	Modulus of elasticity (GPa)	Density (kg/m^3)	Poisson's ratio
Concrete	27.2	2400	0.2
Steel	20	7850	0.25

Soil structure interaction was not considered, and the bridge pier was considered restrained. Also, due to the presence of a shear key in the abutment to prevent the transversal movement of the bridge, the abutment is restricted in the transverse direction in addition to vertical movement.

For the analysis and modeling of the three-dimensional bridges examined, Ansys finite element software and Solid 65 element, including eight nodes, each node containing three degrees of translational freedom, have been used. The Solid 65 element can model reinforced concrete and defined as a percentage of the volume ratio, in this study, the reinforcement for the pier height is 13%, and for the deck, it is considered a value of 2%.

4. Earthquake records

The selection of earthquake records is an essential part of the seismic analysis that will be effective in obtaining results. For this research, three earthquake records for soil type 3 and three earthquake records for soil type 2 were selected according to the standard 2800, and the characteristics of the records are given in Tables 3 and 4.

Table 3.
Characteristics of earthquake recording, soil type 3

Earthquake	Station	Magnitude (Richter)	Rjb (km)	Vs30 (m/sec)
Kobe	HIK	6.9	95.72	256
Northridge	LA – W 70th St	5.28	30.46	241.41
Taiwan SMART1	SMART1 M01	6.5	96.28	268.37

Table 4.
Characteristics of earthquake recording, soil type 2

Earthquake	Station	Magnitude (Richter)	Rjb (km)	Vs30 (m/sec)
Tabas	Bajestan	7.35	119.77	377.56
Northridge	Lake Hughes #4 – Camp Mend	6.69	31.27	600.06
Taiwan SMART1	Fort Tejon	6.61	59.52	394.18

5. Numerical analysis

In order to ensure the correctness of numerical modeling, first, sensitivity analysis is done to determine the proper dimensions of the element and then the validity of the bridge model.

5.1. sensitivity analysis

To perform the sensitivity analysis, we have to reduce the size of the elements in several steps so that the results are independent of the element size. To determine the dimensions of the element, the displacement sensitivity analysis of the middle of the bridge span in the vertical direction (U_y) was performed under static analysis by changing the dimensions of the element and calculating the displacement at each step. In Figure 2, the displacement is shown by changing the size of the element. According to Figure 2, the sensitivity analysis is considered for the element to dimensions from 1.5 meter to 0.25 meter, and according to the time required to analyze, the bridge models have been selected to 0.5 meters element. Then, the number of bridge elements with 12, 30, and 45 meters pier heights is 21030, 21890, and 23712, respectively.

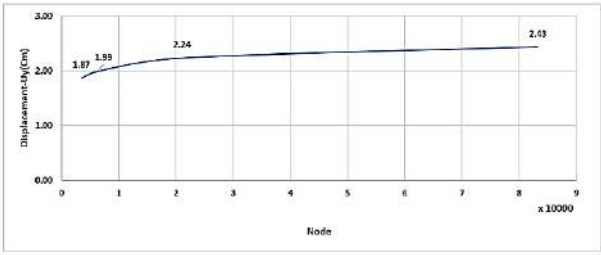

Fig. 2. The displacement sensitivity analysis of the middle of the bridge span with a 12-meter pier height.

6. Validation of the bridge

To verify the bridge model in the Ansys software, the period of the bridge in the reference [13] and the model carried out in this research will be compared. The period is one of the critical indicators that influence the analysis and response of structures, and a slight change in the period of structures will cause differences in the results and responses of the analyses. For this purpose, according to Table 5, it is observed that the difference in the period of reference 13, which was modeled and analyzed with the OpenSees, and the bridge modeling done in this study was very small; it is possible to understand the accuracy of modeling as well as the results of the analysis. In addition to this, the vertical reaction in the supports and its equality with the weight is another proof of the accuracy of the modeling of the present research.

It is noteworthy that for soil type 2, Northridge, San Fernando, and Tabas earthquakes are considered, and the bridge with three different pier heights of 12, 30, and 45 meters have been analyzed, which, due to the limited number of pages, is excluded from its presentation.

Table 5.
Validation of the bridge's period

The Finite Element Model	Period (sec)
Reference [15]	1.29
Ansys model	1.2977

7. Results

Three series of bridges with pier heights of 12, 30, and 45 meters were subjected to the combined effect of six translational and rotational components, as well as three translational components were separately subjected to a far-field earthquake with different soil and shear wave velocity. To compare the results of the time history analysis, the displacements Ux, Uy, and Uz, which are respectively in the transverse, vertical, and longitudinal directions of the bridge, are presented in centimeters, and the principal stresses (S1, S2, S3) are offered in kilopascals. Figures 3 and 4, respectively, show the time history of the displacements and points A, B, and C, and the principal stresses for point B are for the analysis of six and three components of the Northridge earthquake of soil type 3 for a bridge with a pier height of 12 meters. Also, tables 6 to 8 summarize results from other analyses for displacements and principal stresses for bridges 12, 30, and 45(m) of soil type 3.

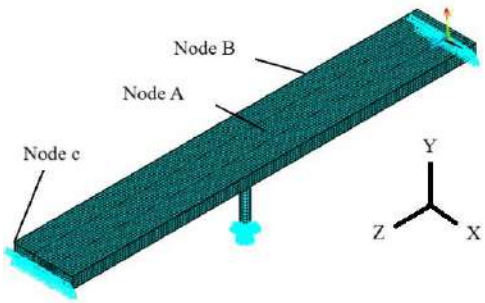

Fig. 3. Maximum points of displacement and stress of the bridge with 12(m) pier height

8. Conclusion

According to the analysis of bridges with different heights and earthquakes, the impact of rotational components on the box bridge is as follows:

- Among the results of the analyses carried out under three and six components of the type 3

soil earthquake, the effect of the rotation component of the Northridge earthquake was more effective and had an increasing impact on the results of the displacements and stresses created in the bridges. As a result of the increase in the pier height, the percentage of the difference between three and six components in stress and displacements increased, which is the result of the effect of the rotational component.

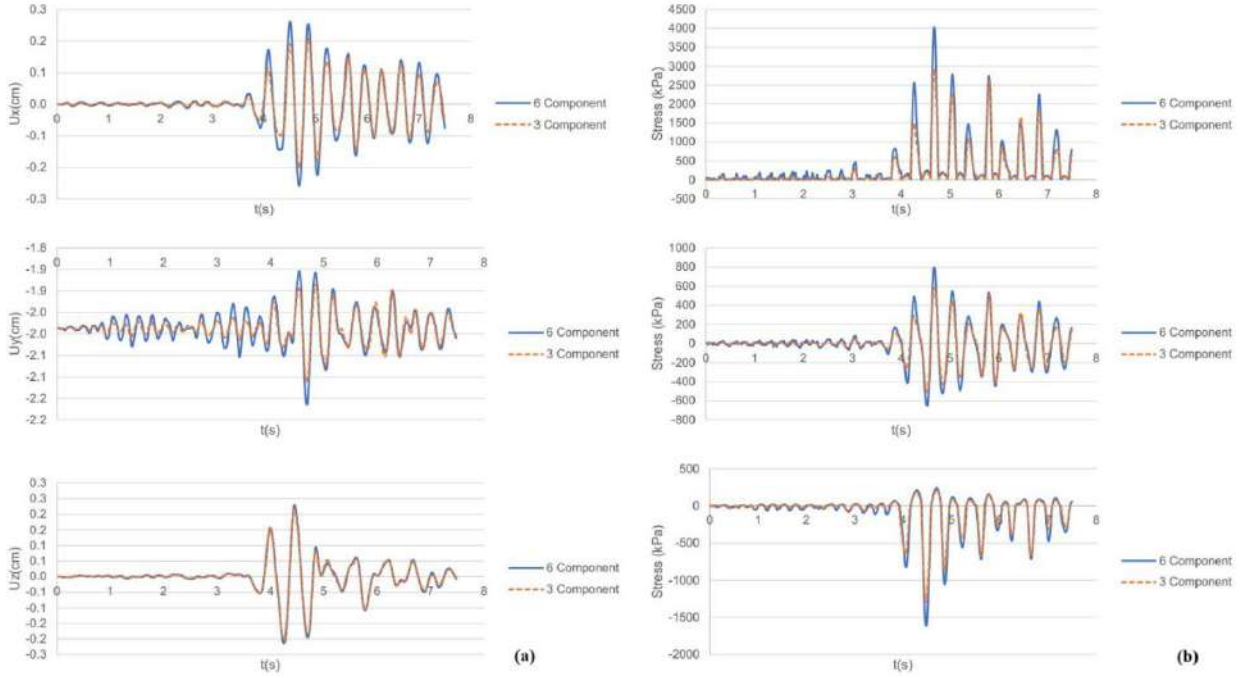

Fig. 4. Time history analysis, a) displacement b) principal stress

Table 6.

Results of bridge analysis with a pier height of 12(m) under soil type 3 earthquake

Maximum Displacement(cm)	**Three-component**			**six-component**		
	Kobe	Taiwan SMART1	Northridge	Kobe	Taiwan SMART1	Northridge
Transverse direction (Ux)	1.13	0.227	0.209	0.896	0.242	0.263
Vertical direction (Uy)	-1.41	-2.144	-2.112	-1.453	-2.205	-2.165
longitudinal direction (Uz)	3.96	1.97	0.217	3.96	1.97	0.23
Principal stresses (kPa)	**Three-component**			**six-component**		
	Kobe	Taiwan SMART1	Northridge	Kobe	Taiwan SMART1	Northridge
S1	18823.5	10575.3	2933.7	18842.6	10553.4	4008.5
S2	2174.9	-2637.13	580.2	2173.7	-2616.14	795.4
S3	-20476.6	-11747	-1284.2	-20469.3	-11750.9	-1610.06

- The maximum increase in displacement values for soil type 3 in the analysis of six components compared to the three components of the bridge with pier heights of 12, 30, and 45 meters is 20.53%, 61.92%, and 39.85%, respectively. And for soil type 2, these values are 13.73%, 14.5% and 19%, respectively.
- The maximum increase of the maximum stress values for soil type 3 in the analysis of six components compared to three components for the bridge with pier height of 12, 30, and 45 meters is 26.8%, 67.3%, and 47.8%,

respectively. And for soil type 2, these values are 20.5%, 26.87% and 48.84%, respectively.

- In the six-component analysis, the rotational component does not always have an increasing effect, and like the soil type 3 Kobe earthquake, it has a decreasing effect on the stress values and displacements. However, in the vertical axis (Y), due to the rotation component that rotates around this axis, the incremental effect of the rotational component is evident in three bridge models. The increase or decrease of the response of the six-component analysis can also be attributed to the frequency spectrum of the earthquake.

- In soil type 2 earthquakes, the difference between the results of three and six earthquake components has increased, which can also be pointed to the effect of the rotational component in soil type 2. Also, compared to the analysis of soil type 3 earthquakes, the reduction effect caused by the rotational component is much less.

Table 7.
Results of bridge analysis with a pier height of 30(m) under soil type 3 earthquake

Maximum Displacement(cm)	**Three-component**			**six-component**		
	Kobe	Taiwan SMART1	Northridge	Kobe	Taiwan SMART1	Northridge
Transverse direction (Ux)	-1.477	-0.297	-0.286	-0.98	-0.297	0.751
Vertical direction (Uy)	-2.171	-1.676	-1.894	-2.29	-1.672	-2.06
longitudinal direction (Uz)	-3.147	2.08	0.203	-3.136	2.129	-0.291
Principal stresses (kPa)	**Three-component**			**six-component**		
	Kobe	Taiwan SMART1	Northridge	Kobe	Taiwan SMART1	Northridge
S1	12061	2050.93	2375.1	8126.2	2422.25	7255.6
S2	2455.8	-487.7	494.8	-1782.6	-482.1	1376.2
S3	-3023.9	-428.7	-391.8	-2378.4	-425.3	-1165.85

Table 8.
Results of bridge analysis with a pier height of 45(m) under soil type 3 earthquake

Maximum Displacement(cm)	**Three-component**			**six-component**		
	Kobe	Taiwan SMART1	Northridge	Kobe	Taiwan SMART1	Northridge
Transverse direction (Ux)	-2.133	0.576	-0.335	1.846	0.636	-0.557
Vertical direction (Uy)	-1.408	-1.66	-1.763	-1.541	-1.657	-1.926
longitudinal direction (Uz)	3.08	-1.843	0.19	3.134	-1.873	0.2
Principal stresses (kPa)	**Three-component**			**six-component**		
	Kobe	Taiwan SMART1	Northridge	Kobe	Taiwan SMART1	Northridge
S1	4726.9	2251	953.8	5825.6	2457.1	1827.2
S2	-2064	811.2	291.4	-19442.2	846.2	548.2
S3	-6325.4	-1642.5	-940.5	-4838.5	-1487.3	-1736

References

[1] Jamshidi, Morteza, and Teymour Sam. "Study of the collapse of Sardabroud-Chalous truss bridge." Journal of Civil Engineering Researchers 4.2 (2022): 46-51. https://doi.org/10.52547/JCER.4.2.46

[2] Alvansazyazdi, Mohammadfarid, et al. "Evaluation of the Impact of Driving Techniques on the Subsoil Stability of Bridge E2 in Manta, Ecuador." Journal of Civil Engineering Researchers 6.3 (2024): 40-46. https://doi.org/10.61186/JCER.6.3.40

[3] Cochard, Alain, et al. "Rotational motions in seismology: theory, observation, simulation." Earthquake source asymmetry, structural

media and rotation effects (2006): 391-411. https://doi.org/10.1007/3-540-31337-0_30

[4] Newmark, Nathan M. "Torsion in symmetrical buildings." PROCEEDING OF WORLD CONFERENCE ON EARTHQUAKE ENGINEERING, 1969.

[5] Li, Hong-Nan, Li-Ye Sun, and Su-Yan Wang. "Improved approach for obtaining rotational components of seismic motion." Nuclear Engineering and Design 232.2 (2004): 131-137. https://doi.org/10.1016/j.nucengdes.2004.05.002

[6] Abdel-Ghaffar, Ahmed M., and Lawrence I. Rubin. "Torsional earthquake response of suspension bridges." Journal of engineering mechanics 110.10 (1984): 1467-1484. https://doi.org/10.1061/(ASCE)0733-9399(1984)110:10(1467)

[7] Sarokolayi, L. Kalani, and B. Navayi Neya. "Dynamic Analysis of Concrete Gravity Dams due to Nonuniform Translation and Rotational Components of Earthquake Considering Reservoir Interaction." Ph.D dissertation, Babol Noshirvani University of Technology, 2013

[8] Kalani Sarokolayi, L., et al. "Seismic analysis of elevated water storage tanks subjected to six correlated ground motion components." Iranica Journal of Energy & Environment 4.3 (2013). https://www.ijee.net/article_64469_e05efe546014916846654c99cfc51ab8.pdf

[9] Esfandiari, F. Sarokolayi, L. Kalani, and B. Navayi Neya. "Linear Dynamic Analysis of Cooling Tower Considering Translational and Rotational Components of Earthquake." Master thesis, Babol Noshirvani University of Technology, 2017

[10] Mohammadi Dehcheshmeh, Esmaeil, and Vahid Broujerdian. "The Effects of Rotational Components of Near-Fault Earthquakes on Self-Centering Base-Rocking Walls." Bulletin of Earthquake Science and Engineering 9.3 (2022): 37-55. https://doi.org/10.48303/bese.2021.245905

[11] Gholampour, Siroos, et al. "Investigating the effect of rotational components on the progressive collapse of steel structures." Engineering Failure Analysis 121 (2021): 105094. https://doi.org/10.1016/j.engfailanal.2020.105094

[12] Raghem Moayed, V. , et al. "The effect of torsional component of earthquake on structural behaviour of bridges." Master thesis, University of Mohaghegh Ardabili, Faculty of Engineering, 2013

[13] Özşahin, Ecem, and Gökhan Pekcan. "Assessment of seismic demand due to torsional ground motions on symmetric skew bridges." Journal of Earthquake Engineering 26.8 (2022): 3938-3953. https://doi.org/10.1080/13632469.2020.1822224

[14] Rahat Dahmardeh, Saman, Mehrtash Motamedi, and Armin Aziminejad. "A study on the effects of torsional component of ground motions on seismic response of low-and mid-rise buildings." The Structural Design of Tall and Special Buildings 29.4 (2020): e1699. https://doi.org/10.1002/tal.1699

[15] Srivastava, Charu, Muhamed Safeer Pandikkadavath, and Sujith Mangalathu. "Effect of material variability on the seismic response of reinforced concrete box-girder bridges for different pier heights." Materials Today: Proceedings 65 (2022): 564-571. https://doi.org/10.1016/j.matpr.2022.03.186

J-Researchers

Journal of Civil Engineering Researchers

Journal homepage: www.journals-researchers.com

Investigation of the Effect of High Temperature on the Microstructure of Conventional Concrete Containing High Grade of Portland Cement

Mohammadhossein Mansourghanaei,[a,*]

[a] *Department of Civil Engineering, Chalous Branch, Islamic Azad University, Chalous, Iran*

ABSTRACT

In this laboratory study, a mixed concrete design containing 500 kg/m3 Portland cement was prepared, and elastic modulus testing, X-ray diffraction (XRD) analysis, and scanning electron microscope (SEM) image analysis were performed on concrete samples at 21 and 600 °C after a curing age of 90 days to investigate and evaluate the microstructure of concrete at room temperature and under high temperature. The results of the tests indicate that high temperature causes a decrease in the results, so that the elastic modulus of concrete experienced a decrease of 71.63% from 73.33 GPa at 21°C to 24.12 GPa at 600 °C, and in the XRD analysis, a decrease in the height of the peaks of hydrated elements is observed. The low peak height of calcium hydroxide in the XRD spectrum indicates a proper polymerization process in conventional concrete. In SEM analysis, at a temperature of 21 °C, due to the completion of a large part of the polymerization process, the tree structure, pores and unhydrated particles are seen in their minimum amount, but after applying a temperature of 600 °C to the concrete sample, with damage to the microstructure of the concrete and the hydrated calcium aluminum sulfate (C-A-S-H) and hydrated calcium silicate (C-S-H) gels, an increase in the tree structure, pores and cracks is evident in the concrete sample.

ARTICLE INFO

Received: January 12, 2025
Accepted: February 26, 2025

Keywords:
Ordinary Concrete
Heat
Modulus of Elasticity
Hydrated Calcium Silicate (C-S-H)
Calcium Hydroxide (Ca(OH)2)

DOI: 10.61186/JCER.7.1.62
DOR: 20.1001.1.2538516.2025.7.1.7.3

1. Introduction

In order to develop national security and passive defense in the field of civil engineering infrastructure, a lot of laboratory work has been done to produce structural concrete for strategic and sensitive centers of the country [1-3]. The strength of reinforced concrete structures of these centers plays an important role in reducing destruction and human injuries caused by enemy defense operations. Improving the strength of concrete can be achieved through the type of materials used in its mixture composition [4-10].

There are various methods to improve the mechanical properties and durability of ordinary concrete, and these goals can be achieved to some extent by increasing the grade of Portland cement in ordinary concrete. Research has shown that by increasing the grade of cement in concrete and keeping the water-to-cement ratio low, the mechanical properties of concrete can be increased, and the weak performance of concrete in these conditions can be

* Corresponding author. Tel.: +989121712070; e-mail: mhm.ghanaei@gmail.com.

compensated by adding superplasticizers [1,2,11]. In concretes with a low water-to-cement ratio, the appropriate amount of cement causes a higher concentration of the cement paste and a reduction in the existing porosity. After the polymerization process (hydration or polymerization), the pores of the concrete become smaller and, as the polymerization reaction continues, these small pores are also blocked [12]. The grade of cement used in the concrete mixture has a direct effect on the elastic modulus of the concrete [13]. Understanding the microstructure of concrete is a great help in understanding changes in the macrostructure and rheological, physical and durability performance of concrete.

The microstructure of concrete consists of various parts. According to the microstructural studies conducted by Mehta and Monteiro [14], the hydrated cement paste in ordinary concrete containing Portland cement consists of four important parts. The first and main part consists of a hydrated calcium silicate gel called tobermorite gel (C-S-H), which constitutes 50 to 60 percent of the volume of the hydrated paste. The second part consists of calcium hydroxide called portlandite (Ca(OH)2), which constitutes 20 to 25 percent of the volume of the hydrated cement paste. This compound plays a reactive role in combination with other cementitious materials in the polymerization process. In well-hydrated concretes, the presence of this compound reaches its minimum level. The third part is the hydrated calcium aluminosulfate gel, known as ettringite gel (C-A-S-H), and the fourth part belongs to the unhydrated clinker grains and other components that did not participate in the polymerization process. According to the definition, the C-S-H gel with a variable chemical formula and amorphous structure constitutes a large part [14,15] of the volume of hydrated cement paste and is the main reason for the mechanical properties and durability of hardened concrete [16,17]. However, studies have shown that the hydrated calcium aluminosulfate gel has a weakness in the vicinity of sulfate environments and Ca(OH)2 crystals have a weakness in the vicinity of acidic environments, so the presence of these compounds in concrete will play a significant role in reducing the durability properties of concrete.

The size of C-S-H gel has been estimated to be in the range of 14 angstroms [17]. Richardson has classified the structure of C-S-H gel into four types: tobermorite, japhite, zenite and metagenite, which follow the pseudo-tobermorite model, zenite having a higher calcium to silica (Ca/Si) ratio than tobermorite (which has a ratio of 1.5) [17]. The structure of zenite was first proposed by Taylor in 1968 [18]. This researcher obtained metagenite by heating zenite in the temperature range of 70–90 °C and developed the metagenite model to japhite. C-S-H gel constitutes the largest volume of hydrated cement paste in ordinary concrete. The main product of hydrated cement paste in conventional concrete with a calcium to silica (Ca/Si) ratio of 1.5 to 2 is C-S-H gel, which has a tobermorite or zenite-like structure [17]. The C-S-H structure may be based on tobermorite or zenite, so the C-S-H structure in one part of the hydrated cement paste may be different from another part of the paste. One of the reasons for this is the changes in the calcium to silica (Ca/Si) ratio at different points in the mixture, which leads to morphological changes in the C-S-H structure, which is effective in changing the density and porosity of the tobermorite gel [19]. Figure 1 shows a diagram of the direct model of the C-S-H gel structure, where P is represented by silicate tetrahedra at the O-O edges connected to the central Ca-O layer (paired tetrahedra) and the unconnected crystals are known as B (bridged tetrahedra) [17]. The C-S-H internal product in relatively large C3S or alite grains appears to consist of small spherical particles, 4–8 nm in size in hydrated pastes at 20 °C, but smaller at higher temperatures, in the range of 3–4 μm [19].

Research has shown that high temperatures have a negative effect on the microstructure of concrete [20-25]. As the temperature increases, the porosity in the microstructure of concrete increases [26]. Heat causes water to evaporate and escape from the concrete mixture, disrupting and weakening the polymerization process and causing damage to various parts of the concrete microstructure. Research has shown that due to the high interstitial pressure, water escapes from the chemical bond space in hydrated calcium silicate gel (as the main product of the polymerization process) leads to concrete failure at temperatures above 450 ℃ [27]. The use of additives with pozzolanic properties in the concrete mixture can improve the production of hydrated gels in concrete [1-5,28]. In this regard, research has shown that the use of nanoparticles with pozzolanic properties can improve the mechanical and microstructural properties of concrete exposed to high temperatures [3-5,28]. The type of materials used in concrete, such as aggregates, has a significant impact on improving the resistance of concrete to high temperatures [30]. In this regard, research has shown that the use of sea sand in the concrete mixture, due to its high mechanical and chemical properties in its microstructure, can make the resulting concrete more resistant to high temperatures (compared to the use of natural sand) [31]. Research has shown that when high temperatures are applied to concrete, the amount of pores in the concrete increases due to the increase in internal vapor pressure [32]. This factor plays an effective role in reducing the mechanical properties and durability of heated concrete. The reduction in the resistance of concrete under heat is mainly attributed to the decomposition of calcium hydroxide, and this phenomenon usually occurs in the temperature range between 450 and 500 ℃ [33]. Hertz has reported that the C-S-H gel structure decomposes at 600 °C and is destroyed at 800 ℃ [34]. The

occurrence of these processes causes a decrease in the resistance of concrete to applied loads and the permeability of concrete in corrosive environments. Other studies show that high temperatures (in the range of 600 ℃) cause a decrease in the modulus of elasticity in concrete [4,5,20,28,35]. Also, the destructive effects of high temperatures (in the range of 600 ℃) on the chemical composition of hardened concrete have been reported according to the results of XRD analysis [3,4,36-38]. Microstructural studies obtained from SEM analysis show that high temperatures (in the range of 600 ℃) cause great damage to the microstructure of concrete [3-5,20,37,39]. In this laboratory study, the investigation of the microstructural properties of ordinary concrete containing high grades of Portland cement is proposed as an innovative design with regard to the modulus of elasticity test and XRD and SEM analysis.

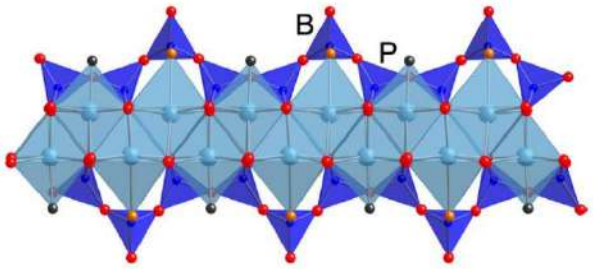

Fig. 1. Structure of C-S-H Gel [17]

2. Materials

The cement used in this laboratory study with a density of 3250 kg/m^3 and a specific surface area of 3100 cm3/g is Portland Type 2, produced by the Gilan Sabz Cement Industries Factory (Dilman), which is produced under the En 197-1 standard. Table 1 shows the chemical characteristics of the cement used. The water used to prepare lime water and make the mixture design in the current study is from the drinking water of Lahijan city. This water has a pH in the range of 5.6 to 5.7 and a density of 1000 kg/m^3. According to Section 9-10-4-2 and 9-10-4-3 of the fourth edition of the National Building Regulations of Iran, water that is drinkable, has no distinct taste or odor, and is clean and clear can be used in concrete without testing, unless previous records indicate that this water is unsuitable for concrete. The aggregate grading curve used is in accordance with Figure 2 within the ASTM C33 standard. The aggregates used were supplied from sand and gravel factories in Lahijan and were cleaned to remove organic impurities. Some of the characteristics of the fine and coarse aggregates used in this study within the aforementioned standard range have been determined based on Table 2. The superplasticizer used in this study is a fourth-generation normal polycarboxylate-based product from Durochem Middle East Company under the trade name Flowcem R700. This material was used in ordinary concrete to compensate for the poor performance and maintain the fluidity of the mortar mixture due to the high grade of Portland cement used. Some of the characteristics of the normal polycarboxylate superplasticizer are presented in Table 3.

Table 1.
Chemical Characteristics of Type II Portland Cement

Existing Material	%
Cl	Max 0/003
SiO2	21-22
Al2O3	4.5-4.8
Fe2O3	3.5-3.8
Cao	42-43
MgO	Max1.45
SO3	2-2.3
Na2O+0.658K2O	MAX 0.6
I.R	MAX 0/7
C3A	5.5-7.5
L.O.I	MAX 1/5

Table 2.
Specifications of Aggregate Used

Concrete Aggregates	Gravel	Sand
Minimum Diameter	4.75 (mm)	75 (µm)
Maximum Diameter (mm)	19	4.75
Modulus of Elasticity (mm)	5.7	2.85
Density (kg/m^3)	2750	2650
Water Absorption (%)	2.2	2.9

Table 3.
Superplasticizer Characteristics

Chemical Formula	Normal Polycarboxylate
Physical Condition	Liquid
Color	Light Brown
Density (kg/m^3)	1100
Consumption Standard	ASTM C494
pH	About 7

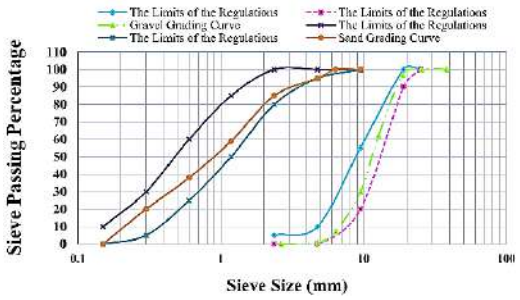

Fig. 2. Aggregate Curve

3. Mix Design and Curing

The conventional concrete mix design in this study was prepared based on the proposal of the American Concrete Association under the recommendation of the ACI Committee 211.1-89 [40], in accordance with Table 4. In this regard, the density of conventional concrete was determined to be 2397.9 kg/m^3 and the water-to-cement ratio was determined to be 0.45. In this regard, first, dry

materials were poured into the rotating mixer and the mixing process lasted for 1.5 minutes, then water and superplasticizer were added to the mixture and the mixing of the materials lasted for another 2 minutes. Next, the concrete molds that had been previously foiled and oiled were filled with concrete in three stages and in each stage, 25 blows were applied to the concrete with a special rod to compact the concrete components. After concreting, the samples were kept in a dry environment at a temperature of 21 ℃ for 24 hours and after demolding, they were kept and cured in lime water at a temperature of 21 ℃ until the test time. In preparing the mixture design in this study, the percentages determined for material consumption were selected based on standards (regarding mixture design and materials used) and the study and review of laboratory research by other researchers on the subject of this study.

Table 4.
Concrete Mix Design Specifications

Materials	Density (kg/m^3)	C.W (kg/m^3)	C.W* (%)	Control Number**
Cement	3250	500	20.85	0.1547
Water	1000	225	9.38	0.225
Gravel	2750	1000	41.7	0.3636
Sand	2650	666.15	27.78	0.2513
PNS***	1100	6.75	0.0028	0.006

* Consumed Weight
** The control number is the result of dividing the weight used by the density, and the sum of the numbers of each design must be 1 (taking into account an error coefficient of up to 3%).
*** Polycarboxylate Normal Superplasticizer

In this regard, the weight of cement used was selected as 500 kg/m^3, and by determining the water to cement ratio (0.45), the weight of water was also determined, the weight of sand in the mixture design was considered constant (1000 kg/m^3 of concrete mixture), and the consumption of superplasticizer was also determined within the range of 0.013 of the weight of cement used, and the amount of sand was also calculated and determined as a variable based on the relationships. In this study, superplasticizer was used in order to increase the efficiency of ordinary concrete due to the high grade of Portland cement and the low percentage of water to cement (0.45). In this regard, the amount of superplasticizer added to ordinary concrete was determined to be such that the slump in ordinary concrete could meet the requirements of the Iranian National Standard Nos. 2930, 6044, and 3203. Also, considering that the concrete produced was not of the air-entraining type, no air-entraining bubble additives were used in the concrete. In this laboratory study, 10 concrete samples were made, of which 6 concrete samples with cylindrical dimensions of 30×15 cm were made to perform elastic modulus testing under ambient temperature (3 samples) and high temperature (3 samples), 2 concrete samples with cubic dimensions of 10×10×10 cm were made to perform SEM analysis under ambient temperature (1 sample) and high temperature (1 sample), and 2 concrete samples with cubic dimensions of 10×10×10 cm were made to perform XRD analysis under ambient temperature (1 sample) and high temperature (1 sample).

4. Standards and Test Methods

The modulus of elasticity test was performed on cylindrical samples with dimensions of 30×15 cm after the concrete was stored in the lime water basin and after 90 days of this process (concrete curing conditions), at room temperature and under 600 ℃ (room temperature and high temperature are the test conditions), in accordance with the ASTM C469 standard [41]. In this regard, the desired sample was placed inside the concrete modulus of elasticity test frame, then the concrete sample with a cross section of 15 cm was placed vertically between the two plates of the concrete breaking jack device, then a load was applied at a speed between 0.5 and 0.9 kN/s until the sample deformed on its vertical axis. The longitudinal deformation of the concrete sample was measured using a gauge or strain gauge attached to the frame. XRD analysis was performed after 90 days of curing at room temperature and under high temperature according to BS EN 13925 [42] using a Philips PW1730 X-ray diffraction spectrometer. In this regard, crushed samples taken from the center of the concrete sample were placed inside the device and during the test, a diffraction diagram of the concrete crystals was prepared. The data obtained from X-ray diffraction is in the form of photon intensity depending on the detector angle 2θ, which is presented as a list of peak locations and their intensities on the graphs. SEM analysis was performed after 90 days of curing at room temperature and under high temperature according to ASTM C1723 [43] using a FEI Quanta200 scanning electron microscope. In this regard, the crushed concrete sample was placed in the device and images were recorded at the desired magnification and then microstructurally examined. Before performing the high-temperature tests, which were performed after a curing age of 90 days, according to the ISO834 standard [44], the concrete samples were placed in a furnace at a temperature of 600 °C for 1 hour, then the samples remained in the furnace for another 1 hour to avoid the effect of thermal shock. After the samples were removed from the furnace, the samples were kept at room temperature for 24 hours to reach temperature equilibrium. The use of this standard in other research on high-temperature tests in concrete has been reported [1,6,45].

5. Test Results and Interpretation

5.1. Elastic Modulus Test Results

The results of the elastic modulus test of concrete after a curing age of 90 days at 21 °C and after applying heat to 600 °C are shown in the graph in Figure 3. The results of each test are the average of the results of three laboratory samples. Based on these results, the elastic modulus at 21 °C and high heat was obtained as 33.73 and 12.24 GPa, respectively, which shows a 63.71% decrease in the elastic modulus after applying high heat to the concrete. Studies show that heat causes water to evaporate from the pores and cavities in the microstructure matrix of concrete, and with increasing porosity and the creation of microcracks in the concrete, the elastic modulus in the concrete will decrease. Evaporation of water from the concrete structure is always accompanied by a loss of weight, which can cause thermal cracks due to shrinkage. Research has shown that the rate of acquisition of elastic modulus of concrete increases rapidly at early ages [46-49]. In this regard, increasing the curing age (in this paper up to 90 days) of concrete has improved the result of elastic modulus in concrete under 21 °C and after applying high heat. This is due to the role of high cement grade consumption in increasing the strength of hardened concrete and the progress of the polymerization process with increasing curing age. Under these conditions, with greater participation of cement particles in the polymerization process, the volume of C-A-S-H and C-S-H gels, which are the final product of the chemical process between water and cementitious materials, increases. The main role of these gels in the composition of concrete is to fill the capillary pores, cavities and cracks in the structure of the cement matrix, on the other hand, it covers the connection in the interfacial transition zones (ITZ) at the aggregate interface. The results of XRD and SEM analysis in this study provide an interpretation of the effective role of C-S-H gel in the polymerization process and changes in concrete under high temperature. Other studies have shown that high temperatures (in the range of 600 °C) cause a decrease in the modulus of elasticity in concrete [20,28,35]. Figure 4 shows a concrete sample undergoing a modulus of elasticity test, in which the deformation of the concrete (due to changes in the gauge attached to the concrete sample) under force application is visible.

5.2. XRD Analysis Results

In this laboratory study, X-ray diffraction (XRD) spectroscopy was used to study and analyze the crystalline structure of the materials and to investigate the presence of grains and particles in the concrete. The results of the XRD analysis after a curing age of 90 days at 21 and 600 °C are shown in Figure 5.

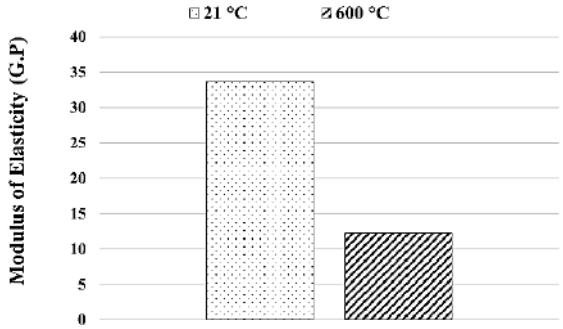

Fig. 3. Concrete Modulus of Elasticity Test Results

Fig. 4. Concrete Deformation in the Modulus of Elasticity Test

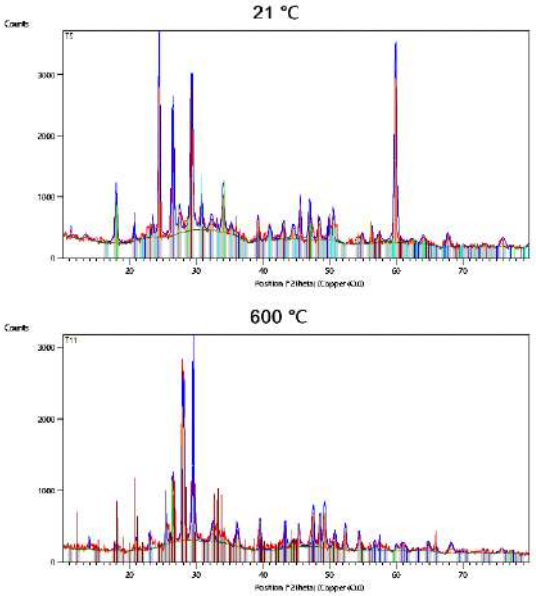

Fig. 5. XRD Test Results

Figure 6 shows a sample image of the XRD device. Based on these results, it is observed that at a temperature of 21 °C, aluminum phosphate compounds with a maximum peak height of 2670 at an angle of 59.85 degrees, followed by calcium hydroxide with a maximum peak

height of 2452 at an angle of 24.41 degrees, titanium oxide with a maximum peak height of 1794 at an angle of 29.24 degrees, calcite with a maximum peak height of 1600 at an angle of 26.45 degrees, and dolomite with a maximum peak height of 671 at an angle of 17.92 degrees, have the highest dispersion. After the removal of some elements in the high-temperature calcination process, compounds such as calcium manganese carbonate with a maximum peak height of 2092 at an angle of 29.47 degrees, carbon with a maximum peak height of 1865 at an angle of 27.9 degrees, hydrated aluminum manganese iron potassium silicate with a maximum peak height of 1712 at an angle of 28.13 degrees, and hydrated calcium aluminum silicate with a maximum peak height of 726 at an angle of 26.42 degrees have the highest dispersion.

Fig. 6. XRD Device

Applying high temperature to concrete samples has reduced the height of the peaks due to the presence of hydrated compounds, this has also been observed in the research of others [3,4], in this regard, the difference in the peak height in the XRD graph at a temperature of 21 °C (with a height of 2092) compared to a temperature of 600 °C (with a height of 2670) is 21.64%. Studies show that under the effect of high temperature in concrete, CH gel does not convert into calcium carbonates such as Calcite and as is clear from the results of the table, CH disappears at high temperature and is actually converted into Carbon and C-A and this is the main cause of the weakness of concrete at high temperature [50,51]. In other research, the destructive effects of high temperature (in the range of 600 °C) on the chemical composition of hardened concrete have been reported according to the results of XRD tests [36-38].

5.3. SEM Analysis Results

The results of the analysis of scanning electron microscope images with a scale of 3 and 20 µm under temperatures of 21 and 600 °C after a curing age of 90 days in the concrete from the current research are shown in Figure 7. Figure 8 shows an example of the SEM device. According to the images, it is observed that the microstructure of concrete consists of three basic separate and different phases as follows [1-5]:

1. The first phase includes the polymerization products containing hydrated C-A-S-H and C-S-H gels, which are mainly dark in the images, in this regard, the C-S-H gel has formed the largest volume of the cement paste.
2. The second phase includes unreacted crystals, which are a result of impurities in the raw materials or unreacted particles in the polymerization process, and are mainly white in SEM images.
3. The third phase includes the way the cement paste bonds with the aggregate in the ITZ.

In the images taken at a temperature of 21 °C, the volume of C-A-S-H and C-S-H gels is seen in a high amount in the mixture, which indicates high quality and density in the concrete, and this is mainly due to the completion of a large part of the polymerization process after the age of 90 days of curing and the use of high cement grade in the concrete mixture. The amount of pores and cracks is seen in a minimum amount in the images. White spots are caused by unhydrated cement particles and Ca(OH)2 not participating in the chemical process, in this regard, finer particles are often related to unhydrated cement particles and coarser particles to Ca(OH)2. Studies have shown that the presence of C-A-S-H crystals in the concrete composition formed due to the chemical weakness of concrete in the vicinity of sulfate environments and Ca(OH)2 crystals formed due to the weakness of concrete in the vicinity of acidic environments can have an adverse effect on the mechanical properties and durability of concrete. The images indicate that applying high heat to the concrete sample has caused damage to the microstructure of the concrete due to the water escaping from the pores and capillary pores. Accordingly, it is observed that the volume of porous areas and tree-shaped structure resulting from the destruction of the concrete matrix under high heat are present in large quantities. The size of the pores in the heated sample is much larger than that of the sample placed at 21 °C. On the other hand, due to the damage to the concrete microstructure, the volume of hydrated C-A-S-H and C-S-H gels in the mixture has been reduced. These factors are the main reasons for the decrease in the results observed in the heated concrete compared to the concrete exposed to ambient temperature in the elastic modulus and XRD tests in this study. Microstructural studies obtained from SEM analysis show that high heat (in the range of 600 °C) causes great damage to the microstructure of the concrete [20,37,39]. The presence of Ca(OH)2 particles in the

images indicates that a major part of this hydrated material has not been able to fully participate in the chemical process, and this could be due to the high cement content in the concrete, which increased the polymerization rate and did not give the opportunity for the chemical participation of some cementitious materials. Studies have shown [4,5,7] that after the materials used in the preparation and manufacture of concrete are combined, the process of chemical reaction (polymerization) between cementitious materials and water begins. The speed and extent of formation of hydrated gels, which are the final product of the chemical composition in concrete, mainly depends on the properties and ratios of cementitious materials and water.

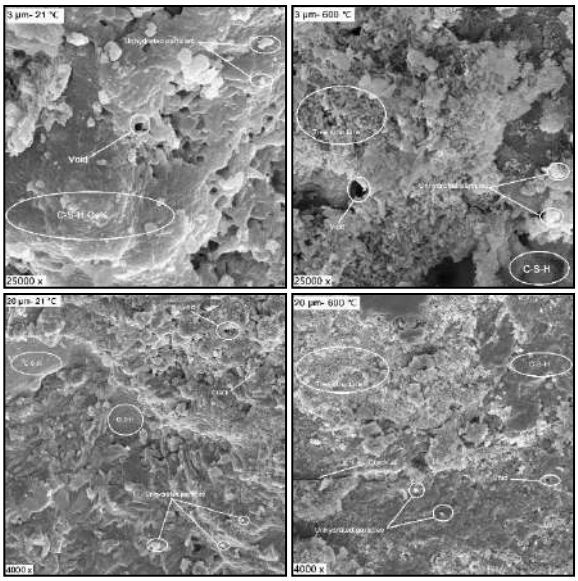

Fig. 7. SEM Images

Fig. 8. SEM Device

6. Conclusion

In this laboratory study, the microstructure of ordinary concrete containing Portland cement with a grade of 500 kg/m3 at a temperature of 21 °C and high heat (600 °C) was evaluated. In this regard, elastic modulus test and XRD and SEM analysis were performed on concrete samples. The results of this study are presented as follows.

1. In the elastic modulus test, applying heat to the concrete sample caused a decrease in the result. So that the elastic modulus of concrete decreased from 33.73 to 12.24 GPa, which resulted in a decrease of 63.71%. Similar results have also been obtained in the study of others [4].
2. In the XRD test at 21 °C, aluminum phosphate compounds with a maximum peak height of 2670 at an angle of 59.85 degrees, followed by calcium hydroxide with a maximum peak height of 2452 at an angle of 24.41 degrees, titanium oxide with a maximum peak height of 1794 at an angle of 29.24 degrees, calcite with a maximum peak height of 1600 at an angle of 26.45 degrees, and dolomite with a maximum peak height of 671 at an angle of 17.92 degrees, have the highest dispersion.
3. In the XRD test at 600 °C, compounds such as calcium manganese carbonate with a maximum peak height of 2092 at an angle of 29.47 degrees, carbon with a maximum peak height of 1865 at an angle of 27.9 degrees, hydrated aluminum manganese iron potassium silicate with a maximum peak height of 1712 at an angle of 28.13 degrees and hydrated aluminum calcium silicate with a maximum peak height of 726 and at an angle of 26.42 degrees have the highest dispersion. In this regard, the decrease in the height of the presence of elements under heat compared to the spectrum of concrete at 21 °C is evident.
4. The presence of Ca(OH)2 crystals with a high peak height in the X-ray diffraction spectrum at 21 °C is due to the incomplete polymerization process in the ordinary cement matrix. The low age of the curing period increases the volume of these crystals in the concrete mixture, which decreases with the age of the concrete. The high grade of cement used in the concrete mixture can intensify the presence of Ca(OH)2 crystals by accelerating the polymerization process. Similar results have also been obtained in the research of others [3].
5. In SEM images at a temperature of 21 °C, the volume of hydrated gels is seen in high amounts. This is due to the use of high grade of cement in

the mixture and the completion of a large part of the polymerization process, which has led to a reduction in the size and number of pores and cracks in the matrix structure of ordinary concrete. Similar results have also been obtained in the research of others [1,2,7].

6. Applying heat of 600 °C to concrete samples has caused water to be removed and microstructural phases in concrete to be destroyed. In this regard, the creation of a tree structure, destruction of the hydrated gel structure and an increase in the number and size of pores are evident in SEM images. Similar results have been obtained in the research of others [3,4,5].
7. Evaluation of SEM images of the microstructure of concrete at temperatures of 21 and 600 °C was in agreement and overlap with the results obtained from the elastic modulus test and XRD analysis.

References

[1] Mansourghanaei, Mohammadhossein, Morteza Biklaryan, and Alireza Mardookhpour. "Durability and mechanical properties of granulated blast furnace slag based geopolymer concrete containing polyolefin fibers and nano silica." KSCE Journal of Civil Engineering 28.1 (2024): 209-219. https://doi.org/10.1007/s12205-023-2202-6

[2] Mansourghanaei, Mohammadhossein, Morteza Biklaryan, and Alireza Mardookhpour. "Experimental study of the effects of adding silica nanoparticles on the durability of geopolymer concrete." Australian Journal of Civil Engineering 22.1 (2024): 81-93. https://doi.org/10.1080/14488353.2022.2120247

[3] Mansourghanaei, Mohammadhossein, Morteza Biklaryan, and Alireza Mardookhpour. "Experimental study of properties of green concrete based on geopolymer materials under high temperature." Civil Engineering Infrastructures Journal 56.2 (2023): 365-379. https://doi.org/10.22059/ceij.2022.345402.1856

[4] Mansourghanaei, Mohammadhossein, and Alireza Mardookhpour. "Analysis of the Numerical Results Obtained from the Experimental Examination of the Mechanical Properties of Geopolymer Concrete." Numerical Methods in Civil Engineering 9.1 (2024): 31-41. https://doi.org/10.61186/NMCE.2402.1047

[5] Mansourghanaei, Mohammadhossein, Morteza Biklaryan, and Alireza Mardookhpour. "Experimental Study of Mechanical Properties of Slag Geopolymer Concrete under High Temperature, Used in Road Pavement." International Journal of Transportation Engineering 11.1 (2023): 1371-1385.

[6] Mansourghanaei, Mohammadhossein, and Alireza Mardookhpour. "Investigating the Properties of Environmentally Friendly Green Concrete (Geopolymer) Under High Temperature." Sustainable Earth Trends 3.4 (2023): 62-69. https://doi.org/10.48308/ser.2024.234846.1038

[7] Mansourghanaei, Mohammadhossein, Morteza Biklaryan, and Alireza Mardookhpour. "Experimental study of modulus of elasticity, capillary absorption of water and UPV in nature-friendly concrete based on geopolymer materials." International Journal of Advanced Structural Engineering 12.2 (2022): 607-615.

[8] Mansourghanaei, Mohammadhossein. "Experimental Evaluation of The Impact Resistance of Alkali-Activated Slag Concrete Under High Temperature." Journal of Civil Engineering Researchers 6.3 (2024): 47-53. https://doi.org/10.61186/JCER.6.3.47

[9] Mansourghanaei, Mohammadhossein. "Investigating the Mechanical and Durability Properties of Geopolymer Concrete Based on Granulated Blast Furnace Slag as Green Concrete." Journal of Civil Engineering Researchers 5.3 (2023): 24-34. https://doi.org/10.61186/JCER.5.3.24

[10] Mansourghanaei, Mohammadhossein. "Evaluation of Mechanical Properties and Microstructure of Pozzolanic Geopolymer Concrete Reinforced with Polymer Fiber." Journal of Civil Engineering Researchers 5.2 (2023): 1-13. https://doi.org/10.61186/JCER.5.2.1

[11] Tadaion, M., Hani Honarmand, and Moosa Kalhori. "Impact of Plasticizers on The Quality of Concrete and The Reduction of the Cement Content." Concrete Research 3.2 (2010): 49-57.

[12] Naderi, Mahmood, Rezvan Valibeigi, and Seyed Mohammad Mirsafi. "Studying the Effects kind of Curing on Strengths and Permeability of Concrete." Journal of Structural and Construction Engineering 5.3 (2018): 106-123. https://doi.org/10.22065/jsce.2017.69343.1013

[13] Kazemian, Sina, and S. Ghareh. "Effects of Cement, Different Bentonite, and Aggregates on Plastic Concrete in Besh-Ghardash Dam, Iran." Journal of Testing and Evaluation 45.1 (2017): 242-248. https://doi.org/10.1520/JTE20160161

[14] Mehta, Povindar K., and Paulo Monteiro. "Concrete: microstructure, properties, and materials." McGraw-Hill Education (2014).

[15] Lin, Weihui, et al. "Dynamic mechanical behaviors of calcium silicate hydrate under shock compression loading using molecular dynamics simulation." Journal of Non-Crystalline Solids 500 (2018): 482-486. https://doi.org/10.1016/j.jnoncrysol.2018.09.007

[16] Juenger, M. C. G., et al. "Advances in alternative cementitious binders." Cement and concrete research41.12 (2011): 1232-1243. https://doi.org/10.1016/j.cemconres.2010.11.012

[17] Richardson, Ian G. "The calcium silicate hydrates." Cement and concrete research 38.2 (2008): 137-158. https://doi.org/10.1016/j.cemconres.2007.11.005

[18] Taylor, H. F. W. "Hydration of Cements." Proc. Fifth Int. Symp. on the Chemistry of Cement.. 1968.

[19] Richardson, I. G. "Tobermorite/jennite-and tobermorite/calcium hydroxide-based models for the structure of CSH: applicability to hardened pastes of tricalcium silicate, β-dicalcium silicate, Portland cement, and blends of Portland cement with blast-furnace slag, metakaolin, or silica fume." Cement and concrete research 34.9 (2004): 1733-1777. https://doi.org/10.1016/j.cemconres.2004.05.034

[20] Tayeh, Bassam A., et al. "Effect of air agent on mechanical properties and microstructure of lightweight geopolymer concrete under high temperature." Case studies in construction materials 16 (2022): e00951. https://doi.org/10.1016/j.cscm.2022.e00951

[21] Li, Yang, et al. "Influence of different alkali sulfates on the shrinkage, hydration, pore structure, fractal dimension and microstructure of low-heat Portland cement, medium-heat Portland cement and ordinary Portland cement." Fractal and Fractional 5.03 (2021): 79. https://doi.org/10.3390/fractalfract5030079

[22] Li, Shuangxin, et al. "Effects of isothermal microwave heating on the strength and microstructure of ultra-high performance concrete embedded with steel fibers." Journal of Materials Research and Technology 14 (2021): 1893-1902. https://doi.org/10.1016/j.jmrt.2021.07.092

[23] Amin, Mohamed, et al. "Effect of high temperatures on mechanical, radiation attenuation and microstructure properties of heavyweight geopolymer concrete." Structural Engineering and Mechanics, An Int'l Journal80.2 (2021): 181-199.

[24] Malik, Manisha, S. K. Bhattacharyya, and Sudhirkumar V. Barai. "Microstructural changes in concrete: Postfire scenario." Journal of

Materials in Civil Engineering 33.2 (2021): 04020462. https://doi.org/10.1061/(ASCE)MT.1943-5533.0003449
[25] Yu, Baoying, et al. "Compressive strength development and microstructure of magnesium phosphate cement concrete." Construction and Building Materials 283 (2021): 122585. https://doi.org/10.1016/j.conbuildmat.2021.122585
[26] Akçaözoğlu, Semiha, et al. "Examination of mechanical properties and microstructure of alkali activated slag and slag-metakaolin blends exposed to high temperatures." Structural Concrete 23.2 (2022): 1273-1289. https://doi.org/10.1002/suco.202000080
[27] Siddique, Rafat, and Deepinder Kaur. "Properties of concrete containing ground granulated blast furnace slag (GGBFS) at elevated temperatures." Journal of Advanced Research 3.1 (2012): 45-51. https://doi.org/10.1016/j.jare.2011.03.004
[28] Tobbala, D. E., et al. "Performance and microstructure analysis of high-strength concrete incorporated with nanoparticles subjected to high temperatures and actual fires." Archives of Civil and Mechanical Engineering 22.2 (2022): 85. https://doi.org/10.1007/s43452-022-00397-6
[29] Althoey, Fadi, et al. "Performance of cement mortars containing clay exposed to high temperature." Arabian Journal for Science and Engineering (2022): 1-9. https://doi.org/10.1007/s13369-021-05583-x
[30] Wang, Hui, et al. "Thermal stresses in rectangular concrete beams, resulting from constraints at microstructure, cross-section, and supports." European Journal of Mechanics-A/Solids 93 (2022): 104495. https://doi.org/10.1016/j.euromechsol.2021.104495
[31] Vafaei, Davoud, et al. "Microstructural and mechanical properties of fiber-reinforced seawater sea-sand concrete under elevated temperatures." Journal of Building Engineering 50 (2022): 104140. https://doi.org/10.1016/j.jobe.2022.104140
[32] Abolhasani, Amirmohamad, et al. "A comprehensive evaluation of fracture toughness, fracture energy, flexural strength and microstructure of calcium aluminate cement concrete exposed to high temperatures." Engineering Fracture Mechanics 261 (2022): 108221. https://doi.org/10.1016/j.engfracmech.2021.108221
[33] Bentz, Dale P. "Fibers, percolation, and spalling of high-performance concrete." Materials Journal 97.3 (2000): 351-359.
[34] Hertz, Kristian Dahl. "Concrete strength for fire safety design." Magazine of concrete research 57.8 (2005): 445-453. https://doi.org/10.1680/macr.2005.57.8.445
[35] Fan, Kunjie, et al. "Compressive stress-strain relationship for stressed concrete at high temperatures." Fire Safety Journal 130 (2022): 103576. https://doi.org/10.1016/j.firesaf.2022.103576
[36] Liu, Chihao, and Jiajian Chen. "High temperature degradation mechanism of concrete with plastering layer." Materials 15.2 (2022): 398. https://doi.org/10.3390/ma15020398
[37] Dash, Manoj K., et al. "Impact of elevated temperature on strength and micro-structural properties of concrete containing water-cooled ferrochrome slag as fine aggregate." Construction and Building Materials 323 (2022): 126542. https://doi.org/10.1016/j.conbuildmat.2022.126542
[38] Mostafa, Sahar A., et al. "Experimental study and theoretical prediction of mechanical properties of ultra-high-performance concrete incorporated with nanorice husk ash burning at different temperature treatments." Environmental Science and Pollution Research 29.50 (2022): 75380-75401. https://doi.org/10.1007/s11356-022-20779-w
[39] Hasan-Ghasemi, Ali, Mahdi Nematzadeh, and Hossein Fallahnejad. "Post-fire residual fracture characteristics and brittleness of self-compacting concrete containing waste PET flakes: experimental and theoretical investigation." Engineering Fracture Mechanics 261 (2022): 108263. https://doi.org/10.1016/j.engfracmech.2022.108263
[40] ACI Committee. "Standard practice for selecting proportions for normal, heavyweight, and mass concrete." Pub. L. No. ACI 211 (2002): 121.
[41] ASTM C469 /C469M-14, "Standard Test Method for Static Modulus of Elasticity and Poisson's Ratio of Concrete in Compression," ASTM International, 2014.
[42] Berti, Giovanni. "EN 13925-1 Non-destructive testing-X-ray diffraction from polycrystalline and amorphous material-Part 1: General principles." (2008): 1-13.
[43] ASTM C1723-16. "Standard guide for examination of hardened concrete using scanning electron microscopy." Annual book of ASTM standards (2016).
[44] ISO, ISO. "834-1: 1999-Fire-resistance tests—elements of building construction–part 1: general requirements." Int Organ Stand (1999).
[45] Kong, Daniel LY, and Jay G. Sanjayan. "Effect of elevated temperatures on geopolymer paste, mortar and concrete." Cement and concrete research 40.2 (2010): 334-339. https://doi.org/10.1016/j.cemconres.2009.10.017
[46] Abd Elaty, Metwally Abd Allah. "Compressive strength prediction of Portland cement concrete with age using a new model." HBRC journal 10.2 (2014): 145-155. https://doi.org/10.1016/j.hbrcj.2013.09.005
[47] Kim, J-K., Y-H. Moon, and S-H. Eo. "Compressive strength development of concrete with different curing time and temperature." Cement and Concrete Research 28.12 (1998): 1761-1773. https://doi.org/10.1016/S0008-8846(98)00164-1
[48] Madandoust, Rahmat, John H. Bungey, and Reza Ghavidel. "Prediction of the concrete compressive strength by means of core testing using GMDH-type neural network and ANFIS models." Computational Materials Science 51.1 (2012): 261-272. https://doi.org/10.1016/j.commatsci.2011.07.053
[49] Pirmohammadi Alishah, Farhad, and Navid Mahmoudzadeh. "Investigation of the effect of bentonite paste index on modulus of elasticity, compressive strength and performance of plastic concrete." Civil and Project 2.5 (2020): 87-109.
[50] Rashad, Alaa M. "The effect of polypropylene, polyvinyl-alcohol, carbon and glass fibres on geopolymers properties." Materials Science and Technology 35.2 (2019): 127-146. https://doi.org/10.1080/02670836.2018.1514096
[51] Morsy, M. S., et al. "Behavior of blended cement mortars containing nano-metakaolin at elevated temperatures." Construction and Building materials 35 (2012): 900-905. https://doi.org/10.1016/j.conbuildmat.2012.04.099

Author Guidelines EditEdit Author Guidelines

GENERAL GUIDELINES FOR AUTHORS

Journal of civil engineering researches invites unsolicited contributions of several forms: articles, reviews and discussion articles, translations, and fora. Contributions should fall within the broad scope of the journal, as outlined in the statement of scope and focus. Contributors should present their material in a form that is accessible to a general anthropological readership. We especially invite contributions that engage with debates from previously published articles in the journal.

Submissions are double-blind peer-reviewed in accordance with our policy. Submissions will be immediately acknowledged but due to the review process, acceptance may take up to three months. Submissions should be submitted via our website submission form (see links above for registration and login). Once you login, make sure your user profile has "author" selected, then click "new submission" and follow the instructions carefully to submit your article. If problems arise, first check the FAQ and Troubleshooting guide posted below. If you are still experiencing difficulty, articles can be submitted to the editors as email attachments.

Each article should be accompanied by a title page that includes: all authors' names, institutional affiliations, address, telephone numbers and e-mail address. Papers should be no longer than 10,000 words (inclusive of abstract 100-150 words, footnotes, bibliography and notes on contributors), unless permission for a longer submission has been granted in advance by the Editors. Each article must include a 100 words "note on contributor(s)" together will full institutional address details, including email address. We request that you submit this material (title page and notes on the contributors) as "supplementary files" rather than in the article itself, which will need to be blinded for peer-review.

We are unable to pay for permissions to publish pieces whose copyright is not held by the author. Authors should secure rights before submitting translations, illustrations or long quotes. The views expressed in all articles are those of the authors and not necessarily those of the journal or its editors. After acceptance, authors and Special Issue guest editors whose institutions have an Open Access library fund must commit to apply to assist in article production costs. Proof of application will be requested. Though publication is not usually contingent on the availability of funding, the Journal is generally under no obligation to publish a work if funding which can be destined to support open access is not made available.

Word template and guidelines

Our tailored Word template and guidelines will help you format and structure your article, with useful general advice and Word tips.

(La)TeX template and guidelines

We welcome submissions of (La)TeX files. If you have used any .bib files when creating your article, please include these with your submission so that we can generate the reference list and citations in the journal-specific style

Artwork guidelines

Illustrations, pictures and graphs, should be supplied with the highest quality and in an electronic format that helps us to publish your article in the best way possible. Please follow the guidelines below to enable us to prepare your artwork for the printed issue as well as the online version.

Format: TIFF, JPEG: Common format for pictures (containing no text or graphs).

EPS: Preferred format for graphs and line art (retains quality when enlarging/zooming in).

Placement: Figures/charts and tables created in MS Word should be included in the main text rather than at the end of the document.

Figures and other files created outside Word (i.e. Excel, PowerPoint, JPG, TIFF, EPS, and PDF) should be submitted separately. Please add a placeholder note in the running text (i.e. “[insert Figure 1.]")

Resolution: Rasterized based files (i.e. with .tiff or .jpeg extension) require a resolution of at least 300 dpi (dots per inch). Line art should be supplied with a minimum resolution of 800 dpi.

Colour: Please note that images supplied in colour will be published in colour online and black and white in print (unless otherwise arranged). Therefore, it is important that you supply images that are comprehensible in black and white as well (i.e. by using colour with a distinctive pattern or dotted lines). The captions should reflect this by not using words indicating colour.

Dimension: Check that the artworks supplied match or exceed the dimensions of the journal. Images cannot be scaled up after origination

Fonts: The lettering used in the artwork should not vary too much in size and type (usually sans serif font as a default).

Authors services:

For reformatting your manuscript to fit the requirement of the Journal of Civil Engineering Researchers and/or English language editing please send an email to the following address:

researchers.services@gmail.com

Noted: There is a fixed charge for these mentioned services that is a function of the manuscript length. The amount of this charge will be notified through a reply email.

FAQ AND TROUBLESHOOTING FOR AUTHORS

I cannot log in to the system. How do I acquire a new user name and password?

If you cannot remember your username, please write an email to (journals.researchers@gmail.com), who will locate your username and notify you. If you know your username, but cannot remember your password, please click the "Login" link on the left-hand menu at homepage. Below the fields for entering your username and password, you will notice a link that asks "Forgot your password?"; click that link and then enter your email adddress to reset your password. You will be sent an automated message with a temporary password and instructions for how to create a new password. TIP: If you do not receive the automated email in your inbox, please check your SPAM or Junk Mail folder. For any other issues, please contact our Managing Editor,Kamyar Bagherinejad (admin@journals-researchers.com).

How do I locate the online submission form and fill it out?

First you need to register or login (see above). Once you are logged in, make sure the "roles" section of your profile has "Author" selected. Once you assign yourself the role of "Author," save your profile and then click the "New Submission" link on your user home page.

Once you arrive at the submission form page, please read the instructions carefully filling out all necessary information. Unless specified otherwise by the editors, the journal section to be selected for your submission should be "Artlcles." Proceed to the remaining sections, checking all boxes of the submission preparation checklist, and checking the box in the copyright notice section (thus agreeing to journals-researchers's copyright terms). Once the first page is completed, click "Save and Continue." The next page allows you to upload your submission. Use the form to choose your file from your computer. Make sure you click "Upload." The page will refresh and you may then click "Save and Continue." You will then proceed to a page for entering the metadata for your article. Please fill out all required fields and any further information you can provide. Click "Save and Continue." The next page allows you to upload supplementary files (images, audiovisual materials, etc.). These are not required, but if you wish to provide supplementary materials, please upload them here (do no forget to click "Upload." Then click "Save and Continue." This brings you to the final page of the submission form. Please click "Finish Submission" in order to close the

submission process. You wil then be notified by email that your article has been successfully submitted. TIP: If you do not receive the automated email in your inbox, please check your SPAM or Junk Mail folder. For any other issues, please contact our Managing Editor, Kamyar Bagherinejad (admin@journals-researchers.com).

Why am I not receiving any email notifications from HAU?

Unfortunately, some automated messages from Open Journal Systems arrive in users' Spam (or Junk Mail) folders. First, check those folders to see if the message was filtered into there. You may also change the settings of your email by editing your preferences to accept all mail from [jcer] and related journals-researchers.com email accounts.

I am trying to upload a revised article following an initial round of peer-review, but I cannot locate where to upload the article. Where do I submit a revised article?

Follow the login process outlined above and when you successfully login you will see on your user home page a link next to "Author" for "active" articles in our system (usually it is only one article, but if you have mulitple submissions currently in our system, the number could be higher. Click the "Active" link and you will be led to a page that lists your authored articles currently in our system. Click the link under the column labeled "Status" and this will take you to a page showing the current review status of your article. At the very bottom of the screen, you will see an upload form under the heading "Editor decision." Here you may upload your revised article. An automated email will be sent to the editors and you may also notify them directly via email. You may then logout.

I successfully submitted an article; how long will it take for the editors to respond to me with a decision.

For all articles that are recommended for peer-review, the editors of JCER strive to notify authors of a decision within 4-6 weeks. You may contact JCER's Managing Editor, Kamyar Bagherinejad (admin@journals-researchers.com). if you have any questions relating to the review process and its duration.

For all other inquiries, please contact: Kamyar Bagherinejad (Managing Editor)

Privacy Statement

The names and email addresses entered in this journal site will be used exclusively for the stated purposes of this journal and will not be made available for any other purpose or to any other party.

Articles

Section default policy

Make a new submission to the Articles section.

Copyright Notice EditEdit Copyright Notice

Journal of Civil Engineering Researchers follows the regulations of the International Committee on Publication Ethics (COPE) and the ethical principles of publishing articles in this journal are set based on the rules of this committee, and in case of problems, it will be treated according to these rules.

Privacy Statement EditEdit Privacy Statement

The names and email addresses entered in this journal site will be used exclusively for the stated purposes of this journal and will not be made available for any other purpose or to any other party.

Scholars Pavilion

Scholars Pavilion or **Scholars Chartagi** is a monument donated by the Islamic Republic of Iran to the United Nations Office at Vienna. The monument architecture is claimed by the Islamic Republic News Agency of Iran to be a combination of Islamic and Achaemenid architecture, although the latter clearly predominates in the decorative features, with Persian columns and other features from Persepolis and other remains from the Achaemenid dynasty. The Chahartaq pavilion form runs through the architecture of Persia from pre-Islamic times to the present.

Statues of four famous Persian medieval scholars, Omar Khayyam, Al-Biruni, Muhammad ibn Zakariya al-Razi and Ibn-Sina are inside the pavilion. This monument donated in June 2009 in occasion of Iran's peaceful developments in science.

J-Researchers